Forschungszentrum Karlsruhe
in der Helmholtz-Gemeinschaftt

Wissenschaftliche Berichte
FZKA 7249

Institute for Nuclear Waste Disposal

Annual Report 2005

H. Geckeis (Ed.)

Institut für Nukleare Entsorgung

August 2006

Forschungszentrum Karlsruhe

in der Helmholtz-Gemeinschaft

Wissenschaftliche Berichte

FZKA 7249

Institute for Nuclear Waste Disposal

Annual Report 2005

H. Geckeis (Ed.)

Institut für Nukleare Entsorgung

Forschungszentrum Karlsruhe GmbH, Karlsruhe
2006

Forschungszentrum Karlsruhe GmbH
Postfach 3640, 76021 Karlsruhe

Mitglied der Hermann von Helmholtz-Gemeinschaft
Deutscher Forschungszentren (HGF)

ISSN 0947-8620

urn:nbn:de:0005-072490

Table of contents

1. Introduction of the Institut für Nukleare Entsorgung

Activities at the Institut für Nukleare Entsorgung (INE) are integrated into the research programme NUKLEAR of the Forschungszentrum Karlsruhe within the Hermann von Helmholtz Gemeinschaft Deutscher Forschungszentren (HGF). INE contributes to the German R&D on long-term safety assessment for final disposal of nuclear waste. Further activities deal with the separation of minor actinides from high-level waste (partitioning) for subsequent transmutation and the immobilization of high-level liquid waste by vitrification.

Over 10.000 t spent fuel containing approximately 100 t plutonium, 8 t minor actinides (neptunium, americium and curium) and 400 t of fission products have been generated in Germany until 2005. About 7000 t were shipped to France and UK for reprocessing to recover plutonium and uranium. The safe disposal of high-level waste consisting of spent fuel and waste arising from reprocessing is in the responsibility of the federal government.

There is an international consensus on the final disposal of highly radioactive waste in deep geological formations. Geological disposal is believed to ensure the effective protection of the population against radiation exposure arising from the waste over very long periods of time. The isolation and immobilization of nuclear waste in a repository is obtained by the appropriate combination of redundant barriers (multi barrier system). INE research focuses on the geochemical aspects of nuclear waste disposal. Special emphasis is laid on actinides and long-lived fission products because of their significant contribution to the radiotoxicity for long periods of time.

Relevant scenarios for the geological long-term behaviour of nuclear waste disposal in general assume radionuclide transport via the groundwater pathway. Thermomechanical studies are performed at INE in order to describe the evolution of the repository after closure. The possible groundwater access to emplacement caverns is assumed to cause waste form corrosion. Radionuclide mobility is then determined by the various geochemical reactions in the complex aquatic systems: dissolution of the nuclear waste form (high level waste glass, spent fuel), radiolysis phenomena, redox reactions, complexation with inorganic and organic ligands, colloid formation, surface sorption reactions at mineral surfaces, precipitation of pure solid phases and solid solutions. Characterisation and quantification of all those processes requires the availability of thermodynamic data and a comprehensive understanding on all processes at a molecular scale. Relevant radionuclide concentrations in natural groundwater lie in the nano-molar range which is infinitesimal small in relation to the main components of the groundwater. Quantification of the chemical reactions occurring in those systems calls for the application and the development of innovative methods and experimental approaches, which provide insight into the chemical speciation of radionuclides. Laser and X-ray spectroscopic techniques are developed and applied at INE. Quantum chemical calculations are currently being applied as an additional tool to confirm the experimental results and to estimate data, which are difficult to derive experimentally.

The long term safety analysis of nuclear waste disposal has to be demonstrated by model calculations being applicable to geological time scales. The experimental research programme at INE aims to acquire fundamental knowledge on model subsystems and to derive model parameters. Geochemical models and thermodynamic databases are developed as a basis for the description of geochemical behaviour of radionuclides in complex natural aquatic systems. The radionuclide migration behaviour in the geosphere becomes predictable by coupling geochemistry to transport. Transferability and applicability of model predictions are examined by designing dedicated laboratory experiments, field studies in underground laboratories and by studying natural analogue systems. This strategy allows to identify and to analyse key uncertainties related to the accuracy and the relevance of the developed models.

The Partitioning & Transmutation (P&T) strategy is pursued in many international programmes in order to achieve a significant reduction of nuclear waste radiotoxicity. P&T is considered as an alternative to ultimate waste disposal of long-lived fission products and actinides. The aim of R&D at INE is to separate and isolate long-lived minor actinides from high-level nuclear waste for the subsequent transmutation into short-lived or stable fission products, thus reducing the time horizon for waste storage from more than 100000 to less than 1000 years. INE develops highly selective extracting agents and performs extraction experiments to derive kinetic and

thermodynamic data for the extraction reaction. The continuous extraction by means of hollow-fibre modules is investigated as a separation technique alternative to classical mixer-settler, pulsed column or centrifugal extractors.

Beside research for the long-term safety assessment of nuclear waste disposal and reduction of nuclear waste radiotoxicity by partitioning, INE contributes to the decommissioning of nuclear facilities. The main process technology for the Karlsruhe vitrification plant (VEK) at the WAK site located at the area of the Forschungszentrum Karlsruhe is essentially developed at INE. This work comprises design of process components incl. the glass melting furnace and the off-gas cleaning installation. The VEK facility is now in the commissioning phase and hot operation is scheduled for late 2006. INE is involved in functional test of major process systems, the preparation of qualification records and the certification of product quality. The basis of the tests are detailed functional test programs and test instructions for each system which have been approved by the licensing authority.

Promotion of young scientists is of fundamental importance to ensure a high level of competence and to maintain a leading international position in the field of nuclear - and radiochemistry. Therefore, close cooperation with universities is indispensable. INE scientists are strongly involved in teaching at the Universities of Heidelberg, Karlsruhe, Mainz, Jena and Berlin. Radiochemistry lectures at the Universtity of Heidelberg are supplemented by practical training courses at FZK and INE laboratories. By this combination, students are educated in the field of nuclear and actinide chemistry, which most universities are not any more able to offer. Hence INE makes a vital contribution to the medium and long-term perspective of maintaining nuclear technology competence. On the European level the Network of Excellence ACTINET has been established recently to educate young scientists in actinides sciences by opening the main facilities in Europe, where handling of transuranium elements is possible, to universities and other national institutions. INE/FZK is one of the core institutions of this network.

INE laboratories are equipped with all facilities necessary to perform radionuclide/actinide research. Alpha glove boxes, shielded boxes with remote control devices and controlled atmosphere boxes are available. Classical α, β, γ spectroscopy instruments exist for the sensitive detection and analysis of radionuclides. Trace element and isotope analysis is made by instrumental analytical techniques such as X-ray fluorescence spectrometry (XRF), atomic absorption spectrometry (AAS), ICP-atomic emission spectrometry (ICP-AES) and ICP-mass spectrometry (ICP-MS). Surface sensitive analysis and characterisation of solid samples is done by X-ray diffraction (XRD), photoelectron spectroscopy (XPS) and atomic force microscopy (AFM). Sensitive laser spectroscopic techniques are developed and applied to the sensitive speciation analysis of actinides such as the laser time-resolved laser fluorescence spectroscopy (TRLFS), the laser photoacoustic spectroscopy (LPAS), the sum frequency infrared spectroscopy, and the laser-induced breakdown detection (LIBD). Structural insight into actinide species is obtained by Extended X-ray fine structure (EXAFS) spectroscopy at the INE-beamline at the Karlsruhe synchrotron source (ANKA).

A non-radioactive vitrification pilot plant consisting of a 1:1 mock-up of the VEK plant is available at INE in order to investigate and to simulate vitrification processes for hot facilities. INE is furthermore equipped with CAD workstations for technical construction and planning.

2. Highlights

Contributions collected in the present report provide a representative overview on the scientific outcome of INE research activities in 2005. The structure of the report follows widely the organisation of the institute according to research topics: Basic understanding of geochemical reactions of radionuclides on a molecular scale is considered a crucial issue. That information, however, has to be implemented into the description of the "reality" i.e. into applied studies of nuclear waste disposal subsystems. Some examples for linking molecular scale information to macroscopic processes are described. They certainly belong to the highlights of INE research. In order to obtain detailed chemical information on radionuclide speciation and structures, INE consequently develops speciation methods and analytical techniques. Beside spectroscopic methods, quantum chemical calculations are increasingly implemented as an additional tool to gain insight into the molecular structure of radionuclide species. Speciation techniques are not only applied to geochemical studies but also to answer questions towards mechanisms underlying the partitioning of minor actinides by solvent extraction using new types of extractants. Research dedicated to the immobilisation of high-level radioactive liquid waste is much more technically oriented. In this field, the long time experience of INE engineers has led to the realization of a vitrification plant on the WAK (Karlsruhe reprocessing pilot plant) site which will start hot operation in the near future.

A selection of milestones and highlights out of the research activities in 2005 are listed below:

A breakthrough has been achieved in understanding **aqueous Pu chemistry**. A consistent description of the solubility controlling reactions of Pu in acidic solution became possible for a wide range of experimental data reported so far in the literature. The occurring reactions are in thermodynamic equilibrium and can be quantified. Thus, the "mystery" of the aquatic chemistry of Pu was solved and the way was opened for further investigations on redox- and geochemical reactions under conditions relevant for a nuclear repository.

On the basis of spectroscopic experiments, all possible **interaction modes of trivalent actinides with clay minerals** have been elucidated spectroscopically: (i) outer-sphere surface complexation at the (001) basal surfaces, (ii) inner-sphere surface complexation at the (hk0) edge surfaces, (iii) cation exchange within the interlayer and (iv) for the first time the possibility of structural incorporation of actinide ions into the octahedral layer has been demonstrated. Molecular scale information on speciation of surface sorbed actinide ions obtained from spectroscopic techniques for a wide pH range is found to support the outcome of surface complexation modelling. Uncertainties of geochemical model assumptions are decreased by this approach and the confidence in model predictions can be considerably enhanced.

First radioactive experiments have been performed at the **INE-Beamline** at the synchrotron radiation source ANKA (Angströmquelle Karlsruhe). The INE-Beamline is dedicated to actinide research, with emphasis placed on spectroscopic speciation investigations related to nuclear waste disposal. After commissioning of the INE-beamline in January 2004, the first spectrum of a Am containing radioactive sample was recorded on February 2005, the same day on which the INE-Beamline was licensed for active operation. The INE-Beamline is now available to the international community for performing synchrotron-based X-ray research on radioactive samples with activities up to 10^6 times the limit of exemption. As such it represents an important component of the 'Pooled facility' of the EU European Network of Excellence for Actinide Sciences (ACTINET). The unique aspect of the INE-Beamline is that it is in close proximity to INE's active laboratories on the FZK site, with all necessary infrastructure for working with radioactive samples and well-equipped with state-of-the-art spectroscopic (notably laser-based) and analytical techniques. This is singular in all of Europe.

By application of non-linear optical **vibrational sum frequency spectroscopy** it was possible to obtain a picture of the mineral/water interface at a molecular level showing the presence of a multitude of surface hydroxyl groups and surface coordinated water molecules of different orientation depending on pH. Such information is crucial for the quantitative understanding of radionuclide interaction at solid/liquid interfaces.

Combining for the first time the **Scanning Transmission X-ray and Laser Scanning Luminescence Microscopy** to the characterisation of Eu(III)-humic acid aggregates offered the possibility to combine speciation information from the organic matter and an interacting metal ion. Both techniques reveal the existence of chemically different areas within a metal ion – humic aggregate which can be attributed to different metal ion binding states.

Those latter two results have been obtained by cooperations within the Virtual Institute: Functional Properties of Aquatic Interfaces, funded by the HGF.

A concerted study by combining EXAFS and ab-initio quantum chemical calculations has been undertaken within the **Partitioning** activities at INE in order to elucidate the Am, Cm, and lanthanide complexation with alkylated 2,6-bistriazinylpyridines (BTP) on a molecular scale. All studies were in agreement with regard to the respective complex structures and the nature of the metal-ligand binding. However, the high selectivity of the extractand for the trivalent actinides over lanthanides could not be explained and is obviously not of structural origin.

INE of Forschungszentrum Karlsruhe plays a decisive role in promoting the **Karlsruhe Vitrification plant (VEK)** towards readiness for hot operation. Major activities in 2005 were the creation of functional test programs and test instructions for the core process systems and the subsequent performance of functional tests of process systems also as well as auxiliary systems. With respect to cold test and hot operation, operational manuals for the core process technique have been completed, forming the basis for granting of the license for cold test operation in late 2005 and also the license for hot operation, which is expected in autumn 2006.

3. National and International cooperation

INE research is involved in a number of national and international cooperations and projects.

INE coordinates the **Virtual Institute Functional Properties of Aquatic Interfaces** supported by the HGF and comprising research groups at the Universities of Heidelberg, Karlsruhe and Münster. Aim of research performed at the virtual institute is the characterisation of the mineral surface/solution interface. Laser spectroscopy, X-ray spectroscopy, acoustic sensors and various microscopic techniques are being developed and applied to investigate solid/liquid interface reactions relevant to the understanding of actinide reactions in the geosphere.

“Fundamental processes of radionuclide migration” (**FUNMIG**) is an Integrated Project within the European Commission’s 6th Framework Program. It started January 2005, with a duration of four years. With respect to the number of partners and geographical distribution it is the largest such project within the EURATOM program. There are 51 Contractors from 15 European countries. There are also 20 Associated Groups from an additional three European countries, Korea and Canada. All types of key players are well represented, i.e. research organizations, universities, SME’s, national waste management organizations and national regulatory bodies. The project is coordinated by INE with Enviros S.L. as the coordination secretariat. The research program builds around five research and technological development components (RTDC’s). Two of these deal with well established and less established processes, applicable to all host-rock types. Three of them deal with processes specific to the three host-rock types under investigation in Europe, i.e. clay, crystalline and salt. Another RTDC deals with integration of the scientific progress towards application to long-term safety assessment of a nuclear repository. An important part of the project is management and dissemination of knowledge, including training.

The "Network of Excellence for actinide sciences” **(ACTINET)** is a consortium gathering more than twenty-five European research institutions. The consortium is supported by the European Commission under a four year contract established in March 2004 as an European Network of Excellence for actinide sciences. The objective of ACTINET is to take steps in order to bring both research infrastructures and human expertise in Europe to an enhanced performance level, thereby contributing to the development of the European Research Area in the fields of physics and chemistry of actinides. INE acts as one of the core members of the ACTINET consortium together with the coordinating institution Commissariat à l’Energie Atomique (CEA, France), the Institute for Transuranium Elements (ITU, European Joint Research Center), and the Studiecentrum voor Kernenergie - Centre d’Etude de l’Energie Nucléaire (SCK•CEN, Belgium). A first priority objective within ACTINET is to pool selected parts of the major facilities for actinide research of some large European institutes (CEA, ITU, INE, SCK-CEN, Forschungs-zentrum Rossendorf (FZR), and Paul Scherrer Institut (PSI)) and to operate this pool as a multi-site user facility, in order to make it accessible to all members through a competitive selection of joint projects. Further objectives are to support training and education in actinide research fields and dissemination of the achieved knowledge in actinide sciences.

INE participates a further European Integrated Project entitled **NF-PRO**: Understanding and physical and numerical modelling of key processes in the near-field, and their coupling, for different host rocks and repository strategies. NF-PRO is a four-year Integrated Project (2004-2007) that investigates key processess affecting the barrier performance of the near-field environment of geological repositories for the disposal of high-level radioactive waste and spent nuclear fuel. The near-field is an important component of the geological disposal system as it plays an essential role in ensuring the overall safety of geological disposal. In particular, the near-field is made of engineered barriers that enclose the disposed waste and contain and minimise the release of radionuclides over extended periods of time.

Two international projects focus onto the influence of colloids on radionuclide migration in crystalline host rock: The Colloid Formation and Migration (**CFM**) experiment is coordinated by NAGRA (National Cooperative for the Disposal of Radioactive Waste, Switzerland) at the Grimsel Test Site and the **Colloid Project** has been initiated by SKB (Swedish Nuclear

Fuel and Waste Management Co., Sweden) and includes field experiments at the Äspö Hard Rock laboratory. INE plays a decisive role in the laboratory programmes of both projects and is also involved in the field activities.

INE is furthermore involved in various bi- and multilateral cooperations with national universities on different topics. Scientific cooperation with various universities within Germany is partly supported by the German ministry for Economy and Technology (BmWI). Those research programs are dedicated to actinide geochemistry and specifically the impact of colloidal and natural organic matter.

4. Fundamental Studies: Process understanding on a molecular scale

This section reports fundamental studies on the chemistry of dissolved actinide species in aqueous solutions, their interaction with minerals and colloid formation processes. Research on plutonium geochemistry still represents a challenge mainly due to the complex Redox chemistry. The first contribution describes the consistent thermodynamic description of Pu solubility data and measured Redox potentials. The structure of actinide aquo ions is subject of ongoing spectroscopic studies. A thorough understanding of those species is a prerequisite for the straightforward interpretation of spectroscopic data as e.g. derived for curium ions by laser fluorescence. First experiments reveal structural changes in the actinide aquo ions at temperatures up to 200°C - a relevant temperature range in a repository for heat producing high level nuclear waste. Sorption at mineral surfaces and incorporation into secondary mineral phases represent important geochemical mechanisms governing the radionuclide retention in the vicinity of a repository. INE studies concentrate on the elucidation of sorption and incorporation mechanisms, the characterization and quantification of formed species and the implementation of this information into geochemical models. Colloids on the other hand side are known to promote radionuclide mobility under certain geochemical conditions. Studies on different colloid generation mechanisms: actinide coprecipitation with colloidal alumosilicates and sorption to clay colloids are investigated by various techniques.

4.1 Chemistry and thermodynamic of actinides in aqueous solution

M. Altmaier, H.R Cho, R. Klenze, P. Lindqvist-Reis, C.M. Marquardt, V. Neck, P. Panak, A. Seibert, C. Walther, J.I.Yun, Th. Fanghänel

Introduction

The objectives were to fill in the gaps of thermodynamic data on solubility and complexation reactions of actinides. In recent years the work was focussed on the tetravalent actinides, including Th, U, Np and Pu, for which notable progress has been achieved. Here we report a breakthrough in understanding of the aqueous Pu chemistry. In the second part, recent results on the hydration of trivalent actinides aquo ions are summarized. Further research was performed on the formation of mixed hydroxo-carbonates of tetravalent actinides, on the fluorescence of Pa(IV) and on the speciation of tri- and tetravalent f-elements in Ca-rich solution.

Hydrous PuO_{2+x}(s): Solubility and thermodynamic data

The solubility and redox reactions of Pu(IV) hydrous oxide were analysed by comparing total Pu concentrations, oxidation state distributions and simultaneously measured redox potentials under air [1] and under Ar containing only traces of O_2 ([2,3], present work). Combining all information strongly indicates that O_2 is scavenged by solid PuO_2(s,hyd) yielding mixed valent PuO_{2+x}(s,hyd) = $(Pu^{V})_{2x}(Pu^{IV})_{1-2x}O_{2+x}$(s,hyd) according to the net reaction of the water-catalyzed oxidation mechanism proposed by Haschke et al. [4]:

$$PuO_2(s,hyd) + x/2\ O_2(g) \rightarrow PuO_{2+x}(s,hyd)$$

At pH < 3 (region A in Fig.1), the oxidised fractions of PuO_{2+x}(s,hyd) (ca. 10 % in the studies of Rai et al. [1] under air and 0.5 % in the present experiment) are completely soluble and lead to a constant level of [Pu(V)] + [Pu(VI)] (under air), which is correlated and limited to the amount of oxygen in the system and/or the amount of oxidised Pu in the original Pu(IV) stock solution. In the present study under Ar, the samples at pH < 2.5 did not contain Pu(VI) but predominantly Pu(V) + Pu(III). At pH > 3, the aqueous Pu concentration is dominated by Pu(V) for both studies under air or Ar. The maximum concentration of PuO_2^+, decreasing with slope -1 in a logarithmic plot vs. pH (regions B and C in Fig.1), is limited to the solubility of PuO_{2+x}(s,hyd) considered as solid solution $(PuO_{2.5})_{2x}(PuO_2)_{1-2x}$(s,hyd). Defining the solubility product as

$$K_{sp}(PuO_{2.5} \text{ in } PuO_{2+x}(s,hyd)) = [PuO_2^+][OH^-]$$

all experimental data in dilute to concentrated electrolyte solutions lead to a consistent value at I = 0, log $K°_{sp}$ = -14.0 ± 0.8 (2σ), which is comparable to the value for $NpO_{2.5}$(s) [5]. The

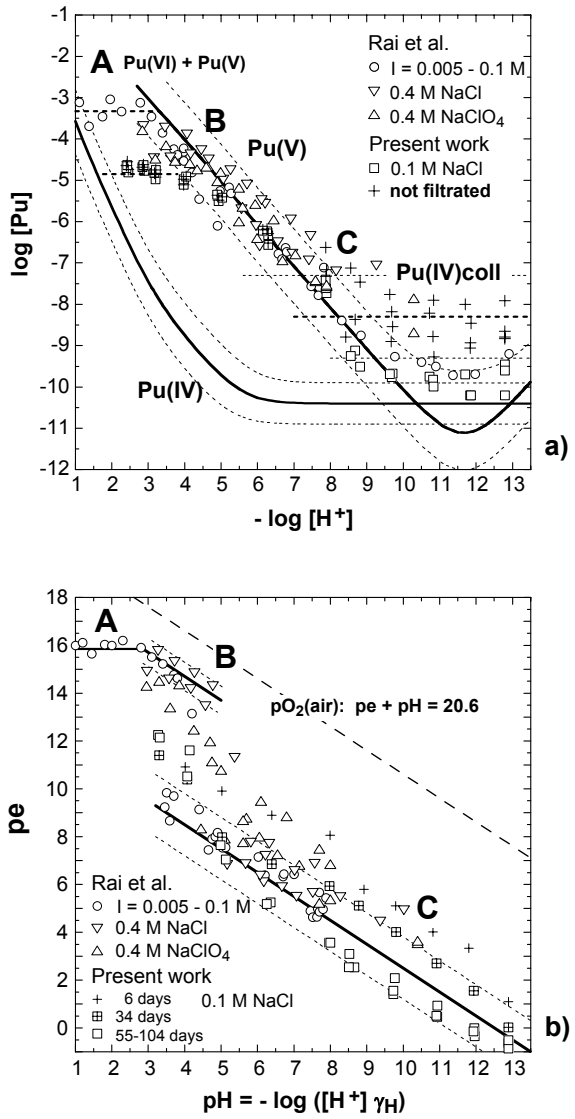

Fig.1 a) Solubility of PuO_{2+x}(s, hyd) at 20 - 25°C; calculated Pu(IV) equilibrium concentration [6], Pu concentration measured after ultrafiltration (open symbols) and $[Pu]_{tot}$ including Pu(IV) colloids/polymers (crosses), b) simultaneously measured redox potentials (pe = 16.9 Eh(V) at 25°C). Comparison of data from Rai et al.[1] under air and present work under Ar (traces O_2).

The low redox potentials at pH 4 - 13 (regions C in Fig.1) were not yet understood [1]. We have shown that they are reproducible (pe + pH = 12.5 ± 1.2), independent of the initial O_2 in the system, and caused by equilibria between PuO_{2+x}(s,hyd), PuO_2^+(aq) and small Pu(IV) colloids/polymers (1.5 - 2 nm) predominant at pH > 7 ($\log [Pu(IV)]_{coll}$ = -8.3 ± 1.0).

The molar standard Gibbs energy for PuO_{2+x}(s, hyd) = $(PuO_{2.5})_{2x}(PuO_2)_{1-2x}$(s, hyd) can be estimated from the solubility data for x = 0.003 (present study) and x = 0.05 (under air [1]):

$\Delta_f G°_m(PuO_{2+x}(s,hyd)) = 2x$
$\Delta_f G°_m(PuO_{2.5}(s, hyd)) + (1-2x)$
$\Delta_f G°_m(PuO_2(s,hyd))$
$= \{2x\ (-\ 971.2 \pm 5.4) + (1-2x)(-\ 965.5 \pm 4.0)\}$ kJ/mol

Accordingly, $\Delta_f G°_m(PuO_{2+x}(s,hyd))$ is only slightly lower than $\Delta_f G°_m(PuO_2(s,hyd)) = -965.5 \pm 4.0$ kJ/mol [5]. Since the experimental data for PuO_{2+x}(s,hyd)) include a certain solid solution stabilisation energy, it is not clear whether PuO_{2+x}(s,hyd)) can be oxidised to values of x > 0.27, the maximum value observed [4]. Possibly, the molar standard Gibbs energy for $PuO_{2.5}$(s,hyd) is slightly less negative than $\Delta_f G°_m(PuO_2(s,hyd)) = -965.5 \pm 4.0$ kJ/mol. Anhydrous Pu(IV) dioxide ($\Delta_f G°_m(PuO_2(cr)) = -998.1 \pm 1.0$ kJ/mol [5]) cannot be oxidised by O_2(g). Known analogous data and observations for hydrated and crystalline NpO_2(s) and $NpO_{2.5}$(s) support the calculated thermodynamic data for PuO_{2+x}(s). The values reported by Haschke et al. [4], $\Delta_f G°_m(PuO_{2.25}(s)) = -1080$ kJ/mol and $\Delta_f G°_m(PuO_{2.5}(s)) = -1146$ kJ/mol are much too negative. They are calculated assuming the oxidation of PuO_2(s) by water according to

$$PuO_2(s) + x\ H_2O \rightarrow PuO_{2+x}(s) + x\ H_2(g)$$

For thermodynamic reasons this reaction is not possible ($\Delta_f G°_m$ > 200 kJ/mol). The observed formation of H_2(g) is most likely caused by experimental artifacts, e.g., radiolysis effects.

In summary, a consistent description of the solubility controlling reactions of Pu in acidic solution has been achieved. The complex reactions of the various involved species are illustrated in Figure 2. The occurring reactions are in thermodynamic equilibrium and have been quantified in thermodynamic terms. Thus the "mystery" of the aquatic chemistry of Pu was solved and the way was opened for further investigations on the redox- and reaction under conditions relevant for a nuclear repository.

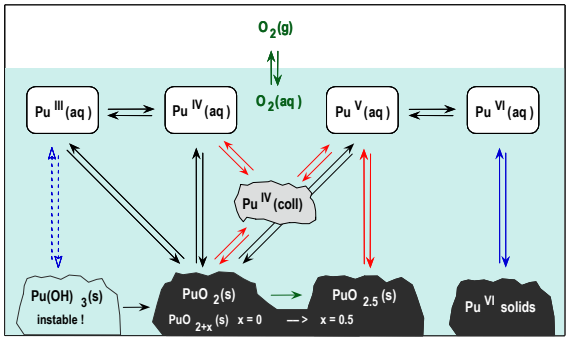

Fig.2: Equilibrium reactions (arrows) of solved (aq), solid (s) and colloidal (coll) Pu species (oxidation states III – VI) in acid solution on exposure to air.

Hydration of the Cm(III) aquo ion

It is well-established that the inner-sphere hydration numbers for the early and the late trivalent lanthanide aquo ions are 9 and 8, respectively [7] (see Fig. 4). However, detailed knowledge of the structure and dynamic properties of the aquo ions in the middle of the lanthanide series is lacking. A similar trend is expected for the trivalent actinide aquo ions, although the transition between 9- and 8-coordination may occur later in this series due to the larger ionic radius. Previously, the An^{3+} hydration numbers have been estimated by interpolation using the values obtained for Ln^{3+} ions with similar ionic radii [7]. From those results the hydration number for Cm^{3+} was estimated to be 8.9, for the heavier ions, Bk^{3+}, Cf^{3+} and Es^{3+}, 8.7, 8.2, and 8.0, respectively, while the lighter ions, Ac^{3+}–Am^{3+}, were all found to be 9-coordinate. More recently, EXAFS has been used to derive hydration numbers and bond distances for the U^{3+}–Cf^{3+} aquo ions. The results, compiled in [8], showed a steady decrease in the An–O bond distance with increasing atomic number, while the reported hydration numbers were somewhat scattered between about 7 and 10. A re-evaluation of the EXAFS data for Cm^{3+}(aq) showed that the first hydration shell is clearly asymmetric, consistent with a tricapped trigonal prism coordination geometry with six shorter and three longer Cm–O distances [9].

We have recently studied the temperature-dependency of Cm^{3+}(aq) with time-resolved laser fluorescence spectroscopy (TRLFS) from 20 to 200 °C [10]. An equilibrium between 9- and 8-hydrated Cm^{3+} was established, with a dominant moiety of the 9-coordinate species at room temperature. Further evidence for the coexistence of such species in aqueous solution obtained last year will be summarized below.

Fig. 3 shows the normalized fluorescence emission spectra of 0.5 μM Cm^{3+}(aq) at 20, 100, 150, and 200 °C. Emission is observed from the first excited $^6D'_{7/2}$ state to the $^8S'_{7/2}$ ground state, both of which are split by the ligand field into four Kramers doublets. The ground state splitting is not resolved, while the thermal population of the higher excited crystal field levels of the emitting $^6D'_{7/2}$ state gives rise to three 'hot bands', A_2–A_4, situated at the blue

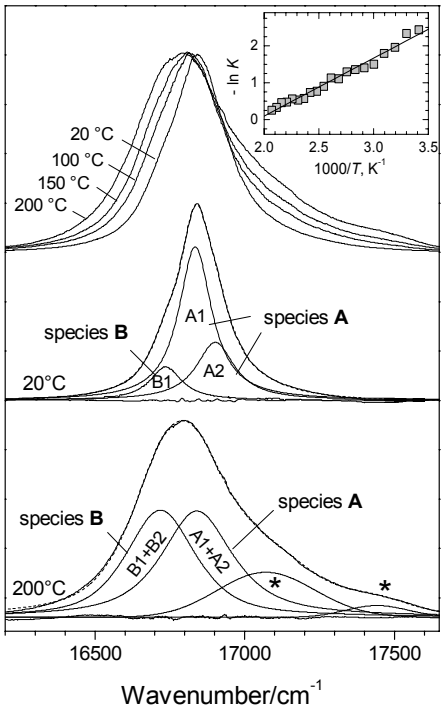

Fig. 3 $^6D'_{7/2} \rightarrow {}^8S'_{7/2}$ emission spectra of Cm^{3+} in: (a) 0.1 M $HClO_4$ aqueous solution at 20, 100, 150, and 200 °C. Species **A** and **B** refer to nona- and octahydrated species, respectively [10].

side of the main transition, A_1. The spectra are broadened asymmetrically and shifted to lower energies with increasing temperature, whilst the emission intensity and lifetime decrease notably [10]. Two spectral components, **A** and **B**, assigned to nona- and octahydrated Cm^{3+}, respectively, can be deduced from the spectra. The spectral composition of these species according to the various emitting levels is shown in the lower part of Fig. 3. The **B/A** intensity ratio follows the Van't Hoff equation with ΔH = 13.1 ± 0.4 kJ mol^{-1} and ΔS = 25.4 ± 1.2 kJ mol^{-1} K^{-1} (insert to Fig. 3); the ratio between **A** and **B** are roughly 90:10 at 20 °C and 60:40 at 200 °C [10]. Hence, at 20 °C the average hydration number is 8.9, which agrees nicely with the predicted value based on the ionic radius and the experimentally determined Ln^{3+} hydration numbers [7,8] (see Fig.4).

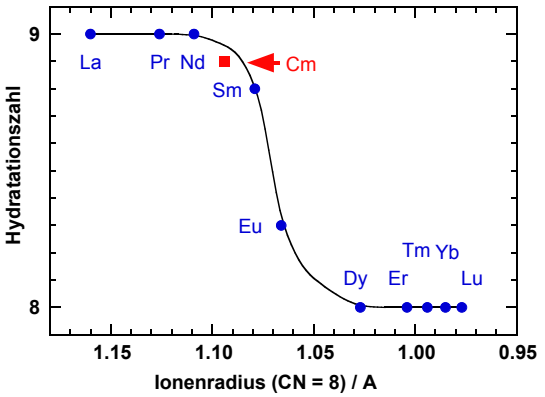

Fig. 4 Average hydration number of the lanthanide aquo ions as a function of their ionic radii [7].

These findings are in good agreement with recent quantum chemical calculations, showing the transition to be entropy driven (see section 6.4, p. 69). Moreover, the assignment of species **A** and **B** is supported by direct comparison with the spectra of the crystalline host compounds $[La(H_2O)_9](CF_3SO_3)_3$ (**1**), $[La(H_2O)_9]Cl_3 \cdot 15\text{-crown-}5 \cdot H_2O$ (**2**), and $[Y(H_2O)_8]Cl_3 \cdot 15\text{-crown-}5$ (**3**). Fig. 5 shows the spectra of $[Cm(H_2O)_9]^{3+}$ in **1** and **2** and $[Cm(H_2O)_8]^{3+}$ in **3**, together with the coordination polyhedron of the host metal ion. The asymmetry/ shoulder seen at the high-energy flanks of **2** and **3** are mainly due to transitions from the A_2 levels, whereas in **1** the A_1 and A_2 levels are rather narrowly spaced and can only be discerned at low temperature. The fact that the energy at peak maximum of

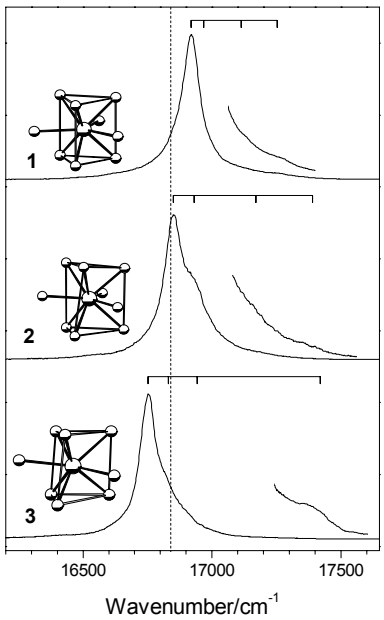

Fig. 5 Emission spectra of **1–3** at 20 °C, in comparison with the Cm^{3+} aquo ion spectrum, represented by the dashed line at 16840 cm^{-1}.

component **A** of Cm^{3+}(aq) and **2** are similar, while that of **1** and **3** are blue- and red-shifted, respectively, suggests that the main Cm^{3+} aquo species have a tricapped trigonal prismatic geometry at room temperature, probably with a lower symmetry than that in **1**, C_{3h}. More information on high-resolution spectra on Cm(III) in crystalline hydrates of diamagnetic lanthanides will be found in section 6.2, (p.57).

The equilibrium is expected to shift from 9- to 8-fold hydration with decreasing activity of water, e.g., with increasing ionic strength. TRLFS spectra of Cm(III) have been recorded in perchloric acid ($HClO_4$) in the concentration range from 7.1 – 12 M. Perchlorate has been chosen as a counter ion because of its low coordination affinity to hard Lewis acids such as Ln^{3+} and An^{3+}. In 7.1 M $HClO_4$ the emission spectra are identical to those at low acid concentration. However, above 7.1 M $HClO_4$ a continuous red-shift of the emission peak is ob-

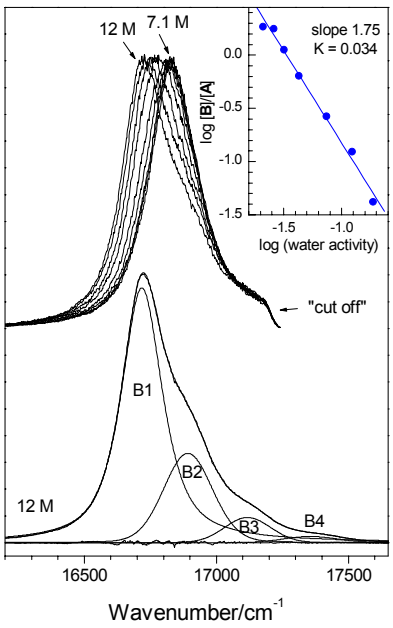

Fig. 6. $^6D'_{7/2} \rightarrow {}^8S'_{7/2}$ emission spectra of Cm^{3+} in 7.1 to 12 M $HClO_4$ at 20 °C. The curve-fitted component bands in the lower part of the figure correspond to the emission contributions from the B_1–B_4 crystal field levels of the exited $^6D'_{7/2}$ state.

served (Fig. 6). This shift is similar to that observed with increasing temperature (Fig. 3). The spectra of a new species, derived by peak deconvolution is shown in the lower part of Fig. 6. It is nearly identical with the spectrum of the 8-fold coordinated high-temperature species, except for the more pronounced hot bands in the latter, due to the elevated temperature. It is reasonable to interpret this redshift as a change in the coordination number from 9 to 8 taking place at high ionic strength where the

water activity is very low (in 12 M $HClO_4$ the water to acid ratio is ≈ 4). This may be understood as a competition for water of hydration between Cm^{3+} and H^+ ions. As shown in the insert of Fig. 6, a linear relationship between the intensity ratio of the 9- and 8- fold hydrated species and the water activity is found. The deviation of the derived slope of 1.75 to the expected value of 1 may be due to ionic strength effects. However, it can to be excluded that at high $HClO_4$ concentrations, ClO_4^- coordinates directly to the Cm replacing two water molecules.

To corroborate this interpretation of a change in the coordination number occurring at very high ionic strength, Cm L_3-edge EXAFS spectra were recorded at the INE-Beamline (ANKA, Karlsruhe) on two different ~10 mM Cm^{3+} aqueous solutions, one acidified with 0.01 M $HClO_4$, and one with 12 M $HClO_4$ [11]. The results show that the coordination number and the Cm-O bond distance decrease slightly when going from 0.01 to 12 M added $HClO_4$. The refined coordination numbers, *N*, and Cm-O bond distances, *r*(Cm–O), in the 0.01 and 12 M $HClO_4$ solutions are: *N* = 8.5(8), *r*(Cm–O) = 2.477(5) Å and *N* = 8.1(6), *r*(Cm–O) = 2.466(4) Å, respectively.

To summarize, we have shown that the $^6D'_{7/2} \rightarrow {}^8S'_{7/2}$ emission spectrum of $Cm^{3+}(aq)$ shifts to lower energy with increasing temperature. This redshift, which is due to an increase of the ligand field, is interpreted as a change in the inner-sphere hydration number of the Cm^{3+} ion from 9 to 8. Spectra of $[Cm(H_2O)_9]^{3+}$ and $[Cm(H_2O)_8]^{3+}$ in crystals support these findings. The hydrated Cm^{3+} ion persists as a stable nonahydrate species in aqueous solution up to very high ionic strength and over a wide concentration range of perchloric acid. However, its coordination geometry changes, most likely to 8-coordination, when the water-to-acid concentration ratio becomes lower than about 4. This is reflected in a slight shortening of the mean Cm-O distance, as determined by EXFAS.

References

[1] D. Rai et al., a) Soil Sci. Am. J. 44, 490 (1980), b) Radiochim. Acta 35, 97 (1984), c) Radiochim. Acta 89, 491 (2001).

[2] C. Lierse, J.I. Kim, Report RCM 02286, Technische Universität München, 1986.

[3] H.R Cho, C.M. Marquardt, V. Neck, A. Seibert, C. Walther, J.I.Yun, Th. Fanghänel, Proceeding of the ACTINIDES 2005

[4] J.M. Haschke, T.H. Allen, L.A. Morales, a) Science. 287, 285 (2000), b) J. Alloys Comp. 314, 78 (2001), c) J. Alloys Comp. 336, 124 (2002).

[5] R. Guillaumont et al. (OECD-NEA TDB), Update on the Chemical Thermodynamics of Uranium, Neptunium, Plutonium, Americium and Technetium, Elsevier, 2003.

[6] V. Neck, J.I. Kim, Radiochim. Acta, 89, 1 (2001).

[7] E. N. Rizkalla and G. R. Choppin, 'Lanthanides and Actinides Hydration and Hydrolysis' in *Handbook on the Physics and Chemistry of Rare Earths. Lanthanides-/Actinides: Chemistry*, eds., K. A., Jr. Gschneidner, L. Eyring, G. R. Choppin and G. H. Lander, Elsevier Science, Amsterdam, 1994, Vol. 18, Chapter 127, pp 529–558.

[8] F. H. David and V. Vokhmin, *New J. Chem.*, 2003, 27 1627 (Table 3 and refs therein).

[9] P. Lindqvist-Reis, R. Klenze, M. A. Denecke, T. Fanghänel and A. Eichhöfer, to be submitted.

[10] P. Lindqvist-Reis, R. Klenze, G. Schubert, T. Fanghänel, *J. Phys. Chem. B*, 2005, 109, 3077.

[11] P. Lindqvist-Reis, R. Klenze, R. G. Haire., T. Fanghänel, unpublished results.

4.2 Actinide sorption onto clay minerals: Adsorption and structural incorporation

D. Bosbach, H. Brandt, P.J. Panak, Th. Rabung, D. Schild, R. Klenze, M.-C. Pierret, A. Bauer, H. Geckeis, Th. Fanghänel
Forschungszentrum Karlsruhe, Institut für Nukleare Entsorgung, Germany

partly in cooperation with M.H. Bradbury, B. Baeyens
Paul-Scherrer-Institut, Labor für Entsorgung, Villigen, Switzerland

Introduction

Clay minerals play a major role in various concepts for the disposal of high-level nuclear waste (HLW) in deep geological formations. Geological clay formations are considered as a host rock for a waste repository. Also, clay based materials may be used as a backfill or buffer, representing a geotechnical barrier within a multi-barrier system. Finally, after contact with ground water, clay minerals will form as secondary phases upon alteration of the waste matrix, such as HLW borosilicate glass, during the geochemical evolution of the repository system over long periods of time. Dissolution of various compounds of the multibarrier system and subsequent reprecipitation of secondary clay minerals may occur. The actinides dominate the radiotoxicity in a high-level nuclear waste repository over long time-scales. Under waste repository relevant geochemical conditions dissolved Am, Cm and some fractions of Pu may occur in the trivalent redox state.

Clay minerals have a high affinity for trivalent actinides and can provide a significant retention potential. However, due to their structural complexity, several molecular level sorption mechanisms have been identified: (i) outer-sphere surface complexation at the (001) basal surfaces, (ii) inner-sphere surface complexation at the (hk0) edge surfaces, (iii) cation exchange within the interlayer and (iv) structural incorporation into the octahedral layer. Adsorption and exchange phenomena (i-iii) and the associated molecular level reaction mechanisms have been studied extensively in the past (e.g. [1]). Additional studies have been performed with well defined Al_2O_3 single crystal surfaces in order to gain insight into the nature of sorbed actinide species. Al_2O_3 surfaces contain different types of Al-OH functional groups which are assumed to exist as well at clay mineral edges.

A molecular level process understanding of key sorption reactions, such as adsorption and structural incorporation, offers many advantages for describing the complex evolution of a nuclear waste repository system over extended periods of time.

Adsorption to Sapphire Single Crystals

An auspicious possibility to get a deeper insight in processes at the mineral surface is the use of single crystal surfaces. The main advantage of using single crystals is the possibility to investigate the metal ion sorption on various well characterized and clear defined crystal plane surfaces. Due to their low roughness and the availability of different crystal planes and dimensions, sapphire (α-Al_2O_3) single crystals were selected as a model system to study interface reactions by a combination of various methods, such as GI-EXAFS, non-linear IR-spectroscopy (see section 6.2, p. 57) and quantum chemical calculations (see 6.4, p. 69). Here we report TRLFS and XPS results on the reaction of Cm(III) at the α-Al_2O_3/water interface, taken as a model for iron(III)oxides and other Al-containing minerals in the nature as clays and gibbsite [2].

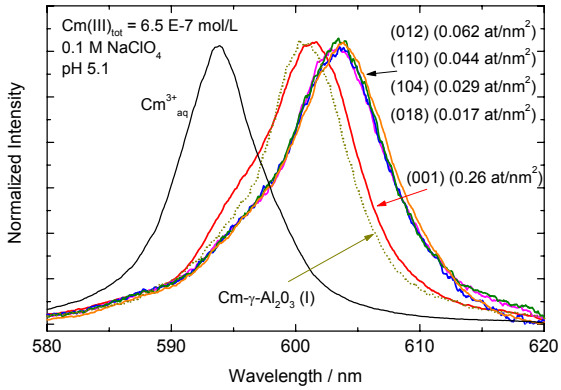

Fig. 1 TRLFS spectra for the Cm(III) sorption onto different sapphire single crystals (001), (110), (012), (104) and (018) at pH 5.1 and 0.1 M $NaClO_4$ normalized to the same peak height. Cm(III) surface concentrations measured by α-spectrometry are added in brackets in atoms/nm^2. Also the spectra for the unsorbed free Cm^{3+} aquo ion and for the first Cm(III) sorption species onto γ-Al_2O_3 derived by peak deconvolution at similar pH are included.

In the present study, the Cm(III) sorption onto different crystal planes (018), (104), (012), (110), (001) of sapphire single crystals (area: 1cm^2) is investigated at low Cm(III) concentrations and at pH 4.5 and 5.1 by time resolved

laser fluorescence spectroscopy (TRLFS), XPS, α-spectrometry and autoradiography [1]. A homogeneous Cm(III) distribution on the sapphire surfaces is demonstrated by autoradiography for all samples. Sorbed Cm(III) concentrations are in the range 2 x 10^{-12} – 7 x 10^{-11} mol/cm^2 or 0.02 – 0.4 atoms/nm^2. TRLFS and XPS spectra of sufficient intensity are obtained for all samples proving the sensitivity of both spectroscopic methods.

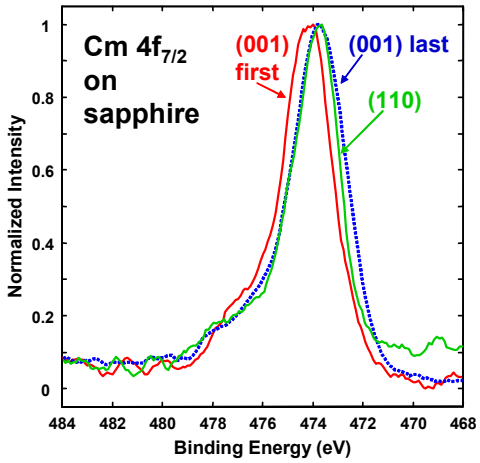

Fig. 2 Cm $4f_{7/2}$ spectra measured by XPS for the Cm(III) sorption onto (001) and (110) sapphire single crystal planes. In case of the (001) surface the first and the last spectrum is shown within an intensive XPS study (large measuring time, high power etc.).

TRLFS spectra of Cm(III) sorbed onto the (001) surface show distinct differences with regard to peak position and fluorescence lifetime compared to those obtained for the four other crystal planes (Fig. 1). Similar information is available from XPS. The extent of Cm(III) sorption differs for the individual crystal planes with the highest sorption taking place at the (001) the lowest at the (018) orientation. Similar TRLFS spectra for Cm(III) sorbed at the (001) plane, onto colloidal γ-Al_2O_3 and onto clay mineral surfaces suggest the presence of similar surface species. Variations in the TRLFS and XPS spectra for Cm(III) sorbed at the Al_2O_3 (001) plane after high vacuum treatment and after water contact suggest an important influence of surface relaxation processes on the surface properties. Such an effect is much less pronounced for the other sapphire crystal planes.

Sorption to clay

Sorption of Cm(III) and Eu(III) at trace concentrations onto Ca-montmorillonite (SWy-1) and Na-illite (Illite du Puy) has been studied under anaerobic conditions by batch sorption experiments and time-resolved laser fluorescence spectroscopy (TRLFS) [3]. Comparison of the results from spectroscopic and batch sorption experiments with Cm and Eu indicates the existence of outer-sphere complexes at pH < 4 in the experiments with Na-illite (0.25g/L clay; 2.5 x 10^{-7} mol/L Cm; 0.1 mol/L $NaClO_4$). In the case of Ca-montmorillonite, (0.25g/L clay, 2.5 x 10^{-7} mol/L Cm or 10^{-6} mol/L Eu, 0.066 mol/L $Ca(ClO_4)_2$), Cm/Eu outer-sphere complexes do not form at significant levels due to the Ca^{2+} competition for the clay cation-exchange sites. TRLFS spectra indicate the formation of inner-sphere surface complexes at pH > 5 for both clay minerals (Fig. 3). Five H_2O/OH^- molecules remain in the first metal ion coordination sphere of the sorbed Eu/Cm. Measured fluorescence lifetimes of sorbed Eu/Cm and peak de-convolution of Cm-spectra are consistent with the formation of surface complexes of the form $\equiv$S-O-Eu/Cm$(OH)_x^{(2-x)}(H_2O)_{5-x}$. At pH $\geq$ 12 Cm becomes incorporated into a surface precipitate at the Ca-montmorillonite surface presumably composed of $Ca(OH)_2$ or calcium silicate hydrate. A dramatic shift of the fluorescence emission band by more than 20 nm and a clear increase in the fluorescence lifetime suggest the almost complete displacement of coordinated H_2O and OH^- (Fig. 3).

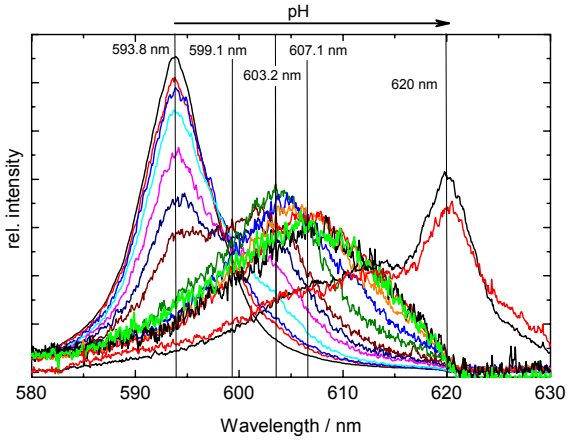

Fig. 3 Ca-montmorillonite. Cm fluorescence spectra normalized to the same peak area. Total Cm concentration = 2.5 x 10^{-7} mol/L, S:L ratio = 0.25g/L, 0.066 mol/L $Ca(ClO_4)_2$ solution. b) Na-illite. Cm fluorescence spectra normalized to the same peak area; total Cm concentration = 2.5 x 10^{-7} mol/L, S:L ratio = 0.25g/L, 0.1 mol/L $NaClO_4$ solution.

The pH dependent Eu sorption data obtained in batch experiments are congruent with spectroscopic data on Eu and Cm within experimental uncertainties thus demonstrating the validity of Eu as a homologue for trivalent actinides. The experimental data were modelled using a quasi-mechanistic sorption model [4] (the two site protolysis non electrostatic surface complexation and cation

exchange 2SPNE SC/NE model). This work has been done in cooperation with M.H. Bradbury and B. Baeyens from Paul-Scherrer Institute, Switzerland. For both clay minerals the Eu sorption edges could be quantitatively modelled in the pH range ~3 to ~10 using cation exchange reactions for Eu^{3+}/Na^{+} and Eu^{3+}/Ca^{2+} and three surface complexation reactions on the strong sorption sites forming $\equiv S^{S}OEu^{2+}$, $\equiv S^{S}OEuOH^{+}$ and $\equiv S^{S}OEu(OH)_2^{0}$ inner sphere complexes which appear successively with increasing pH.

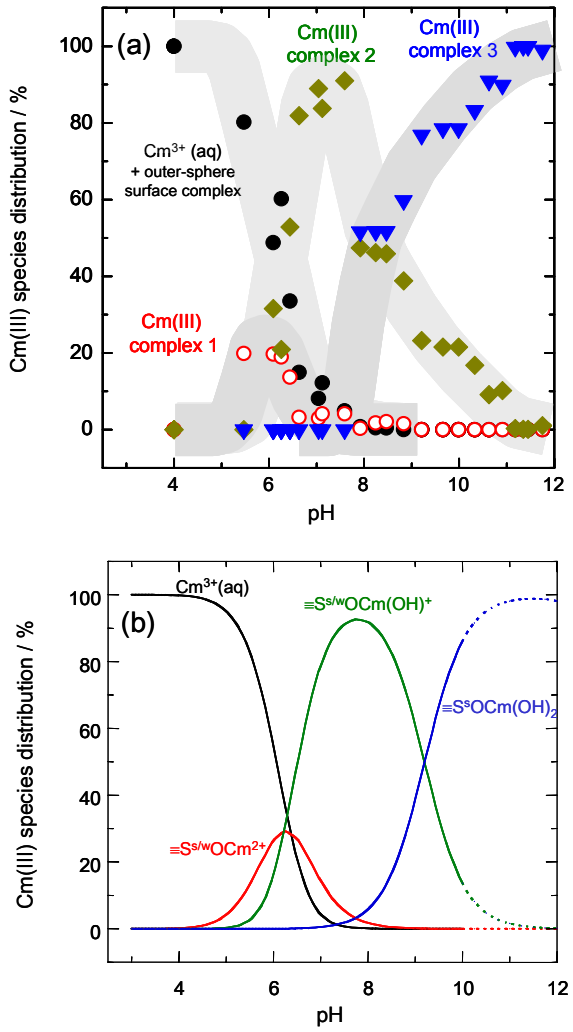

Fig. 4 Surface species distribution plots for Cm on Ca-montmorillonite (a) deduced from TRLFS measurements and (b) modelled using the 2SPNE SC/CE model and the modified Cm hydrolysis data. (Conditions: S:L = 0.25 g L^{-1}, Cm = 2.5 10^{-7} M, 0.066 M $Ca(ClO_4)_2$.)

De-convolution of the normalised laser fluorescence spectra measured at different pH values indicated three distinct Cm surface complexes, Cm complexes 1, 2 and 3 for both clay minerals, in agreement with model predictions, but with different distribution functions for the individual species.

Under the assumption that Eu and Cm exhibit essentially the same hydrolysis and sorption behaviour, the Eu surface complexation constants were used to predict surface species distribution functions for Cm under the same experimental conditions used in the TRLFS measurements. Comparison of modelled and deduced species distributions indicated that for both clay minerals peak heights and widths of the three peaks did not correspond particularly well.

It is shown that the calculated species distribution functions are sensitive to the values of the hydrolysis constants used in the calculations, whereas modelling the sorption edge measurements by applying the 2SPNE SC/CE approach is much less sensitive. By modifying the values of the hydrolysis constants within their uncertainty range and re-modelling the sorption edge, considerably better correspondence between the modelled and TRLFS species distribution functions was found. In particular, peak positions, heights and widths for the model predicted peaks for the $\equiv S^{S}OCm^{2+}$ and $\equiv S^{S}OCmOH^{+}$ species distribution, and those for Cm complexes 1 and 2 derived from TRLFS, were found to be very close for both clay minerals. Fig. 4 shows spectroscopic data (a) in comparison with modeling (b). However, discrepancies were still apparent between the profile for the calculated $\equiv S^{S}OCm(OH)_2^{0}$ surface species and the Cm complex 3 species.

Structural incorporation

In addition to adsorption reactions at external clay mineral surfaces (including interlayer), incorporation of trivalent actinides into the bulk structure during the formation of clay minerals may occur via coprecipitation. Structural substitution within the octahedral and tetrathedral sheets of various clay minerals in nature has been known for many decades. However, it is not unambiguously known whether trivalent actinides (5f elements) and chemical homologous (trivalent) rare earth elements (REE, 4f elements) can occupy an octahedral lattice site, despite their large ionic radii (e.g. $Cm(III)^{[VI]}$=0.97Å). From a crystal chemical point of view, trivalent actinides could occupy a 6-fold oxygen coordinated lattice site (Pauling's first rule). In case a divalent cation is substituted, charge balance could be achieved via a coupled substitution within the octahedral and the tetrahedral sheet or the cation substitution in the interlayer, as typical for smectites. However, compared to the size of cations which typically occur in the octahedral sites of sheet silicates (e.g. Mg^{2+}, Fe^{2+}, Al^{3+}, Fe^{3+}), the substitution by trivalent actinides

seems not to be favorable due to the large strain induced by a substitution with such large cations [5].
We have synthesized hectorite at 90°C in the presence of Cm(III) following a procedure developed by Carrado et al. [6-8].

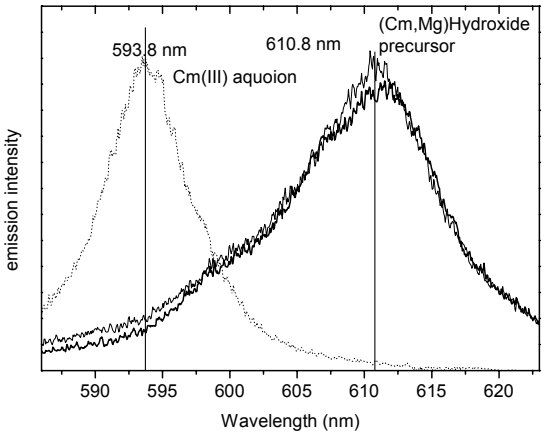

Fig 5 Cm(III) fluorescence emission spectra of Cm(III) aquoion (593.8 nm), freshly preciptated Cm/Mg Hydroxide (610.8 nm) and in the presence of all synthesis compounds (LiF, TEA, silica sol).

The Cm(III) aquo ion contains 9 H_2O molecules in the first coordination sphere . The Cm(III) fluorescence lifetime seems to be only slightly affected due to hydrolysis at higher pH values, whereas a red shift to 598.8 nm ($CmOH^{2+}$) and 603.5 nm ($Cm(OH)_2^{+}$) occurs [9].
After adding NH_4OH up to a pH of 9-10, a Cm(III) containing $Mg(OH)_2$ (brucite) precipitate forms. The 593.8 nm peak of the Cm(III) aquo ion disappears completely. Instead an emission band at 610.8 nm occurs (fig. 5). Such a large red shift of 17 nm indicates a significant change in the first coordination sphere, which has been observed for structural incorporation of Cm(III) into a host mineral.

From the monoexponential decay of the fluorescence signal in our experiments, the lifetime of the Cm containing brucite precipitate was determined to be 165 µs, which indicates the presence of 3 H_2O or OH^- molecules in the first coordination sphere. Therefore, we can exclude that Cm is bound to the brucite via surface complexation. This leads to the idea that Cm(III) is structurally incorporated into a solid phase. We conclude that in our experiments Cm(III) is structurally incorporated into a brucite-like (Mg,Cm)-hydroxide, despite the large difference of the ionic radii between Cm(III) and Mg(II).
The next step within the organo-hectorite synthesis protocol involves the sequential addition of LiF and TEA. It is well known that Cm(III) is complexed by F^-, as indicated by a Cm(III) emission peak at 601.3 nm with a lifetime of 65µs. Further, the formation of sparingly soluble solid CmF_3 upon addition of LiF can be excluded, since CmF_3 exhibits an emission band at 597.0 nm [12]. Therefore, our Cm(III) fluorescence measurements do not indicate any change upon addition of LiF solution to the (Mg,Cm)-hydroxide (fig. 6). We conclude, that Cm(III) is not removed from the (Mg,Cm)-hydroxide and complexed by TEA.
The addition of silica sol had no immediate effect on the Cm(III) emission (peak position and lifetime). In a separate series of experiments the Cm / silica sol interaction was studied [13, 14]. A Cm – silica complex yields an emission band at 605.1 nm with a lifetime of 417.1 µs. A similar peak shift has been observed for the interaction of Cm(III) with silica colloids – 606.2 nm with a lifetime of 310 µs [15]. However, this indicates a significantly different Cm(III) complexation state compared to the (Cm,Mg)-hydroxide precursor as observed in our experiments.
This means that a relatively stable Cm-complex with 3 H_2O/OH- ligands has formed almost instantaneously during the formation of Mg-hydroxide. The complexation state is not affected by the presence of the synthesis components (LiF, TEA, silica sol).

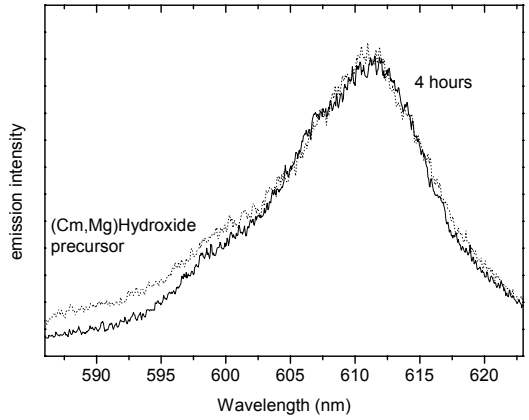

Fig 6 Cm(III) fluorescence emission spectra of freshly preciptated Cm/Mg Hydroxide (610.8 nm) (solid line) as well as aged for 4 hours in the presence of silica sol and LiF at the start of silica condensation (610.8 nm) (dotted line).

Sampling after 4 hours – The lifetime of the Cm(III) emission changes to 231 µs after 4 hours, compared to 165 µs for the (Cm,Mg)-hydroxide. This refers to 1.9 H_2O/OH^- molecules in the first coordination sphere. However, no change in the emission can be detected (610.8 nm, fig. 6). It is known that 4 hours after adding the silica sol the condensation of single [SiO_4]-tetrahedra onto the pre-existing (Mg,Cm)-hydroxide octahedral

sheets has started [6]. The condensation reaction connects the Cm-containing brucite layers with the [SiO_4]-tetrahedral sheets. As a consequence water molecules are released from the forming hectorite, leading to a reduced number of H_2O/OH^- quenchers and therefore a longer lifetime.

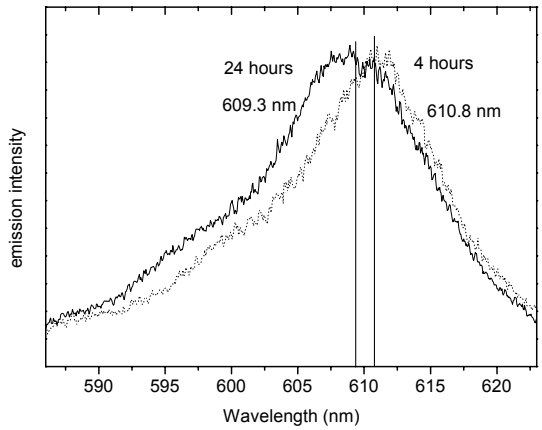

Fig 7 Cm(III) fluorescence emission spectra of Cm/Mg Hydroxide in the presence of slica sol and LiF after 4 hours (610.8 nm) (dotted line) and 24 hours (609.3 nm) (solid line).

Sampling after 24 hours – After 24 hours of reaction time, the Cm(III) emission has shifted to a shorter wavelength of 609.3 nm (fig. 8). Also, the peak broadness has increased. Further more, the lifetime does not follow a mono exponential decay law as it did during the early stages of the synthesis, but seems best to be explained by a bi-exponential decay, thus indicating the presence of two Cm(III) species. One Cm(III) species has a fluorescence life time of 246 µs which refers to 1.75 H_2O/OH^- molecules in the first coordination sphere. A second Cm(III) species exhibits a lifetime of 86 µs and 6-7 H_2O/OH^- ligands. Peak deconvolution reveals that the 1st Cm species exhibits an emission band at 611.0 nm and the 2nd Cm species at 607.1 nm. Both observations – change in peak position and in lifetime - demonstrate a significant change in the Cm ligand field at this stage of the hectorite synthesis.

It is known from the work of Carrado et al. [6-8] that after 24 hours of reaction time at 100°C, the SiO_4-tetrahedra condensation on [$Mg/Li/Cm(O/OH)_6$]-fragments is finished and loosely linked hectorite-like TOT-layers have been built. Obviously, during this process a fraction of the incorporated Cm is released and re-adsorbed onto the reaction product. As a result, two distinct Cm(III) species can be detected. The reaction product contains after TOT-layer formation structurally incorporated Cm(III) with still 1-2 H_2O/OH^- quenchers in the inner coordination sphere and a surface sorbed Cm(III) species (6-7 H_2O/OH^--ligands). The remaining 1-2 H_2O/OH^- quenchers in the inner coordination sphere of the incorporated Cm(III) are in accordance with the two OH-groups at the unconnected corners of the [$Mg/Li/Cm(O/OH)_6$]-octahedra within the octahedral layer.

The emission peak broadening as well as the shift to shorter wavelength is a consequence of the presence of two Cm species, revealed by peak deconvolution. The 1st Cm species exhibits an emission band at 611.2 nm and the 2nd Cm species at 607.3 nm. The 2nd species could be related to a surface complexed Cm(III). On the contrary, the 1st Cm species represents an incorporated species. Compared to the peak position of Cm(III) in the (Cm,Mg)-hydroxide precursor (610.8 nm), the condensation of the tetrahedral sheet results in a further red shift to 611.2 nm. The similarities in peak position and lifetime suggest that Cm(III) remains in the octahedral site. An important structural consequence of the condensation of the tetrahedral sheets onto the octahedral sheets is a distinct change in the distance between adjacent octahedral sites. The spacing changes from 3.142 Å in brucite to 3.026 – 3.033 Å in hectorite. Due to the larger ionic radius of Cm(III) compared to Mg(II), the exact distances are not known but should follow the same trend. The change in bond distance of Cm – O bonds could have an effect on the peak position of the Cm(III) emission, but not necessarily on the lifetime, which primarily depends on the number of coordinating H_2O/OH^- quenchers.

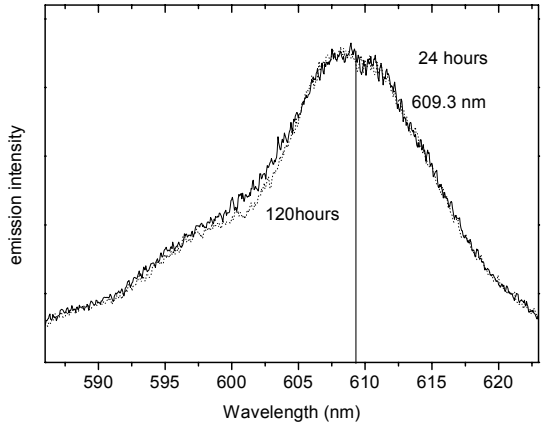

Fig 8 Cm(III) fluorescence emission spectra of Cm/Mg Hydroxide 24 hours (609.8 nm) (solid line) and 120 hours (609.8 nm) (dotted line) after adding silica sol and LiF. Hectorite formation is completed after 5 days.

Due to its size, the structural compatibility of octahedrally coordinated Cm within hectorite is limited and local structural deformation can be expected. This also could affect the Cm(III) emission – in particular with respect to an additional peak broadening. The fact that some

of the initially incorporated Cm(III) into the (Cm,Mg)-hydroxide precursor is released during the condensation of the tetrahedral sheet might be a consequence of the limited compatibility.

Nevertheless the TRLFS data indicate that a significant fraction of the Cm(III) is structurally incorporated into the hectorite-like TOT layers.

Sampling after 120 hours – The Cm(III) emission spectrum shows no detectable difference compared to the TRLFS measurements after 24 hours (fig. 8). Also, a bi-exponential decay as well as the associated lifetimes of 246 µs and 86 µs were found. After 120 hours the layer-layer correlations are optimized and larger TOT-packages built hectorite particles with the TEA organic additive in the interlayer [7]. Further, identical synthesis experiments in the presence of Eu(III) have demonstrated that Eu(III) has no effect on the kinetics of hectorite formation [14]. Apparently the formation of TOT-packages has no effect on the complexation state of the Cm(III). There are two Cm(III) species present, which are structurally incorporated into octahedral sites and inner-spherically adsorbed at the hectorite's external surface, respectively.

Conclusions

Based on TRLFS measurements distinct sorption reactions of trivalent actinides and clay minerals could be identified and characterized on a molecular level. With respect to adsorption phenomena, the spectroscopic data are fully consistent with surface compexation models. With respect to structural incorporation, the spectroscopic information will be used as a baseline for future thermodynamic solid solution models.

References

[1] T. Stumpf et al., Environ. Sci. Technol., 2001, 35(18), 3691-3694.
[2] T. Rabung, et al., J. Phys. Chem., 2004. 108(44), 17160-17165.
[3] T. Rabung et al., Geochim. Cosmochim. Acta, 2005. 69(23), 5393-5402.
[4] M.H. Bradbury, B. Baeyens et al., 2005, Geochim. Cosmochim. Acta 69(23), 5403–5412.
[5] N. Allan, et al., Trace element incorporation in minerals and melts, in Sold-solutions in silicates and oxides, C. Geiger (Edt.), 2001, Eötvös University Press: Budapest, Hungary.
[6] K.A. Carrado, Appl. Clay Sci., 2000. 17(1-2), 1-23.
[7] K.A. Carrado, P. Thiyagarajan, K. Song, Clay Minerals, 1997. 32(1), 29-40.
[8] K.A. Carrado et al., Langmuir, 1997. 13(10), 2895-2902.
[9] T. Fanghanel et al., Radiochim. Acta, 1994. 66-7, 81-87.
[10] J. Tits et al., Environ. Sci. Technol., 2003, 37(16), 3568-3573.
[11] N. Edelstein et al., Coord. Chem. Rev., 2006, (in press).
[12] N.A. Stump et al., Radiochim. Acta, 1993, 61, 129-136.
[13] H. Pieper, Kristallchemischer Einbau trivalenter f-Elemente in trioktaedrische Smectite, in Wissenschaftliche Berichte. 2005, Forschungszentrum Karlsruhe, Germany: Karlsruhe.
[14] H. Pieper et al., Clays clay min., 2006, 54(1), 45-53.
[15] P.J. Panak et al., Radiochim. Acta, 2005, 93, 133-139.

4.3 Colloid formation processes

P. J. Panak[1], M. Bouby[1], M. A. Kim[2], J. I. Yun[1], D. Breban[1,2], A. Priemyshev[2], J. I. Kim[1], H. Geckeis[1], Th. Schäfer[1]

[1]Forschungszentrum Karlsruhe, Institut für Nukleare Entsorgung, Germany
[2]Technische Universität München, Institut für Radiochemie, Garching, Germany

Introduction

Aquatic colloids are ubiquituous in natural water. They are either formed due to oversaturation and subsequent precipitation of colloidal species or are generated in groundwater by erosion from the sediment or rock. Actinide ions of high charge (z > 3+) may interact by incorporation into precipitating colloidal matter or by surface sorption processes. As a result, aquatic colloids can play a carrier role for actinide migration in natural aquifer systems without substantial geochemical retention [1-4]. The present report deals with different modes of actinide-colloid reactions.

Interactions of actinides with hydroxy-alumino-silicate colloids in "statu nascendi"

Hydroxyaluminosilicate (HAS) colloids form by coprecipitation of silicic acid and/or oligomeric ($Si_xO_z(OH_{4x+y-2z}^{y-}$) species with dissolved aluminum ions and/or aluminum hydroxo species and are assumed to be precursors of natural aluminosilicates. The characterization of the colloids is performed by laser-induced breakdown detection (LIBD), AFM, EDX, and XPS. More detailed information on LIBD is given in section 6.3 (p. 63). The particle size of the colloids is in the range of 10 nm – 50 nm with a mass concentration of 10 – 50 ppb and a Si/Al ratio of 0.7-1.2 [3,5].

For studying their interaction with actinides, coprecipitation is performed in the presence of trace amount of actinides, such as Cm(III), Am(III), Th(IV), Np(V), and U(VI). Ultrafiltration studies on tetra-, penta- and hexavalent actinides show that stable colloidal actinide-HAS-species (after 35 d conditioning time) are formed for Am(III), Th(IV), and U(VI), whereas Np(V) does not incorporate into HAS colloids The activity fraction (in %) of colloid-borne actinides formed by coprecipitation with polysilicic acid ([Si]=10^{-2} mol/L; upper part) and monosilicic acid ([Si]=10^{-3} mol/L; central part) is given in Fig. 1.

Because of the excellent fluorescence properties of Cm(III), speciation of colloidal species of trivalent actinides can be performed by time-resoved laser fluorescence spectroscopy (TRLFS) [3-5]. The interaction of HAS-colloids with trivalent actinides is investigated by TRLFS as a function of pH. The pH dependent evolution of the fluorescence spectrum shows the presence of four different Cm species (cf. Fig 2, upper part): the Cm^{3+} aquo ion, with its emission peak at 593.8 nm, and three colloid-borne species, indicated as Cm-HAS species 1, 2, and 3, with emission peaks at 598.5, 601.8 and 606.8 nm [5].

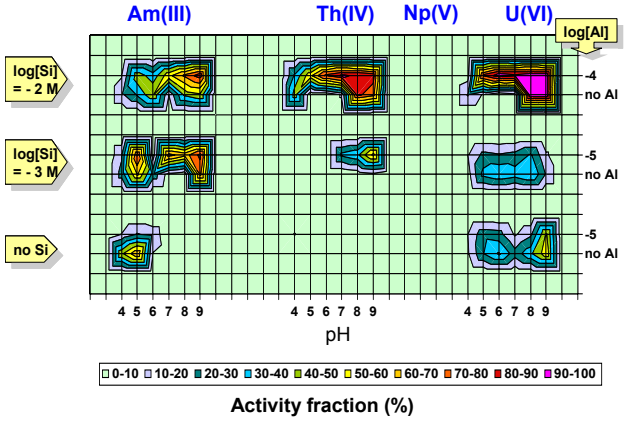

Fig. 1 Activity fractions (%) of Am(III), Th(IV), Np(V), and U(VI) in the colloidal phase.

As also shown in Fig. 2b, the lifetime of the Cm^{3+} aquo ion (67 ± 3 μs) corresponds to nine coordinating water molecules. Complexation of Cm(III) with hydroxyaluminosilicate colloids leads to an increase of the lifetime to 83.5 ± 3.7 μs (Cm-HAS(1)) and 88.3 ± 5.2 μs (Cm-HAS(2)), corresponding to 6.9 ± 1 and 6.5 ± 1 water molecules, respectively. Cm-HAS(3) becomes the predominant species at pH > 6.3, displaying an emission band red shift of 13 nm and a fluorescence life time of 518.5 μs corresponding to 0.4 water molecules. These results show that for Cm-HAS(3) the Cm(III) has lost its primary hydration sphere and is imbedded into the aluminosilicate structure of the colloids (formation of "solid solution").

In order to obtain more information on the coordination sphere of the incorporated species (Cm-HAS(3)) structural investigations are performed by EXAFS using Eu(III) as a non-radioactive homologue of trivalent actinides [6]. The spectra exhibit two significant peaks corresponding to backscattering from oxygen and silicon atoms in the first and second Eu coordination sphere. The Eu incorporated into silica colloids is surrounded

by 7-8 O atoms (coordination number as fit result, N:7.8) at a distance of 2.40 Å and 5 Si atoms (N: 4.8) at a distance of 3.70 Å. These results are in good agreement with our time-resolved laser fluorescence spectroscopy results [5], confirming the incorporation of trivalent actinides into the structure of hydroxyaluminosilicate colloids.

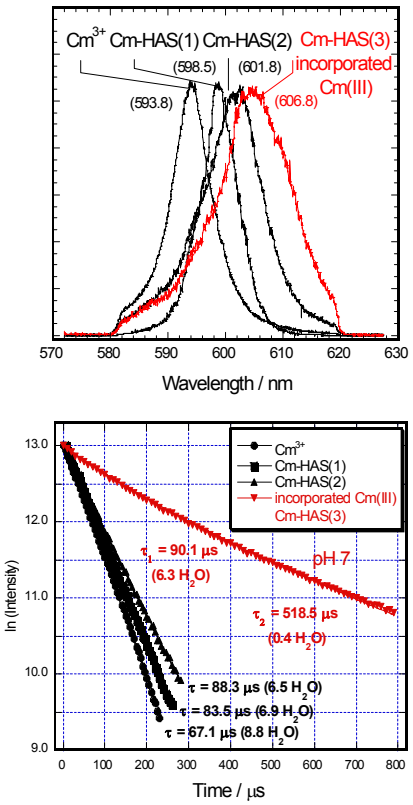

Fig. 2 Fluorescence spectra of Cm(III) with hydroxyaluminosilicate colloids (a) and fluorescence decay of the Cm^{3+} aquo ion, Cm-HAS(1), Cm-HAS(2), Cm-HAS(3) (b).

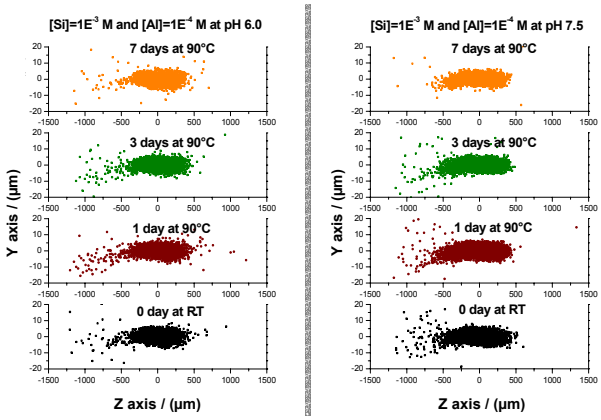

Fig. 3 Spatial distribution of breakdown events within the laser beam focus volume as a function of heating time at pH 6.0 (left) and 7.5 (right).

The long term stability of the aluminosilicate colloids is monitored by 2-dimensional laser-induced breakdown detection (LIBD). Two samples at pH 6.0 and 7.5 are heated at 90° C for 7 days to accelerate aging processes. The average colloidal size from two –dimensional recordings of the plasma light emission generated by breakdown events within the laser beam focus volume is determined as a function of heating time. Thereby, the spatial distribution of breakdown events within the laser focus volume is proportional to the particle size of the colloids [7]. The results are given in Fig. 3.

The unchanged 2-D distribution (x,y-plane) of the breakdown events around the center of the optical focus of the laser beam, before and after prolonged heating periods, proves that the periods of increased temperature do not change the colloidal state.

In addition to the stability of the colloids, the species distribution of the colloid-borne Cm species (Cm-HAS(1), Cm-HAS(2), and Cm-HAS(3)) is monitored at various pH values during a time period of 63 days [5]. Fig. 4 shows the fraction of the incorporated Cm-species (Cm-HAS(3)). At pH 9 the Cm-HAS(3) species prevails and remains stable with time. The fraction of Cm-HAS(3) decreases with lowering pH but at pH-values between 6 and 9 the corresponding Cm-HAS(3) fraction remains stable with time. These results confirm the long term stability of the colloidal species of trivalent actinides formed with aluminosilicate colloids under natural conditions (pH 6-9).

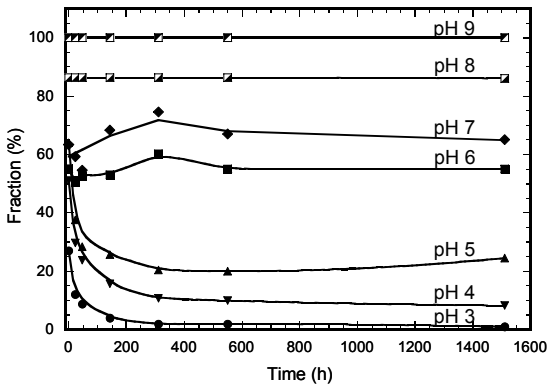

Fig. 4 Stability of Cm-HAS(3) as a function of time at different pH-values

Conclusions

Aluminosilicate colloid generation in presence of trivalent actindes leads to the formation of three colloid-borne Cm(III) species (Cm-HAS(1), Cm-HAS(2), and Cm-HAS(3)). By the use of spectroscopic methods we can differentiate between surface sorbed and incorporated species. For pH > 6 trivalent

actinides are incorporated into the structure of aluminosilicate colloids forming Cm-HAS(3). Long-term measurements confirm the stability of the aluminosilicate colloids and the colloidal Cm-species under natural aquifer conditions (pH > 6). The formation of colloid-borne species facilitates the migration of actinides, which is of major concern for the safety of nuclear waste repositories and has to be taken into account for long-term performance assessment.

Eu(III), Th(IV), U(VI) interaction with clay colloids: the influence of humic acid

Bentonite is in many disposal concepts foreseen as backfill and component of the engineered barrier system. In contact with groundwater it may as well act as a colloid source by releasing clay colloids [8]. In order to assess the influence of those colloids on radionuclide transport from a nuclear waste repository the nature of radionuclide-colloid interaction, notably the reversibility of the binding, has to be identified [9]. Moreover, the geochemical parameters controlling the colloid-colloid interaction and thus the colloid stability have to be quantified. The behaviour of Eu(III) taken as a chemical homologue to trivalent actinides and Th(IV) and U(VI) as representatives of tetra- and hexavalent actinides with clay colloids has been studied in a natural groundwater from the Grimsel test site (GTS, Switzerland; pH=9.6±0.2; Ionic strength=1.2 10^{-3} mol·L^{-1}). Concentration for each metal ion was 10 µg·L^{-1} (~4.2-6.6·10^{-7} mol·L^{-1}). The reversibility of metal binding was tested by addition of natural humic acid as competing ligand. The influence of the clay colloids presently studied on the actinide migration in a fractured zone at the Grimsel Test Site is discussed in section 5.2 (p. 29).

Colloid characterization and stability

Size distribution and stability of colloids derived from FEBEX bentonite [10] have been studied by Flow Field-Flow Fractionation (FFFF) coupled to ICP-mass spectrometry (detailed information is given in section 6.3, p. 63). Colloidal dispersions were obtained from the initial Febex bentonite material after several suspension / centrifugation / resuspension cycles in pure Grimsel groundwater. The suspensions, which have been prepared directly in pure Grimsel groundwater, exhibit sizes between 100 nm up to 250 nm for a final colloidal concentration ~ 180 mg·L^{-1}. After an initial homo ionisation of the bentonite with Li^+, the colloid yield is much higher with a final colloidal concentration ~ 1230 mg·L^{-1}. The dispersion contains much smaller colloids with a total size distribution ranging from 30 nm up to 200 nm. Agglomeration of those colloids is observed after dilution in Grimsel groundwater to a final colloid concentration of 20 mg·L^{-1}. Finally a steady state for the colloid size distribution established comparable to that obtained without previous homo ionisation with Li^+. This is illustrated in Fig. 5. Al is measured by ICP-MS as an elemental indicator for the clay colloids. These experiments demonstrate the dynamic colloid behaviour driven by ion exchange processes at the basal planes of the clay colloids platelets even at the high pH and the low ionic strength conditions of the pure Grimsel groundwater. The observed agglomeration is explained by the exchange of the Li^+ bound to the clay particle ion exchange sites by Ca^{2+} ions in the groundwater (c_{Ca}: 1.4·10^{-4} mol·L^{-1}).

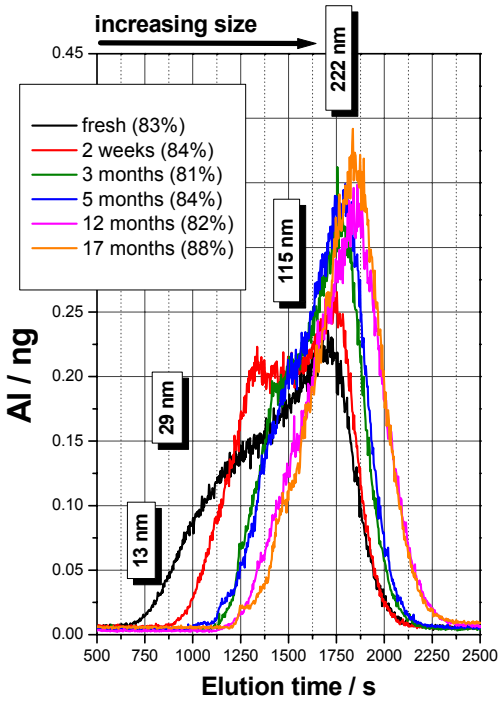

Fig. 5: Evolution of the size distribution of bentonite colloids in Grimsel groundwater with time up to 17 months; Al is taken as the indicator element for clay colloids; the colloids have been obtained after a initial Li-homo ionization and dilution in pure Grimsel groundwater to a final colloid concentration of 20 mg·L^{-1}; % values in brackets in the legend indicate colloid recovery after size fractionation; values on colloid size are obtained by calibration with reference polystyrene (latex) colloids.

The colloid recovery after fractionation is satisfactorily high and demonstrates the good performance of the method (appropriate FFFF-membrane and carrier solution).

Influence of humic acid

The reversibility of the radionuclide-colloid binding is one of the most critical parameters for the assessment of colloid relevance to radionuclide migration. According to an FFFF-ICP-MS study U(VI) does not sorb significantly to the clay colloids under the given conditions. Eu(III) and Th(IV) are completely colloid-borne, in agreement with previous in-situ studies [11]. The time-dependent desorption of Eu(III) and Th(IV) from colloids is studied by addition of humic acid (10 $mg \cdot L^{-1}$) as a competing ligand again by FFFF-ICP-MS. The different colloid types (humic acid and clay colloids) can be separated by this technique due to their different sizes (humic acid< 5 nm; clay colloids > 10 nm). The addition sequence of the metal ions to either humic acid first or bentonite colloid first was also varied. In the case of Eu(III), the results point to the establishment of an equilibrium in favor of the humic acid complexation. A clearly different behavior is stated for the Th(IV) desorption from bentonite colloids. A strong kinetic inhibition of the desorption reaction is found with no equilibrium being achieved after more than 1 year. This is illustrated in Fig. 6 which represents the Th(IV) fraction remaining clay colloid bound (open points) and the fraction desorbed by humic acid (full points) for different Th-colloid contact times prior to humic acid addition. The crosses represent the results of complementary ultrafiltration studies while the stars represent the Th-distribution in the system where all components have been mixed together simultaneously. This distribution does not vary with time and is thus taken as the equilibrium state lying quite close to the result of scoping calculations based on existing complexation constants.

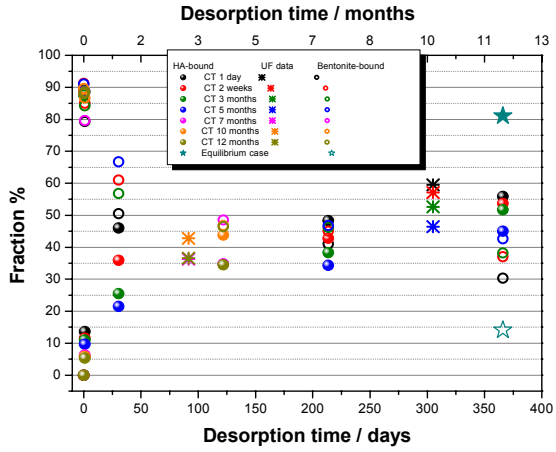

Fig. 6 Strongly kinetically hindered Th-desorption from bentonite colloids after humic acid addition followed for more than one year.

Complementary work to these first studies [12] are now underway to scrutinize the Th(IV) binding to the clay colloid surface. The question to be answered is whether new solid Th(IV) phases have formed at the colloid surface or whether the establishment of surface complexation equilibria is extremely slow for tetravalent actinide ions.

Conclusions

Clay colloids derived from a natural bentonite can dominate the aquatic speciation of tri- and tetravalent metal ions through surface sorption processes. Different to the trivalent metal ions, the tetravalent actinide ions reveal extremely slow desorption kinetics when bound to colloid surfaces. Underlying reasons are presently not understood. The strong kinetic hindrance of tetravalent actinide desorption from colloid surfaces may play an important role for the long range transport of those metal ions widely considered as immobile.

References

[1] J.I. Kim, Radiochim. Acta, 52/53, 71-81 (1991).
[2] W. Stumm, Colloids and Surfaces A, 73, 1-18 (1993).
[3] M.A. Kim, P.J. Panak, J.I. Yun, J.I. Kim, R. Klenze, K. Koehler, Colloids and Surfaces A 216, 97-108 (2003).
[4] P.J. Panak, M.A. Kim, J.I. Yun, J.I. Kim, Colloids and Surfaces A, 227, 93-103 (2003).
[5] M.A. Kim, P.J. Panak, J.I. Yun, A. Priemyshev, J.I. Kim, Colloids and Surfaces A, 254, 137-145 (2005).
[6] P.J. Panak, P. Loiseau, K. Dardenne, J. Rothe, M.A. Denecke, R. Klenze, M.A. Kim, J.I. Kim, Th. Fanghänel, ANKA/FZK Annual Report 2003, p. 51-52 (2003).
[7] T. Bundschuh, W. Hauser, J.I. Kim, R. Knopp, F.J. Scherbaum, Colloids and Surfaces A, 180, 285-293 (2001).
[8] T. Missana, U. Alonso, M.J. Turrero, J. Contam. Hydrol., 61, 17-31 (2002)
[9] Th. Schäfer, H. Geckeis, M. Bouby, Th. Fanghänel, Radiochim. Acta, 92, 731-737 (2004)
[10] M. V. Villar et al., FEBEX bentonite: origin, properties and fabrication of blocks, Enresa Technical report 05/98 Madrid, Spain (1998)
[11] H. Geckeis, T. Schäfer, W. Hauser, Th. Rabung, T. Missana, C. Degueldre, A. Möri, J. Eikenberg, Th. Fierz, W.R. Alexander, Radiochim. Acta, 92, 765-774, (2004)
[12] M. Bouby and al., Environ. Sci. Technol., in prep.

5. Applied Studies: Radionuclide retention in the multibarrier system

Studies reported in the present section are dedicated to the description of radionuclide behaviour in the multibarrier system of a repository. Radionuclide release from spent fuel and high-level waste glass is studied in leaching experiments under simulated repository near-field conditions. Previous experiments concentrated on radionuclide behaviour in saline groundwater typical to a rock-salt repository environment. These studies have been extended and the influence of clay rock porewater on spent fuel and glass corrosion was investigated in 2005. Near field chemistry is significantly influenced by the radiation emitted from the waste. Subject matter in this research field was the quantification of the interactive impact of radiolysis, H_2 evolution during container corrosion and presence of halogenide ions in the natural groundwater on spent fuel corrosion. Radionuclide migration in the repository far field under close to natural conditions was studied in underground rock laboratories. INE participates in experiments at the Äspö Hard rock laboratory, Sweden, and the Grimsel Test Site (GTS), Switzerland. Focus of both studies is laid on the behaviour of Redox sensitive radionuclides such as Tc and U in Äspö and the influence of colloids on radionuclide migration at the GTS. Beside inorganic colloids, colloidal humic matter is also known to influence radionuclide speciation and mobility. Recent investigations concentrated on model approaches to describe actinide complexation with humic acid, the application of microscopic techniques to identify heterogeneities of metal ion-humic acid binding states, the elucidation of Pu redox behaviour in presence of humic acid, and the characterization of clay bound organic matter as a potential source of mobile humic or fulvic acid in clay rock. The last two report contributions deal with the hydromechanical description of excavations in rock salt and concepts on how to prepare a geochemically based safety assessment for a repository in the Asse salt mine, Germany.

5.1 Determination of key processes influencing the near field source term for spent nuclear fuel and HLW glass

E. Bohnert, M. Kelm, B. Kienzler, A. Loida, B. Luckscheiter, V. Metz, N. Müller, M. Nesovic

Introduction

The geochemical environment in the near field, i.e. fluids and geomatrix, affects stability of radioactive waste forms, solubility of radionuclides and radionuclide retention. The fate of spent nuclear fuel, HLW glass and the associated release of radionuclides depend on thermodynamic constraints as well as on kinetics of corrosion of primary waste forms, leaching of radionuclides, and formation of secondary solid phases. The corrosion reactions change the geochemical environment (composition of groundwater and solid phases) in the near field, resulting in significant changes of radionuclide solubilities .

Radiolysis of groundwater is of high importance to spent fuel corrosion at least for the first ~10^4 years of the post closure phase. Aqueous solution in contact with spent nuclear fuel could radiolytically produce sufficient oxidants to convert the relatively stable UO_2(s) matrix into much more soluble U(VI) and thus promote radionuclide release. It is observed in several studies that hydrogen inhibits significantly the radiolytic decomposition of aqueous solution as well as corrosion of spent fuel. Still, there is little knowledge about the mechanisms of inhibition of radiolysis processes by hydrogen and the hydrogen effect on spent fuel corrosion.

In this section we report on our current research on key processes influencing the near field source term for spent nuclear fuel and HLW glass in a deep bedrock repository. Our research work focuses on the interaction of both waste forms with potential groundwater and geotechnical barrier materials. The aims of the present experimental studies are the following: 1) to measure the corrosion of a doped HLW glass simulate in synthetic argillaceous groundwater, 2) to determine the interaction of spent fuel with an argillaceous rock and 3) to determine the effect of dissolved hydrogen and dissolved bromide on the yield of γ-radiolysis products.

Long-term corrosion tests with the HLW glass GP WAK1 in two synthetic pore waters of Opalinus and a lower cretaceous (uKr) clay

The long-term corrosion behaviour of simulated and high-active waste glasses has been investigated by numerous corrosion tests in brines. Besides rock salt formations also granite and clay formations have been recently discussed in Germany as potential

repository host rocks. Most clay rock contains calcite as accessory component. The interstitial clay water is in chemical equilibrium with the calcite and could contain high carbonate concentrations. The presented corrosion experiments aim to reveal the effect of carbonate concentration on the glass corrosion and the release behaviour of rare earth elements and U.

Experiments are performed with the simulated HLW glass GP WAK1 in two synthetic argillaceous solutions both with and without $NaHCO_3$ (1.64 x 10^{-3} mol/L) and calcite (4 g/L) added to the solutions to demonstrate the effect CO_3^{2-}/HCO_3^- anions on the release of the various elements. The composition of the studied synthetic clay water is based on the composition of the pore solutions in Opalinus clay and an argillaceous Lower Cretaceous formation ("uKr" Konrad type solution) [2]. The tests are performed under Argon at 50°C and 90°C over 2 years at an S/V ratio of 5000 m^{-1}. In the meantime solution samples were taken after 14, 60, 130 and 365 days and analysed by ICP-MS and ICP-AES. Each reaction vessel contained a small glass disk to study the formation of alteration products. Further, an iron cube (carbon steel St37) was added to simulate the effect of canister material on the glass dissolution and to adjust more reducing conditions in the solutions. The alteration products on the glass disks are analysed by SEM-EDX.

The pH during glass corrosion in Opalinus clay water increased slowly from about 8.2 at the beginning to 8.6 after 365 days at both temperatures. In uKr water the initial pH was lower at 6.9 and 7.5 (at 90° and 50°C, respectively) and remained nearly constant with time. The lower pH in the $MgCl_2$-rich uKr water is explained by the formation of Mg-hydroxosilicates (clay-like minerals) [3]. Even though the tests were performed under Argon and in presence of Fe cubes, the conditions are slightly oxidising; the measured Eh(SHE) values ranged between +15 and +140 mV. Fig. 1 shows the normalised mass loss of various elements in Opalinus clay water at 90°C with (solid lines) and without (dashed lines) added $NaHCO_3$ and calcite after 14, 60, 130 and 365 days. The alkali elements Li and Cs as well as B, Sr and Mo show the highest normalised mass loss. The release of these elements is rather similar and increases slowly with time. After 130 days their concentration remains nearly constant and, accordingly, the glass corrosion rate is very low at about 5×10^{-4} $g\cdot m^{-2}\cdot d^{-1}$ between 130 and 365 days. Clearly lower is the mass loss of silica, Si has attained saturation concentration at about 75 mg L^{-1} (2.7 x 10^{-3} mol/L) Si after 14 days. Afterwards the Si concentration increases slowly up to 98 mg L^{-1} (3.5 x 10^{-3} mol/L) as the Ca and Mg concentrations in the solution decrease with time due to sorption and/or precipitation of Mg- and Ca-silicates, presumably. Lowest is the mass loss of Ce, U and Nd, after a strong increase up to 60 days their concentrations remain about constant. There are only small differences in the release behaviour of the diverse elements in solution with and without added $NaHCO_3$ and calcite. The release of Cs, Sr, Si and Mo (also of Li and B, not shown) is nearly identical in both solutions. In presence of carbonates the release of Ce, Nd and U is somewhat higher (factor 2). Obviously, carbonate ions have only a small effect on the release behaviour in Opalinus clay water.

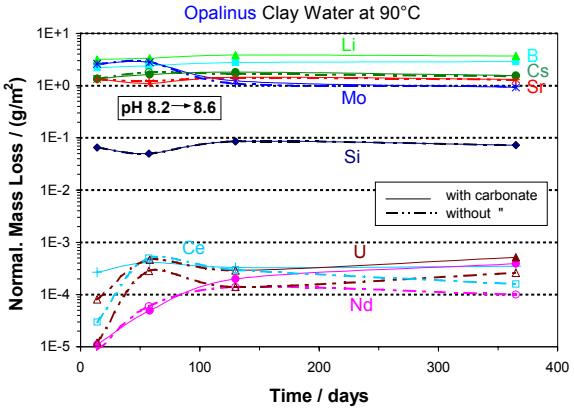

Fig. 1: Normalised mass loss of various elements in Opalinus water at 90°C and S/V = 5000 m^{-1} during corrosion of glass GP WAK1.

Compared to Opalinus clay water, the Si concentration and the Mo release is clearly lower in uKr water. The lower Si concentration results from the high $MgCl_2$ concentration [4] in the uKr water. The lower release or concentration of Mo can be explained by the lower pH in uKr water. The solubility of molybdates, e.g. $CaMoO_4$, is low between about pH 4 and 8. Above pH 8 the solubility of solid molybdate phases ($CaMoO_4$) increases strongly which explains the higher Mo concentration in Opalinus water at pH above 8. Because of the lower pH in uKr water, the release of B, Cs ,Sr and also U is higher by about a factor of 2 to 3 than in Opalinus water. The release of REE is similar in both pore water solutions and so are the corrosion rates after 130 days. The concentrations of Nd and U are rather low between about 1 and 3×10^{-7} mol/L at 90°C.

The small effect of carbonates added to the reaction vessels on the release of REE and U can be explained by the rather low carbonate concentrations in all solutions studied. The carbonate content in the solutions without

added calcite and $NaHCO_3$ may arise from the CO_3^{2-} content already existent in the water and/or the chemicals used for preparing the pore solutions. The alteration products on the glass chips in the reaction vessels were investigated after 130 and 365 days corrosion time by SEM/EDX. On most glass chips small tetragonal-pyramidal powellite ($CaMoO_4$) and needle-like baryte ($BaSO_4$) crystals were found. REE could not be detected in the powellite crystals. At 90°C in Opalinus and uKr water also agglomeration of fine-grained, clay-like particles were detected consisting of Mg-silicates, each containing up to 5% Ca and 7% Fe. Further, bar-like $CaSO_4$ crystals were observed, obviously precipitated from the Ca- and SO_4-rich solutions. In Opalinus water also newly formed rhombohedral calcite crystals were found.

Retention of Radionuclides in Compacted Bentonite Contacting High Burnup Spent Fuel

The Spanish FEBEX bentonite is frequently studied as representative for bentonite backfill material in a spent fuel repository. If radionuclides are released from the spent fuel package after contact with groundwater, it may be expected that they are retained by the bentonite backfill. In the framework of this study, the contribution of compacted bentonite blocks to the retention of radionuclides is studied. In order to determine the effect of bentonite alone, experiments were carried out without any added iron simulating the presence of container material.

A slice of 3.2 g high burnup spent fuel (K12a) was used for a 4.5 years-long immersion test in close contact with FEBEX bentonite. Another slice of 2.7 g from the same fuel was used for a comparative test in the absence of bentonite (K 20a). Before the test was started, the FEBEX powder was compressed by using a mechanical press equipment in order to form a pellet-like block of Ø 10 mm and a length of 10 mm, or 14 mm respectively. Afterwards, the spent fuel slice K12a was placed sandwich-like between both compacted bentonite blocks using a stainless steel immersion cell. This equipment assured close contact of the fuel slice with the bentonite pellets after closing the container. Access of solution to the bentonite is possible by passing through a 10 µm stainless steel pore filter on the top and the bottom of the immersion cell. The reaction cell containing the fuel slice contacting the bentonite pellet was immersed into 200 ml synthetic granite-bentonite groundwater using a 500 ml Ti/Pd lined stainless steel autoclave under initial Ar-atmosphere over 1629 days. The comparative test using fuel sample K20a and 200 ml of the same groundwater, but in the absence of bentonite was performed over 167 days. Details on the used spent fuel sample, FEBEX and groundwater are given in [5]. At the end of the immersion experiments, samples of the gas phase and the immersion solution were taken. The spent fuel slice and the compacted clay were recovered and prepared for radiochemical and mineralogical characterization.

Radiolysis of the groundwater took place as indicated by the formation of 2×10^{-8} mol (g HMxd)$^{-1}$ radiolytic hydrogen during this time. In the absence of bentonite encapsulation (comparative test K 20a), the radiolytic H_2 production was found to be 1×10^{-7} mol (g HMxd)$^{-1}$, although the reaction time was about 10 times shorter. The associated formation rate of radiolytic oxygen was found to be roughly 1×10^{-7} mol (g HMxd)$^{-1}$, which is, as expected, somewhat less than half of the H_2 production rate. The amount of oxygen in the presence of bentonite encapsulation was below the detection limit, which indicates most likely its consumption by oxidation processes of the fuel and by the bentonite. The release of the fractions of fission gases (Kr, Xe) into the free gas space, and the release of the fractions of Cs and Sr in presence of bentonite encapsulation into solution was relatively low in comparison to the experiments in absence of bentonite encapsulation, as shown in Fig. 2.

After 4.5 years contact time, concentrations of actinides and fission products were relatively low in the groundwater in contact with the bentonite spent fuel sandwich. pH remained about constant in this experiment, i.e. pH 8.6, due to buffering by the bentonite. The pH in the experiment without bentonite decreased to 6.2. In the presence of bentonite encapsulation, concentrations of dissolved Cs and Sr were at 5×10^{-7} and 3×10^{-8} M, respectively. Concentrations of dissolved Cs and Sr were about one order of magnitude higher (7×10^{-6} and 2×10^{-7} M, resp.) in the absence of bentonite encapsulation. In the presence of bentonite, concentrations of dissolved Am and Pu were below detection limit (10^{-10} M), while U increased to 4×10^{-8} M. Am, Pu and U concentrations were significantly higher (2×10^{-9}, 2×10^{-9} and 2×10^{-5} M, resp.) in the experiment without bentonite. The release of Kr/Xe (6,7 % of the fuel sample inventory) into the free gas space of the vessel was found to be significantly lower than during corrosion tests using the same fuel, but without bentonite encapsulation. Auto-radiography investigations of surfaces of the compacted bentonite pellets showed a uniform distribution of β/α-activity.

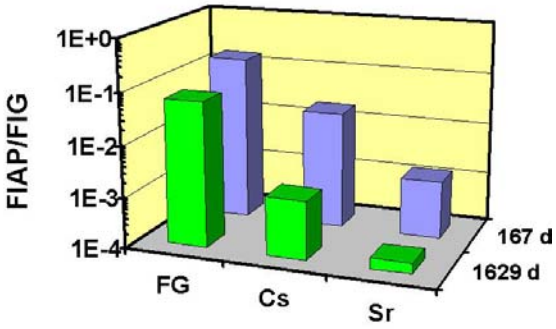

Fig. 2: Integrated release of fission gases (FG), Cs and Sr from studied spent fuel in the presence (1629 d) and in the absence of bentonite (167 d).

Effect of hydrogen and bromide on the yield of γ-radiolysis products

If spent nuclear fuel is disposed in a repository within a rock salt formation one considers the intrusion of brine to the waste as an accident scenario. Radiolytic decomposition of concentrated NaCl solution is accompanied by the formation of H_2 and O_2. These gases remain dissolved as long as the pressure built-up in a final disposal site (e.g. at a depth of up to 1000 m) does not exceed the hydrostatic pressure of about 10 MPa. H_2 overpressure has been reported to significantly inhibit spent fuel corrosion be radiolysis products [10]. Previous studies on γ-radiolysis in homogeneous salt brine have shown that radiation chemically active components such as Br^- compete with hydrogen for oxidative radiolytic products [6,7].

As a consequence the partial pressure of H_2 and O_2 can exceed 100 bar, and a reliable protective H_2 effect with respect to radiolytic solution decomposition and spent fuel corrosion may be reduced if not overridden. Still, there is a lack of experimental data to determine the radiation chemical reactions which control the competing effects of H_2 and Br^-.

In the present study, we measure radiolytic decomposition of 5.3 mol L^{-1} NaCl solution under γ-irradiation without any gas phase formation. The experiments are performed in autoclaves thermostated at 35°C. All autoclave components in contact with the solution are manufactured from a Ni-base alloy. Half of the autoclave volume (350 mL) is occupied by a bellow, which can be pressurized with Ar. During irradiation the bellow transfers a pressure of 250 MPa onto the solution, thereby forcing radiolysis gases to remain dissolved. Initial concentrations of dissolved of H_2 and Br^- vary between 0 – 10^{-2} mol L^{-1} and 0 – 10^{-3} mol L^{-1}, respectively. Solution pH is not adjusted and is close to neutral. Radiolysis of NaCl solution in the presence of non-doped UO_2(s) is investigated in two of the autoclave experiments. In these experiments an UO_2(s) pellet is mounted on an Al_2O_3(s) sample holder, which is placed in the middle of the NaCl solution. In addition to the autoclave experiments, radiolysis of NaCl solution with gas phase formation is studied in a closed glass vessel. 30 mL of 5.3 mol L^{-1} NaCl solution and a UO_2(s) pellet is given into a deaerated glass ampoule, leaving a headspeace of about six times the solution volume. Details on the pretreatment and characterization of the UO_2(s) samples (EC Reference Material #110; each pellet having a mass of 0.2 g) are given in [8]. Irradiation takes place in the GB77 ^{60}Co-source at the Institut für Oberflächenmodifizierung, Leipzig. The mean γ-dose rate in the autoclaves and the ampoule measured with a Fricke dosimeter varies between 350 – 560 Gy h^{-1}. During the autoclave experiments the irradiation is interrupted and the pressure on the bellow is released stepwise at varying time intervals. From the position signal of the bellow, the volume of radioysis gases released from the brine is calculated as well as the total amount of gases formed during the irradiation considering pressure, temperature and the gas solubility according to Henry's law. The ampoule experiment has been terminated and compositions of solution, gas phase and UO_2(s) pellet have been analyzed. Both autoclave experiments with UO_2(s) pellet are still running.

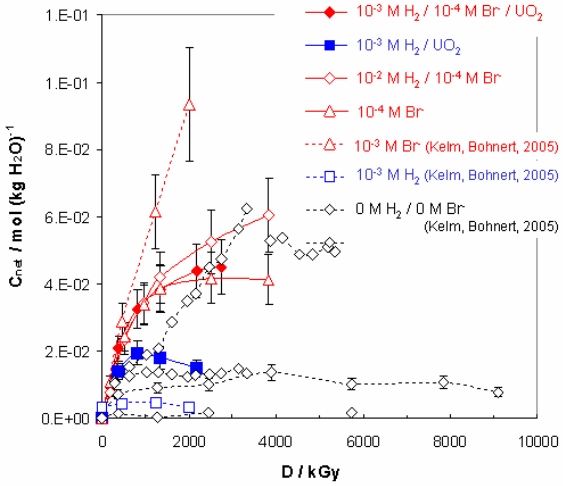

Fig. 3: Produced radiolysis gas concentrations (sum of dissolved H_2 and O_2) as function of applied γ-dose. Filled and closed symbols denote results of the present study and of [7], respectively.

The reaction progress in the brine is simulated using a kinetic reaction model [6] and the code

MACKSIMA-CHEMIST [9]. Presentation of the calculation results is out of scope of the present report.

Fig. 3 shows the total amount of dissolved gases (H_2 + O_2) as a function of applied γ-dose observed in the present autoclave experiments together with results takrn from [7]. The total gas concentration increases with increasing γ-dose until approaching a plateau, where net radiolysis production becomes zero within the experimental error. Experiments without Br^- approach zero net radiolysis at relatively low γ-dose values. In the experiments with 10^{-3} mol L^{-1} H_2 the total gas concentration is higher in the presence of the UO_2(s) pellet than in the experiment without UO_2(s). With the exception of the experiment with the highest Br^- concentration (10^{-3} mol L^{-1} Br^-, [7]), a plateau is achieved after a relatively high γ-dose and at significantly higher total gas concentrations as compared to the experiments in the absence of Br^-. Experimental results and MACKSIMA-CHEMIST simulations are in good agreement. The rate constant for the reaction

$H_2 + Cl^{\cdot} = H + H^+ + 2Cl^-$ $k = 4\times10^5$ L mol^{-1} s^{-1}

was estimated in [7] and is used in the current calculations. This rate constant is examined in an ongoing pulse radiolysis study. As predicted in the calculations, (a) total gas concentration increase with increasing Br-concentration and (b) total gas concentration is higher in the experiment with 10^{-4} mol L^{-1} Br^- and 10^{-2} mol L^{-1} H_2 than in the experiment with 10^{-4} mol L^{-1} Br^-. A similar radiolysis gas production is observed in the experiment with Br^-, H_2 and UO_2(s). Composition of the radiolysis gases of the ampoule experiment is dominated by H_2 (~71 mol%) and a minor contribution of O_2 (~29 mol%). Concentration of dissolved U increased to 5×10^{-7} M, which corresponds to the solubility of $UO_3{:}2H_2O$(cr) / $Na_2U_2O_7{:}H_2O$(s) at the studied solution composition.

Summary and conclusions

The long-term corrosion of the glass GP WAK1 in Opalinus clay and uKr water is rather slow and proceeds in a quite similar way in both test solutions. The small differences in the released amounts of various elements and in the release rates, being slightly higher in uKr than in Opalinus water, can be explained by the lower pH value (around 7) in uKr water as compared to that in Opalinus clay water (8.5). As the pH values in both solutions remain below 9, hydrolysis of the orthosilicic acid does not take place. Therefore, silica saturated conditions are attained within a few days and the Si concentration remains below 100 mg L^{-1}. The effect of carbonate added to the solutions is rather small. The carbonate concentrations remain very low between about 1×10^{-4} and 3.5×10^{-4} mol/L CO_3^{2-} at 90°C in all solutions studied. The corrosion behaviour of the HLW glass in the pore solutions resembles the behaviour found in pure water and NaCl-rich solution at corresponding temperatures. In all these solutions the pH remains between about 7 and 9 and it appears that the pH value determines mainly, besides the temperature, the glass corrosion behaviour.

The experiment on interaction of compacted bentonite in direct contact with spent fuel during immersion in granite groundwater show retention of actinides and fission products. Observed Cs, Sr and U concentrations indicate that the groundwater reached the fuel through the compacted bentonite and mobilized radionuclides from the UO_2(s) fuel matrix plus the instant release fraction out of the solids. However, solution concentrations of Am and Pu, which are below the detection limit, indicate their retention within the bentonite. Analyses of the spatial distribution of radionuclides within the bentonite block show clearly the ability of the bentonite to retain radionuclides, in particular Cs, Sr, U and Pu. Their amount encountered in the bentonite is observed to be at a factor of about one order of magnitude (Sr, Cs) and by a factor 20 - 50 (U) higher than in the surrounding groundwater (without contact to bentonite) used for the immersion of the reaction cell. No concentration gradient across the profile through the bentonite pellet is observed for Cs and Sr. In contrast, the level of Pu close to the contact area with the fuel is observed to be roughly 1.5 orders of magnitude higher than in the residual bentonite, whereas no pronounced concentration gradient is observed for U.

The results of the γ-radiolysis experiments in concentrated NaCl brine indicate that an H_2 inhibition effect on radiolysis gas production and on UO_2(s) corrosion is overridden by Br^-, even at an initial H_2 concentration being 100 times higher than the initial Br^- concentration. Measured U concentrations demonstrate that UO_2(s) corrosion in NaCl solution under γ-irradiation is controlled by the solubility of U(VI) rather than by an H_2 inhibition effect. The present observations are related to the competitive reactions of OH radicals with H_2, Cl^- and Br^-. The presence of UO_2(s) does not affect the radiolysis yield at the studied V/m ratio of 1.8 L g^{-1}. Since H_2 inhibition effect is considerably stronger in diluted aqueous solutions than in brines, it is not clear if the results of the present study are applicable to

groundwater with significantly lower Cl^- concentrations.

References

[1] V. Metz, B. Kienzler, W. Schüßler, J. Cont. Hydrol. 61, 2003, 265-279.

[2] B. Luckscheiter, B. Kienzler, D. Bosbach, Literaturstudie zum Korrosionsverhalten von HAW-Gläsern in Ton. Forschungszentrum Karlsruhe Wissenschaftl. Ber., FZKA 7064, 2004.

[3] A. Abdelouas, J.L. Crovisier, W. Lutze, B. Grambow, J.C. Dran, R. Müller, J. Nucl. Mater. 240, 1997, 100-111.

[4] B. Grambow, R. Müller, Mater. Res. Soc. Symp. Proc. 176, 1998, 229-240.

[5] A. Loida, Studies upon alteration of spent fuel in clay environment: Retention of radionuclides in compacted bentonite contacting high burnup spent fuel. NF-PRO deliverable 1.5.6., 2005, 12.

[6] M. Kelm, E. Bohnert, A kinetic model for the radiolysis of chloride brine, its sensitivity against model parameters and a comparison with experiments. Forschungszentrum Karlsruhe Wissenschaftl. Ber., FZKA 6977, 2004.

[7] M. Kelm, E. Bohnert, J. Nucl. Mater. 346, 2005, 1-4.

[8] E. Bohnert, M. Kelm, B. Kienzler, C. Marquardt, V. Metz, D. Schild, Flow-through studies on UO_2 dissolution as a result of alpha-radiolysis - experimental set-up and speciation analysis method. NF-PRO deliverable 1.5.5., 2006.

[9] M. B. Carver, D. V. Hanley, N. Ross, C. Austin, MACKSIMA-CHEMIST. Atomic Energy of Canada Ltd., Chalk River Nuclear Laboratories, AECL-6413, 1987.

[10] K. Spahiu, L. Werme, U. Eklund, Radiochim. Acta 88, 2000, 507.

5.2 Radionuclide retention in the Far Field

A. Bauer, H. Geckeis, W. Hauser, B. Kienzler, Chr. Marquardt, J. Römer, Th. Schäfer, D. Schild, Th. Rabung, P. Vejmelka

Introduction

Our studies focus on the migration behaviour of actinides and long-lived fission products in natural aquatic systems, and their reactions with representative geo-matrices. Studies are performed on radionuclide migration in sedimentary, clay/argillaceous and crystalline rock. Special attention is directed to natural inorganic and organic colloids, which can stabilize radionuclides in solution and facilitate their migration. For the parameterization of geochemical/transport models and to examine the transferability of laboratory results to natural conditions, radionuclide behavior is investigated under site specific conditions in underground laboratories. Field experiments are performed in underground research laboratories at Äspö (Sweden), at Grimsel (Switzerland), and are planned to be initiated at the Bure site (France) and in Mont Terri (Switzerland).

Actinide Migration Experiment at Äspö HRL

The following contribution presents the final part of a series of laboratory and in-situ migration experiments performed within a bilateral cooperation with SKB, Sweden, since 1998.

The objectives of the investigations performed by INE are focusing on the quantification of the retention of different actinide elements in single fractures of a granite host rock and the investigation of the sorption mechanisms. To guarantee undisturbed groundwater conditions, the experiments are designed to be compatible with the CHEMLAB 2 probe. The CHEMLAB probe contains of solution reservoirs, the experimental borecore and various pumps and tubings connecting the in situ groundwater reservoir with the fractured borecore. The effluent is fractionated and collected in an inert gas glove box for subsequent analysis (see ref. [1]). The experiments aim to show whether radionuclide retention coefficients measured in laboratory batch experiments can be applied to in-situ conditions and whether they will reduce the uncertainties in the present knowledge on the retardation behaviour of Am, Np and Pu, U and Tc.
An in-situ migration experiment with the CHEMLAB 2 probe was started in May 2004 and terminated in April 2005. In this in-situ experiment, HTO, ^{233}U and ^{99}Tc are used as tracers. The injected cocktail did not contain significant amounts of natural ^{238}U. The flow rates were in the range of 0.03 - 0.05 ml h^{-1}. In our previous annual report [1], breakthrough curves for HTO and ^{233}U were shown. Sharp spikes observed in the U tracer breakthrough curve occurred after temporary interruptions of the groundwater flow during the experiment. In Natural ^{238}U was also determined in the effluent. ^{238}U concentrations followed the ^{233}U tracer concentration (Fig. 1).
The simultaneous breakthrough of added tracer and natural uranium is surprising. Natural uranium in the natural granite is expected to exist in the tetravalent state. The U concentration in equilibrium with U(IV) phases, such as UO_2(am) lies in the range of $1 \cdot 10^{-9}$ mol·L^{-1} which is in good agreement with the measured concentration in the groundwater collected at the Äspö site. ^{238}U concentrations in the effluent of the experiments with core #7 were in the range $2\text{-}3 \cdot 10^{-7}$ mol·L^{-1} being a factor of 20 higher than the measured ^{233}U concentration which has been added to the groundwater in the hexavalent state.

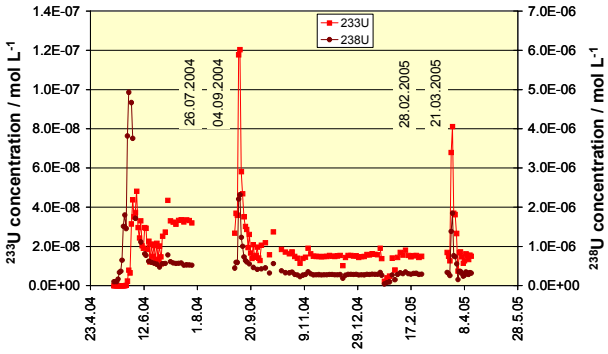

Fig. 1 Breakthrough of ^{233}U tracer and natural ^{238}U as function of time in the in-situ experiment with core #7.

The most reasonable explanation for the observed uranium breakthrough behaviour is that both uranium isotopes are present in the hexavalent redox state in solution and in the core#7 at least at the fracture surfaces being in contact with the groundwater. Oxidation of uranium in the core occurred very likely during drilling and storage. Another source for oxygen could be diffusion of air through the excavated disturbed zone into the groundwater bearing fracture. Redox measurements (flow through cell) at the Chemlab 2 drill hole confirm oxidising conditions in the groundwater

entering the CHEMLAB probe. A mean redox potential of E_h = +248 mV (SHE) was determined. The finding that the concentrations of both U-isotopes increase under stagnant groundwater conditions and immediately decrease when the flow is re-initiated points to the conclusion that U(VI) release is determined by out-diffusion from micro fractures within core#7.

After termination of the experiment, core #7 was transferred to FZK-INE, cut in slices and analysed with respect to the sorbed tracers. Fig. 2 shows the ^{99}Tc and ^{233}U distribution along core #7 as well as the distribution of natural uranium. In a distance of ~100 mm from injection, significant concentrations of natural U and sorbed ^{233}U tracer are found. Also the ^{99}Tc concentration is increased in this region.

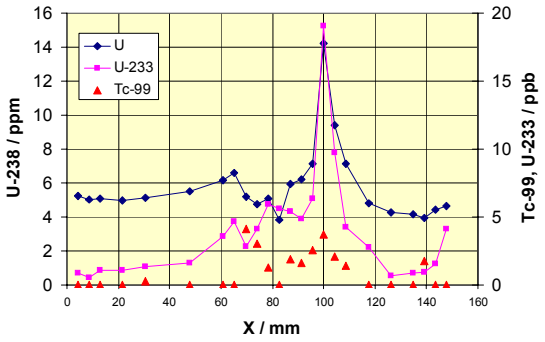

Fig. 2 Tracer concentrations determined by dissolution and ICP-MS measurements of the abraded material obtained by slice cutting of core #7.

The reason for this accumulation may be attributed to the quantity and composition of altered fracture materials or is due to the geometry of the fracture. Fig. 3 shows a SEM-EDX element mapping for the fracture zone of slice 23 (X = 100 mm, see Fig. 2) from core #7.

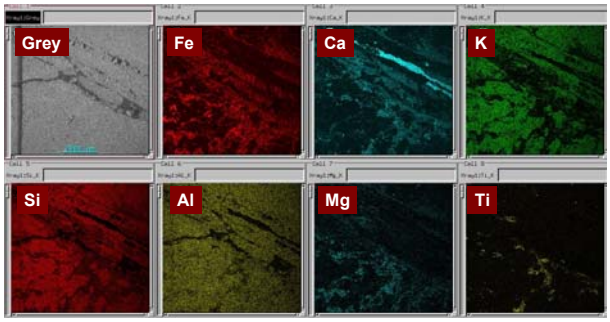

Fig. 3 Lateral element mapping of the fracture zone of slice 23 from core #7.

Areas with almost pure calcium phases exist which may is attributed to calcium carbonate. Grains of the rock matrix are identified to be composed of 15 % Al, 28 % K and ~55% Si in average. Grain boundaries contain mainly Fe and Ca. The fracture zone is characterized by a high Fe content of up to 15 atom % which is significantly higher than found in other slices (average values: 2-3 % Fe). Those mineral phases rich in Fe are assumed to be epidote and/or chlorite. The enrichment in Fe containing mineral phases in the area where U/Tc are accumuled suggests retention of both radioelements either by preferential adsorption to iron containing minerals or reduction and subsequent precipitation or sorption of reduced species by Fe(II).
Complementary experiments are performed on sorption of Tc and actinides onto well defined mineral constituents of granite and fracture filling material obtained from the Äspö Hard Rock Laboratory. α-autoradiography and XPS were applied to quantify sorption of individual elements. Main result of those studies is that reduction to low soluble tetravalent species by Fe(II) containing mineral phases is predominant for the sorption of Np(V). U sorption also correlates strongly with the occurrence of Fe oxide phases. Whether redox reactions are involved is not clear at the moment. Pu retention is in general significantly stronger than observed for Np(V) or U(VI). A correlation of Pu-sorption with specific mineral phases is, however, not found. Results and conclusions are reported in [1-2].

Colloid mediated actinide migration in fractured rock studied at the Grimsel Test Site (GTS)

A very controversially discussed issue which is now investigated for more than 20 years is the influence of colloids on radionuclide migration. Since 1984 it is known that groundwater colloids can interact with notably the polyvalent actinide ions and colloidal species can even dominate radionuclide speciation in groundwater [3]. A number of experiments revealed the ability of groundwater colloids to mobilise various radionuclides.
The aim of in-situ experiments performed at the Grimsel test site (GTS: underground hard rock laboratory in Switzerland, operated by the Swiss cooperation for nuclear waste disposal - NAGRA) was to study the role of inorganic clay colloids on the migration of different relevant actinides (Am(III), Th(IV), Pu(IV), Np(V), U(VI)) and fission products (Cs, Sr) in a water conducting fracture [4]. The groundwater chemistry of high pH=9.6 and low ionic strength (~10^{-3} mol/L) favours clay colloid stability very strongly. The Grimsel groundwater geochemistry represents so to speak ideal conditions for the colloid mediated radionuclide migration. At first sight the outcome of the in-situ studies at the GTS is in

agreement with the expectations: Tri- and tetravalent lanthanides/actinides and partly Cs (<1%) are found to migrate colloid borne over distances up to 5 m. Recoveries for the tri- and tetravalent actinides are quite high (70-90 %). Further in-situ and laboratory experiments, however, show a relationship between colloid recovery and residence time in the granite fracture (see Fig. 4).

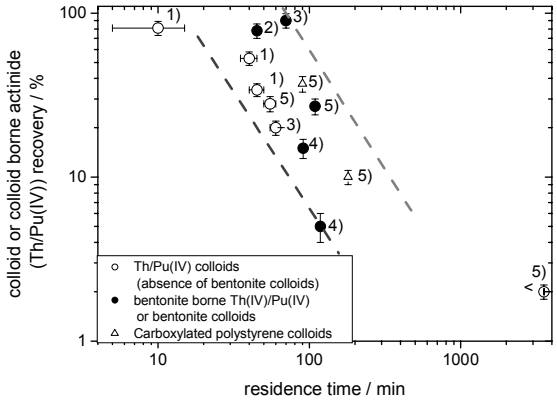

Fig. 4 Recovery of colloids or colloid-borne actinides depending on residence time in a granite fracture; Experiments are conducted with Th/Pu(IV) in Grimsel groundwater in presence and absence of bentonite clay colloids and with carboxylated polystyrene colloids under in-situ conditions at the GTS or in laboratory studies with bore-cores and groundwater from the GTS (data are taken from various refs. cited in [5])

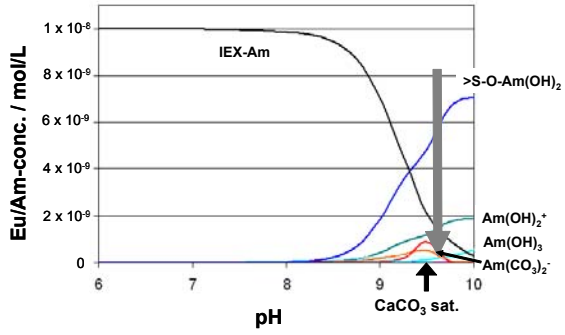

Fig. 5 Speciation of Am in Grimsel groundwater; 20 mg/L smectite colloids; pH~9.6; $I=10^{-3}$ mol/L; $pCO_2=3.5x10^{-6}$ bar; the solution becomes at pH≥9.5 saturated with regard to $CaCO_3$; carbonate concentration is then kept constant (small arrow); the large arrow indicates groundwater pH (9.6) (IEX-Am: Ion-exchange bound Am; >S-O-Am$(OH)_2$: inner-sphere surface complex).

The decreasing recoveries for colloid bound radionuclides and colloids with increasing residence time clearly point to a kinetically controlled radionuclide desorption from colloids and/or attachment of colloids to the rock/sediment surface. The application of the 2SPNE SC/CE surface sorption model [6] to simulate the Am speciation in Grimsel groundwater in presence of 20 mg/L smectite colloids gives the results shown in Fig. 5.

The calculation shows consistently with the experimental result that most of the Am (~ 75%) is colloid borne under given conditions at pH=9.6. The model predicts the formation of ~ 16% ion-exchange bound Am (IEX-Am) and 59 % >S-O-Am$(OH)_2$. In TRLFS studies with bentonite colloids dispersed in Grimsel groundwater and Cm as a fluorescent tracer simulating Am, a rather broad peak is observed being composed of the emission bands of at least two species [4]. The major Cm-fraction could be attributed to an inner-sphere complex at the colloid surface while the identification of the second species is more difficult. Previously, it was suggested that Cm in this fraction is bound to natural organic matter contained in the natural bentonite colloids (~0.5 mass %) [4]. Recent studies rather suggest the existence of hydrolysed Cm species bound to ion exchange sites in agreement with the speciation calculation. The consistent result of calculation and spectroscopic study shows that at least the trivalent actinide binding to colloids is a surface process which should be fully reversible. This explains the slow dissociation of colloid borne actinides found in batch and migration experiments [4].

Rapidly reversible radionuclide binding to colloid and sediment/rock surfaces allows the fast establishment of sorption equilibria and in general enhances radionuclide migration only slightly. It is emphasized that reactions leading to a kinetic inhibition of radionuclide desorption from colloids may enhance the relevance of colloid facilitated radionuclide migration significantly. Possible processes leading to strongly kinetically controlled radionuclide-colloid migration as e.g. actinide incorporation into the colloid structure (see e.g. P. Panak et al. in this report) are also conceivable.

A further issue that deserves care is the colloid interaction with natural rock/sediment surfaces. Many attempts to include colloid interaction with rock/sediment surfaces into PA calculations rely on the classical filtration theory, which is however known to fail very often for natural systems. As a consequence one may find then compelled to assume that no colloid retardation takes place for conservatism reasons. Experimental data shown in Fig.4 demonstrate that even under conditions strongly favouring colloid stability, as it is the case in Grimsel groundwater, colloid retention is observed. Processes leading to such observations are presently studied in more detail.

Actinide Diffusion Experiment in Natural Clay

Little information is available on the impact of the natural variability of samples on the diffusion properties. Variations in the mineralogical compositions, e.g. content of smectite and calcite are typical for natural clay. To support the basis for the up-scaling of laboratory derived data to model the radionuclide migration in the field, FZK-INE established an autoclave system for carrying out actinide diffusion experiments with Mont Terri and Callovo-Oxfordian claystones as a function of different mineralogical composition. First diffusion experiments have been started.

To counteract the swelling of clay in contact with groundwater and to simulate the confining stress in undisturbed clay-rock, a specifically adapted experimental set-up was development: A thin-walled stainless steel sample cell contains the cylindrical clay sample (∅ 20 mm, thickness 10 mm) and the tubing for wetting the clay from both sides. Tubing is as well used for tracer addition and sampling. The whole cell is placed in an autoclave where the confining pressure can be applied (Fig. 6). Due to the construction of the cell, the confining pressure acts isotropically onto the clay sample. The tubing for tracers and sampling are constructed in a way that they are kept under ambient pressure and tracer injection and sampling can be performed in closed circulation loops. This technique allows excluding advective transport processes. Specific attention is paid to avoid boundary effects (periphery flow) and to obtain homogeneous diffusion profiles. For diffusion experiments with actinides, an inert coating of the whole system will be applied. The experimental set-up was tested using an organic dye as tracer. A series of Opalinus clay samples (in total four) with varying mineral composition are mounted in the cells and autoclaves and have been installed in a glove box. The box is equipped with a pressure control system, pumps for tracer injection and sampling, reservoirs for spiked and unspiked groundwater and the liquid sampling systems.

Presently, the first set of samples is in the process of being saturated with solution. Tests with HTO tracers and actinides will be started soon.

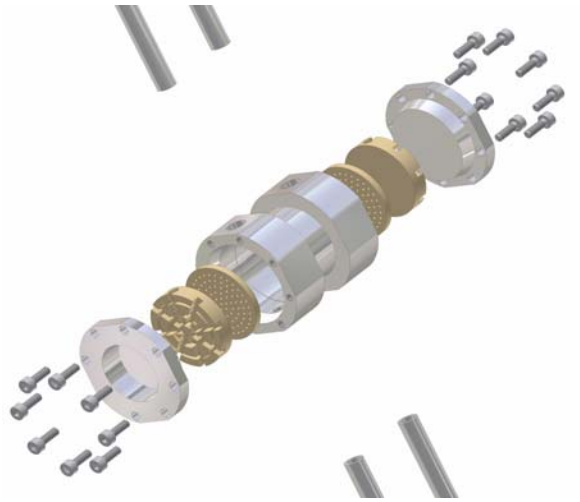

Fig. 6: FZK-INE diffusion cell to be inserted in an autoclave

Humic colloid mediated Pu migration

Over the last years laboratory experiments proved the humic colloid-borne actinide migration in the subsurface aquatic environment. Humic colloids were shown to play an important role in several interaction processes of metal ions in natural aquatic environments. A crucial factor in the migration behavior of several of the actinides is their redox sensitivity, e.g. for neptunium and plutonium [2,8].

Therefore, the mobility of the redox sensitive plutonium was studied by column experiments under near-natural conditions. A Pleistocene sand from the Gorleben region equilibrated with Gorleben groundwater (GoHy-532) was used in 50 x 10 cm columns. The contact time of Pu with the groundwater prior to the injection into the column and the migration time through the column were varied, as well as ^{14}C-labelled humic acid (GoHy-573HA) applied to monitor directly the humic colloid migration behaviour. Special efforts were made to determine reliable redox speciation for the different plutonium experiments.

Results with injected solutions containing Pu concentrations of 10^{-9} mol/L and Pu(III)/Pu(IV) ratios (10:90, 40:60) show the following qualitative trends [9]:

- Retardation factors slightly below 1 show the humic colloid-borne plutonium migration.
- Pu recovery is a function of contact time at high flow velocities; this effect appears to diminish at long residence times (v_{slow}).

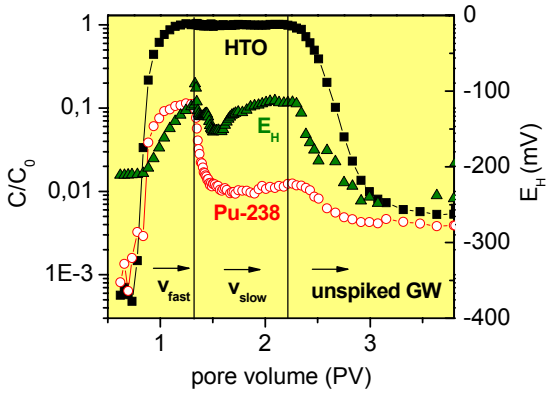

Fig. 7: Breakthrough curves of Tritium and Plutonium under variation of flow velocity. Additionally given is the in-line monitored redox potential (SHE) at the column outlet.

- Stop flow experiments show a dynamic equilibrium even at v_{slow} and sorption reversibility indicating a kinetically controlled interaction of the humic colloid-bound plutonium with the sediment. This can explain the observed higher absolute recoveries for Am(III) experiments (performed at very similar experimental conditions).
- At near natural flow velocities (~1.5 m/a) humic colloid associated Pu recovery is ~0.25%.
- Ultrafiltration shows a humic colloid size increase with Pu association even at trace concentrations (10^{-9} mol/L) fading out in the tailing of the breakthrough curve (lower metal load).

Future work will focus on Pu(III) migration experiments and higher Pu concentrations to combine the migration studies with speciation by capillary electrophoresis (CE).

References

[1] Kienzler, B.; Vejmelka, P.; Römer, J.; Schild, D.; Marquardt, C.; Schäfer, T.; Soballa, E.; Walschburger, C., Actinide migration experiment in the ÄSPÖ HRL in Sweden: results for uranium and technetium with core # 7. (Part IV). FZKA-7113 (Mai 2005)

[2] Kienzler, B.; Vejmelka, P.; Römer, J.; Schild, D.; Jannson, M., Conclusions from in-situ actinide migration experiments in ÄSPÖ HRL. Migration 2005, Avignon, September 18-23, 2005, Book of Abstracts S.39

[3] J.I. Kim, G. Buckau, F. Baumgärtner, H.C. Moon, D. Lux, in: McVay, G.L. (ed) Scientific Basis for Nuclear Waste Management VII, North-Holland, New York, 31-40 (1984)

[4] H. Geckeis, T. Schäfer, W. Hauser, Th. Rabung, T. Missana, C. Degueldre, A. Möri, J. Eikenberg, Th. Fierz, W.R. Alexander, Radiochim. Acta 92, 765-774 (2004)

[5] H. Geckeis, Mat. Res. Soc. Symp. Proc. (2006), in print

[6] M.H. Bradbury, B. Baeyens, Geochim. Cosmochim. Acta 69, 875–892 (2005)

[7] R. Artinger, Marquardt, C.M., Kim, J.I., Seibert, A., Trautmann, N. and Kratz, J.V., 2000. Radiochim. Acta, 88: 609-612.

[8] C. M. Marquardt, Seibert, A., Artinger, R., Denecke, M. A., Kuczewski, B., Schild, D. and Fanghanel, T., 2004. Radiochim. Acta, 92(9-11): 617-623.

[9] T. Schäfer, A. Seibert, C.M. Marquardt and Fanghänel, T., Environ. Sci. Technol. (in preparation)

5.3 Influence of natural organics

G. Buckau, C.M. Marquardt, Th. Schäfer, A. Seibert, A. Naber, M. Plaschke, J. Rothe, H. Hofmann, Th. Fanghänel*

Forschungszentrum Karlsruhe, Institut für Nukleare Entsorgung, Germany
** Universität Karlsruhe, Institut für Angewandte Physik, Karlsruhe, Germany*

Introduction

Humic substances (HS) are part of natural organic matter, i.e. naturally occurring organic substances with a comparably high residence times. Examples are peat, lignite and clay organic matter. HS are a class of organic compounds with a large number of similarities, for example in the aforementioned comparably long residence time/chemical stability. The elemental composition varies around $CHO_{0.5}$. A fraction of HS are called humic and fulvic acids (HA and FA), distinguished by the solubility behaviour. In some cases a third class is added, called humin, operationally defined as the part of organic matter that can be extracted by ethanol.

The proton exchanging functional groups of HA/FA are mainly carboxylic and phenolic with a total proton exchange capacity around 5 to 8 meq/g. One topic of considerable progress in the recent decade is the correct measurement of the molecular mass distribution. Contrary to previous ideas, the number weighted mass distributions of HA and FA are around 450 and 500, respectively ([1] cf. also below). Finally, HS have an inventory of redox sensitive functional groups and the redox state will reflect their physico-chemical environment. These redox sensitive functional groups are very important for reactions with redox sensitive actinide ions.

With respect to the geochemical behavior of actinides, dissolved and clay mineral/sediment bound natural organic matter may play a key role. In solution, actinide ion solubility is enhanced by complexation with HA/FA. These complexes are mobile due to charge repulsion between these complexes and the natural mineral surfaces. As shown by investigations at INE, natural organic matter/humic substances on natural mineral surfaces are generally strongly bound, partly by covalent bonds, and show a lower inventory of carboxylic groups. They can block mineral surface functional groups but can also add interacting functional groups through their own inventory of such groups. Based on these results, the frequently assumed dynamic exchange between dissolved and mineral bound humic substances will not take place.

There are still many open questions for adequate description of the overall influence of humic substances on the geochemical behavior of actinide ions and their mobility in deep groundwater systems. Some of these are discussed below, namely proper description of basic metal ion complexation properties, influence on the redox state of actinide ions and the characteristic properties, actinide interaction function of sediment bound natural organic matter and the existence of heterogeneities in metal ion binding in humic acid aggregates studies by microscopic techniques.

Basic description of complexation with radionuclides

Published description of metal ion complexation with humic and fulvic acids are mainly built on two basic approaches. For the application of the mass action law, the problem arising is definition of the total ligand concentration of HA/FA. For good reasons, the reacting functional groups are assumed to be carboxylic and phenolic groups. There is agreement on using the free ligand concentration as the total concentration minus the concentration of metal complexes. The free metal ion concentration is a directly measured value and is normally not subject to debate. One basic approach is based on measuring the maximum concentration of complex formed under given conditions and using this number to deduce the total HA/FA ligand concentration. The other basic approach defines a total ligand concentration function based on the content of ionized proton exchanging functional groups and the assumed influence of overall charge. Experimental data show that the ligand concentration is lower than the concentration of ionized functional groups (see Fig. 1). The resulting deficiencies in the application of the mass law by this second basic approach have been assigned to polyelectrolyte effects. The debate is still ongoing and in the concerned community, agreement is not yet achieved about the correct basic approach.

The development of these two basic approaches partly has historical reasons. For decades it was assumed that HA/FA are macromolecules with a large number of functional groups per molecule. For metal ion

humate interaction, this leads to models based on polyelectrolyte properties. More recently, the second basic approach also refers to this macromolecule properties by double layer charge as a key parameter varying with degree of protonation and metal ion complexation. Another reason for lack in agreement on the basic approach is that detailed investigations indicate more than one kinetic mode of the complexed metal ions and the possibility for enhanced complexation strength at very low degree of ligand saturation by metal ion complexation.

The mass action law can be approached from two sides, based on the same basic principle. The statistic approach is based on the mean distribution of reactants, the kinetic approach on the ratio of forward and backward reaction rates. In laboratory investigations where multi-charged metal ions are added to HA/FA solutions, followed by measurement of the dissociation kinetics, at least three relevant kinetic modes are identified. The two dominating ones have dissociation half-lives in the order of hours and days. They coexist in relatively comparable amounts (around each one half of the complex inventory). This leads to a distribution coefficient between the two different modes of about 2, or in logarithmic scale in the order of 0.3 units. In bulk investigations, thus they both fall within the error range and become averaged out.

The second basic approach rests on:
- A set of complexing functional groups, represented by average protonation constants and distribution widths,
- A set of complexation constants, and
- An electric double layer varying with the degree of protonation and metal ion complexation.

Problems are:
(i) Representation of proton exchanging functional groups by different distributions is not necessarily related to the metal ion complexation properties, especially where more than one functional group are involved.
(ii) Representation of proton exchanging functional groups by different average distributions does not regard neighboring effects,
(iii) The set of complexation constants is not based on unambiguous identification of the different complexes by, for example spectroscopic investigations, and
(iv) Since about the mid-nineties, mass spectroscopy, Overhauser NMR and careful assessment of diffusion based methods (GPC / HPLC and FFF) indicate that the number averaged mass distributions of HA/FA centers around about 500 and 450 mass units, respectively. Given this low mass, assumption of a significant electric double layer impact has no bearing.

The first basic approach leads to very simple straightforward results, with one bulk complexation constant per complexant (metal ions, including hydrolyzed ones), possibly with higher complexation constants at very low metal ion concentrations (cf. kinetic approach above). Until now, the main problem with this approach was that a thorough physico-chemical explanation for this ligand function was missing.

Under this umbrella, the measured maximum complex concentrations have either been used directly (complexation capacity) or they have been related to the inventory of proton exchanging (carboxylic) groups and normalized to the formal charge of the complexants ("charge neutralization model (CNM)"). The CNM is a post-treatment of the measured complexation capacities; justified by the assumption that HA and FA consist of macromolecules. The outcome in the sense of complexation constants, however, is the same as both approaches at the end use the measured maximum concentrations as the total HA/FA ligand concentrations.

Problems in accepting the CNM approach are related to:
(i) The post-treatment of the measured complexation capacities in the CNM is not unambiguous, and
(ii) Inconsistencies in the description of mixed/ternary complexes because the humate/fulvate ligand concentrations vary depending on the formation routes.

Recent analysis taking the complexation capacities, the protonation behavior and the number averaged mass distribution of HA and FA into account results in a different picture. In Fig. 1, the degree of protonation and the degree of complexation with Am^{3+} and UO_2^{2+} are shown for one humic acid (Gohy-573) as a function of pH. In the pH range from 3.3 to 6 both quantities show almost linear dependency with the same intercept at pH 2.5. A constant slope ratio of 3.4 is found between the concentrations of ionized groups and the maximum concentration of complexes formed. This shows that for both Am^{3+} or UO_2^{2+}, the humic acid ligand concentration decreases by one unit for protonation of an average of 3.4 ionized groups. Extrapolation to pH of 10.25, where all the proton exchanging groups are

ionized, gives a ligand concentration of 1.88 mmol/g. The inverse of this value is the average molecular mass of the ligands, and agrees well with the number averaged mass distribution (about 530 g/mol). This means that one ligand corresponds to one molecule. In addition, taking the number averaged mass distribution and the proton exchange capacity, the number of proton exchanging functional groups per molecule is calculated to be around 3.5.

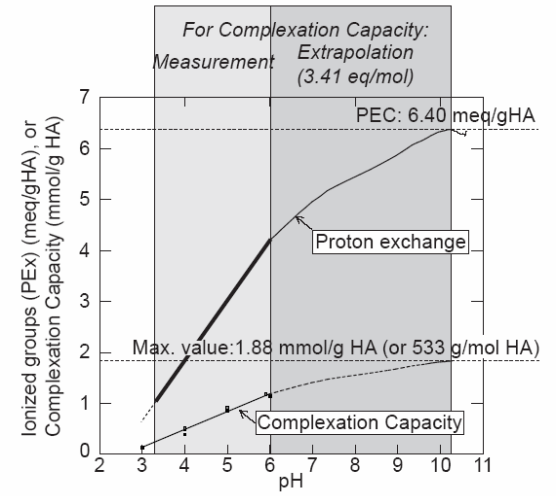

Fig. 1: Proton exchange function (upper curve, meq./g HA) as well as Am^{3+} and UO_2^{2+} complexation capacity (lower curve, mmol/g HA) with Gohy-573(HA) in 0.1 mol/L $NaClO_4$. The left shaded area shows the range where pH titration and complexation capacity measurements overlap. The right shaded area shows the range where the complexation capacity is extrapolated by the dependency to the protonation behavior as found in the overlapping range, i.e. 3.41 eq./mol. This number corresponds also to the number of proton exchanging groups per number weighted average humic acid molecule. The maximum complexation capacity at pH ≈ 10.25 (1.88 mmol/g HA) is equivalent to a molecular weight of 533 g/mol (the inverse value). This latter number agrees well with the number weighted average molecular mass of humic acid as measured by mass spectrometry.

This physico-chemical basis has been published by INE [1]. It provides the justification for the very simple approach to metal ion humate complexation. It also provides the basis for consistent evaluation of ternary complexes. Preliminary analysis of the ligand function with weaker complexing metal ions shows that not all molecules react but only a fraction of them. This again provides the required consistent description of the complexation reaction, coinciding with experimental observations that humic acid does not fully flocculate at ligand saturation with the weaker complexing NpO_2^+ ion. The reason is simply that this metal ion with its weaker complexation constant does not complex with part of the humic acid inventory.

In the next future, this approach will be used for continued analysis especially of mixed ternary complexes. Furthermore, in cooperation with European partners, interpretation of competition between metal ions will be analyzed.

Interaction of humic substances and hydroquinones with redox sensitive Actinide ions

Objective of these studies is to get insight into the redox interaction between humic substances and plutonium. Thermodynamic calculations are used for the description of the experimental results considering latest results of thermodynamic studies on plutonium redox chemistry including solid phases and colloids of tetravalent plutonium [2]. The output of the investigations will be thermodynamic parameters applicable for performance assessment (PA).

Hexavalent plutonium (PuO_2^{2+}) was added to a hydroquinone (H_2Q) solution at various pH values and 0.1 M $NaClO_4$ as background electrolyte. The final Pu and H_2Q concentration were typically $1\text{-}2\cdot10^{-4}$ M and $2\text{-}3\cdot10^{-3}$ eq/L, respectively, at seven pH values between pH 1 and 7. The reduction process has been followed by absorption spectroscopy and solvent extraction with BMBP [3] as chelating agent. In a first step the reduction of PuO_2^{2+} to pentavalent Pu (PuO_2^+) was studied. The reduction is fast and complete within less than one minute. To get the stoichiometry of the reaction a solution of $1\text{-}2\cdot10^{-4}$ M Pu(VI) was titrated with $1\cdot10^{-3}$ M H_2Q until all Pu(VI) is reduced. 2 mol of Pu(VI) are reduced at pH 3 by 1 mol hydroquinone that confirms the following redox reaction, where H_2Q stands for $C_6H_4(OH)_2$, and Q stands for $C_6H_4O_2$:

$$2\ PuO_2^{2+} + H_2Q \leftrightarrow 2\ PuO_2^{+} + Q^{2-} + 2\ H^{+}$$

This result coincides with observations made by Newton [4], who performed the experiment in 1 M $HClO_4$ solution.

The next step in the reaction sequence is the reduction of Pu(V) to lower oxidation states Pu(III) and (IV). Here, we have focused first on the rates and on the Pu oxidation state distribution. An excess of H_2Q was added to the solutions after the titration experiment and the evolution of the lower oxidation states were observed with time. Reaction rates for this step are much slower as Pu-oxygen bonds in the

plutonyl cations have to break first. The reduction is completed after about two months. Depending on the pH value, Pu(III) or Pu(IV) are the prevailing Pu oxidation states. Pu(III) is mainly formed at pH below 3, and Pu(IV) is dominating at pH values above 3. The results are illustrated in Fig. 2. In the upper part the absorption spectrum of Pu^{3+} is observed at pH 1 and 3. An increasing background appears in the spectrum at pH 3 due to generation of colloidal Pu(IV) and superposes the Pu(III) spectrum. Only the structureless background spectrum of colloidal Pu(IV) is observed at higher pH values, as shown in the lower graph of Fig. 2.

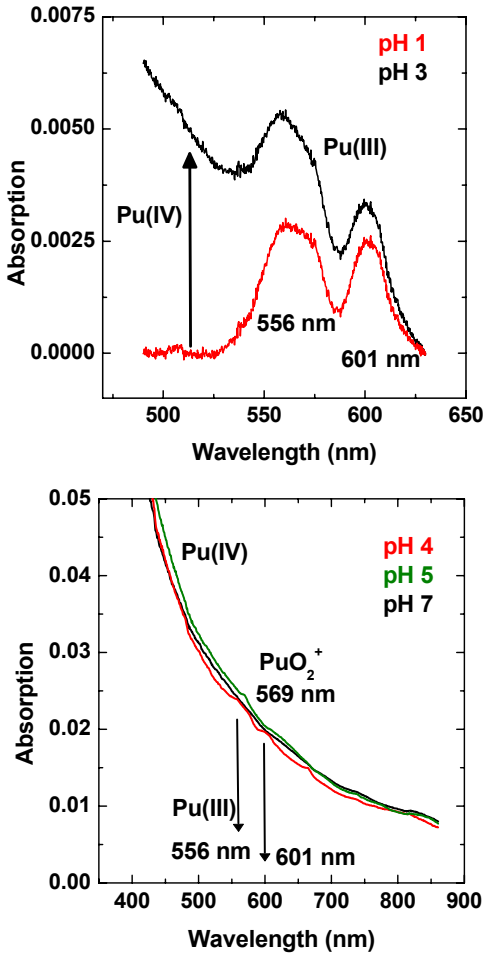

Fig.2: Absorption spectra of Pu, added as Pu(V), in hydroquinone solutions after a reaction time of 2 months. Upper figure: pH 1 and 3; lower figure: pH 4, 5, 7.

Similar experiments have been just recently performed with Pu and purified GoHy-532 fulvic acid. The results obtained so far show in agreement with the hydrochinone experiments, that Pu(VI) is reduced and the resulting Pu species are mainly Pu(III) or Pu(IV) depending on pH. Again, Pu(III) dominates in the acidic pH range, whereas Pu(IV) is the most stable oxidation state at near neutral pH.

From our results, we can conclude that Pu(V) and Pu(VI) are not relevant under anoxic conditions and in presence of hydroquinone bearing organic compounds. Hence, oxidized Pu species can be disregarded in PA considerations focusing on far field conditions. Under anaerobic conditions and at pH values relevant to natural aquifer systems (pH 5-9) mainly tetravalent Pu will exist in solution. It must be emphasized that this conclusion only applies to homogeneous solutions in absence of iron(II) species. In presence of iron(II) species and particularly in aquatic systems being in contact with minerals containing iron(II), the situation might be totally different and Pu(III) may become dominant. Furthermore, in aquifers containing organic compounds being more reductive than purified GoHy-573-FA, generation of trivalent Pu might be favored. This is the focus of future studies.

Characterization of natural organic matter

Synchrotron radiation based Scanning Transmission X-ray Microscopy (STXM) in conjunction with X-ray Absorption Near-Edge structure (XANES) spectroscopy and synchrotron-based Fourier transformed infrared spectromicroscopy has been proven to be a very powerful technique to characterize natural organic matter for several years. Beside the main focus of characterizing hydrophilic organic matter (i.e. humic and fulvic acids), the characterization of sedimentary immobile organic matter was started.

Clay-rich low-organic carbon formations (i.e. Callovo-Oxfordian argillite and Opalinus Clay) are considered as host rocks for radioactive waste disposal. Experimental studies have demonstrated that clay-associated organic carbon can have an impact on the chemical reactivity and complexation behavior of these clays [6,7]. For this reason, the nature of the clay organic carbon and the release of humic (HA) and fulvic acids (FA) like material of the undisturbed host rock were investigated. HA and FA were extracted using the standard International Humic Substance Society (IHSS) isolation procedure. Up to about 8% could be rapidly released (within about 24 h in alkaline medium) by this procedure. Synchrotron based (C-, K-, Ca-, O- and Fe-edge XANES) STXM and μFT-IR were used to identify the distribution of clay organic matter with different functionality. The data were evaluated by principal component and cluster analysis. In combination with target spectra analysis, also the origin of extractable HA (smectite rich regions) and FA (illite mixed layer mineral

regions) could be determined in a sample from Oxfordian argillite (447 m depth, borehole EST 104). FA influenced by marine origin (associated to illite) shows a size distribution different to that of terrestrial FA, and has a low content of chromophoric C functionalities. This characterization shows that especially in the Callovo-Oxfordian clay, original features of the organic matter, reflecting terrestrial and marine deposition around 150 Ma ago, are preserved in the HAs and FAs [8,9]. Furthermore, curium(III) is complexed by both isolated HAs and FAs. Differences in fluorescence behavior of complexed Cm(III) are probably related to the fluorescence quenching by Fe colloids. The complexation constants log (β) indicate a typical complexation behavior in comparison with FAs derived from brown coal [10]. Further characterization and complexation studies are planned or underway.

Beside the work in clay-rich formations, studies in the Gorleben aquifer system, overlaying a Permian salt dome, have been continued. Groundwaters in the system show a range of compositions, especially with respect to salt content and dissolved organic carbon (DOC) concentration. An uncertainty for safety analysis is the mobility of metal-complexing dissolved organic acids. Hence, isotopic data and carbon/sulfur K-edge XANES spectroscopy have been used to determine the mobility of fulvic acids (FAs). Isotopic data (^{13}C, ^{14}C, ^{3}H) show that FAs from the recharge zone are mobile over the entire depth, including the salt dome influenced brines.^{14}C and $\delta^{34}S$ (up to 34 per mill) analyses show furthermore that enhanced DOC (mainly HA and FA) concentrations originate from microbiologically mediated turnover of lignite intercalations in sandy Miocene sediments (‘‘in situ generation’’). XANES revealed that these in situ generated FAs have a high C_{arom}/C_{aliph} ratio (~2.8), and a decreased carboxyl/carbonyl content (less hydrophilic). A red shift in the C_{arom}=C_{arom} peak at 285.2eV indicates a heteroatomic substitution and aromatic ring distortion. These FAs also feature a highly reduced S content (~69%). Shallow recharge groundwater and deep brine derived FAs exhibit a similar C_{arom}/C_{aliph} ratio (1.1–1.4), indicating invariance in the backbone structure during long residence times and variations in geochemical conditions. C(1s) XANES data also suggest that only FAs with destabilized aromatic ring structures and hetero atomic substitutions are stable in the brines. Sulfur XANES revealed 43% reduced S in recharge FAs, whereas the channel brine FAs have a higher content of reduced S (61%) and additionally oxidized S mainly as sulfate. The oxidized S is assumed to originate from cap rock derived channel brine sulfate bound by esterification to the FA. Sulfur redox speciation therefore reflects geochemical conditions and reactions, and it reveals a high stability of reduced sulfur species in more aerobic channel brine environments. The high mobility of FAs over a range of groundwater conditions and residence times verifies the potential for dissolved humic substances to enhance radionuclide transport [10].

Further studies using carbon XANES and synchrotron- based FTIR-ATR spectroscopy focused on the influence of land use on the composition of humic substances (HA and FA) that are expected to be major DOC sources in recharge groundwater (e.g. Gorleben aquifer system). Investigations on samples of very well documented vegetation history over the last century [11] have shown a decrease of polysaccharides and increase of recalcitrant aromatic-C in the historical sequence between natural forests and cultivated fields. This result shows the impact of long-term anthropogenic activities on the composition and biogeochemical cycling of organic C in terrestrial ecosystems.

Synthesis of natural clay organic matter

The effect of clay minerals associated organic matter (OM) on the stability (dissolution behavior) of clays under high alkaline conditions has been a matter of research for several years. The chosen conditions are representative for the initial cement corrosion. Observed effects under these near-field conditions raise the question how the clay-OM association generally affects the reactivity and the radionuclide complexation behavior of clay minerals in the natural argillaceous host rocks. Investigations focus in a first step on the effect of clay mineralogy, of exchangeable cation composition (Na^{+}, Ca^{2+}, Fe^{3+}), and of temperature (25°C, 80°C) on the polymerization of OM. Aim of those studies were to simulate the generation of natural clay-OM compounds and to study their nature. The following OMs were regarded as starting compounds: catechol, glycine and glucose, glycine, synthetic OM, melanoidins or natural humic and fulvic acids. First results on the polymerization of glucose and glycine in presence of Na, Ca, Fe exchanged Ibeco bentonite at 25°C and 80°C were obtained by UV/VIS, µFTIR and STXM. An increase of polymerization with temperature was observed in presence and absence of smectite. Furthermore, the variation of exchangeable cation composition changes the degree of polymerization in the order Fe^{3+}>>Ca^{2+}>Na^{+}. Smaller clay size fractions (<0.1µm) showed the highest aromatic content indicating a

surface area catalyzed polymerization reaction. The results point to a catalytic effect of the mineral surface and the importance of cations at the mineral surfaces forming bridges to accumulating organic matter for the formation of aromatic structures and macromolecules. The polymerization reaction seems to be triggered in the first step by the OM sorption density, which is highest for Fe^{3+}-exchanged smectite. However, the results also indicate that the smectite associated synthetic OM polymers still have considerable higher oxygen containing functional group content in comparison to the clay mineral associated OM found in Opalinus Clay and Callovo-Oxfordian argillite.

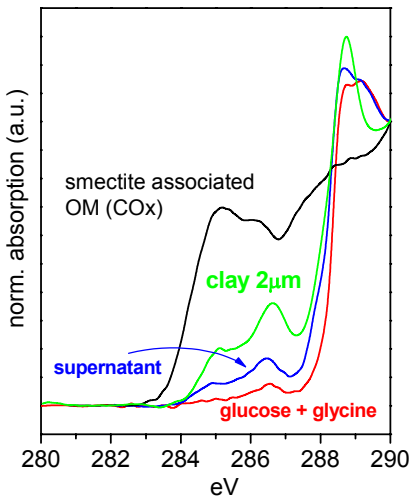

Fig. 3: Carbon XANES of glucose + glycine polymerization (80°C, 30 days) in absence of smectite (red) and in presence of Na-exchanged smectite, supernatant after centrifugation (blue) and 2µm smectite associated OM (green). For comparison a spectrum for smectite associated OM in Callovo-Oxfordian argillite from [8] is inserted.

Future work will focus on the questions (a) if the polymerized OM modifies clay reactivity in chemical disturbed systems and (b) how radionuclide complexation is influenced by the clay surface polymerized organics.

Scanning Transmission X-ray and Laser Scanning Luminescence Microscopy of the Carbon and Eu(III)-Distribution in Humic Acid Aggregates

The exact nature of metal ion binding to natural organic matter is still under investigation and unequivocal mechanistic understanding is still missing. Carboxylic and phenolic groups have been identified by spectroscopy as primary functional groups interacting with hard Lewis acids such as the polyvalent actinide and lanthanide ions. However, the heterogeneity of natural materials has been very often invoked to explain deviation from 'ideal' complexation behaviour of humic acid. The present study focuses on the question whether heterogeneities in the binding of Eu(III), taken as a chemical analogue to trivalent actinides, to humic mater can be visualized by appropriate techniques. Eu(III)-humic acid (HA) aggregates are investigated *in situ* by laser scanning luminescence microscopy (LSLM) and scanning transmission x-ray microscopy (STXM).

Methods

In this study STXM/NEXAFS investigations are performed at the STXM endstation (X-1A Outboard-STXM) at the National Synchrotron Light Source, Brookhaven, NY [12]. STXM at the carbon K-edge measures the absorption within a sample at soft X-ray energies. If the photon energy is changed across the carbon absorption edge the carbon distribution within the sample can be determined. C 1s-NEXAFS (Near Edge X-ray Absorption Fine Structure) provides direct speciation of carbon containing macromolecules from their characteristic 1s $\rightarrow$ π^*, σ^* resonances. As known from our previous STXM investigations, the aggregation of Aldrich HA induced by Eu(III) is accompanied by the segregation into zones with characteristic morphologies, different optical densities and distinct spectral signatures [13, 14]. In the NEXAFS of Eu(III)-HA a strong decrease of the C 1s (COOH) $\rightarrow$ $\pi^*_{C=O}$ transition (carboxylic peak) intensity and a new feature appearing at lower energy adjacent to the carboxylic peak are interpreted as a direct result of Eu(III) complexation [15, 16]. This interpretation is confirmed by similar spectroscopic trends observed for polyacrylic acid (PAA) acting as HA model compound [15]. Thus, if the segregation of Eu(III)-HA resulting in optically 'dense' and 'light' zones is indeed induced by Eu(III) complexation, an enrichment of Eu(III) may be expected in the dense zones of the organic microstructures. In order to measure the Eu(III) distribution in Eu(III)-HA, laser scanning luminescence microscopy (LSLM) is implemented. Since the luminescence yield of lanthanide ions is rather low compared to good fluorophores like organic dyes (less by a factor of ~10^5), advanced optical detection techniques are indispensable to map a distribution of submicrometer-sized Eu(III) containing colloids. We are using a home-build LSLM capable of sensing the fluorescence of a single organic molecule to image the Eu(III) distribution through its relatively intense $^5D_0 \rightarrow {}^7F_{1,2,4}$ emission lines in the spectral range of 580-710 nm [5]. For luminescence excitation a

frequency-doubled diode-laser is employed and tuned to the wavelength of the Eu(III) absorption line $^7F_0 \rightarrow {}^5L_6$. Results of the LSLM measurements are discussed in the context of previous STXM/C1 s-NEXAFS studies.

direct comparison of both microscopy techniques reveals that zones with high optical density in the STXM image correlate with high Eu(III) luminescence intensity (LSLM). Therefore, we conclude that Eu(III) is enriched in these zones. Fig. 5 shows the intensity line

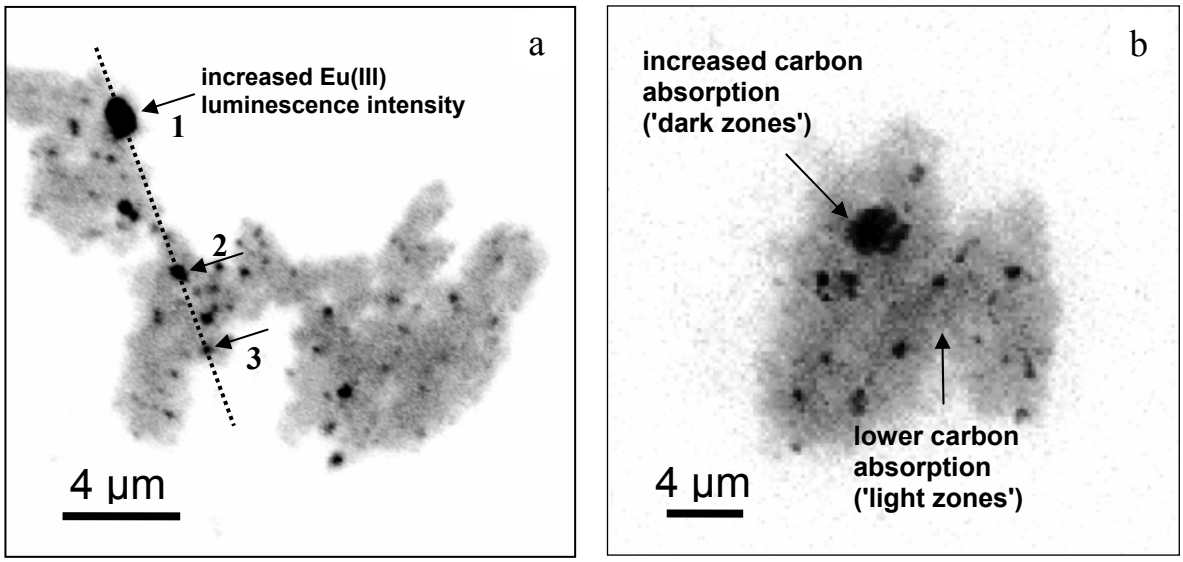

Fig. 4 Comparison of (**a)** Eu(III) luminescence intensity distribution in Eu(III)-HA by LSLM (excitation wavelength 393.5 nm, profile of the dashed line is plotted in Fig. 2, confined patches with increased Eu(III) luminescence intensity are marked with arrows) and (**b**) specific carbon absorption by STXM (recorded at 288.7 eV, image taken from Ref. [14]) of Eu(III)-HA aggregates; see text.

Results and Discussion

In Fig. 4 LSLM- and STXM-micrographs of Eu(III)-HA aggregates are compared. The contrast mechanism in these techniques is based on different physical processes, i.e., C K-edge absorption (STXM) vs. Eu(III) luminescence emission (LSLM). The finest discernable structures in the LSLM image (Fig. 4a) are in the range of 200 nm which is close to the diffraction limit. The smallest features in the STXM micrograph (Fig. 4b) are in the same size range, although STXM has the potential for higher image resolution. Fig. 4b represents the STXM absorption contrast image recorded at 288.7 eV (energy corresponding to the carboxyl transition peak). In the STXM image dark areas correlate with increasing optical density of the carbonaceous material. In previous investigations it has been shown that carboxyl groups are significantly enriched in the optically dense zones [15]. Fig. 4a depicts a LSLM image of these Eu(III)-HA aggregates. Dark areas correlate with increased Eu(III) luminescence intensity ($^5D_0 \rightarrow {}^7F_{1,2}$ transitions). Both microscopy techniques reveal similar aggregate morphologies, consisting of confined dark patches (with diameters ranging from 200 nm to 2 µm) embedded in a lighter matrix. The profile of the Eu(III) luminescence extracted along the dashed line in Fig. 1a. Most of these patches (e.g., areas 2 and 3 in Figs. 4a and 5) exhibit a three- to fourfold intensification of the Eu(III) luminescence compared with the surrounding matrix. This corresponds well to the three to four times higher carbon absorption detected for the dark zones compared with the light zones in Fig. 4b as reported in [15, 16]. However, there are also few zones with significantly higher Eu(III) luminescence intensity (e.g., area 1 in Figs. 4a and 5) and carbon absorption (Fig. 4b).

The very similar morphologies revealed by STXM and LSLM point to a segregation of HA into fractions with different metal ion affinities. Thus, the macroscopic properties attributed to HA – including cation loading capacities and complexation constants – are only averaged values. These values are not sufficient for a molecular understanding of the underlying processes. The future goal of our work is to implement time resolved LSLM. In combination with STXM we expect to gain additional insight into the metal ion binding mechanisms of the different HA fractions.

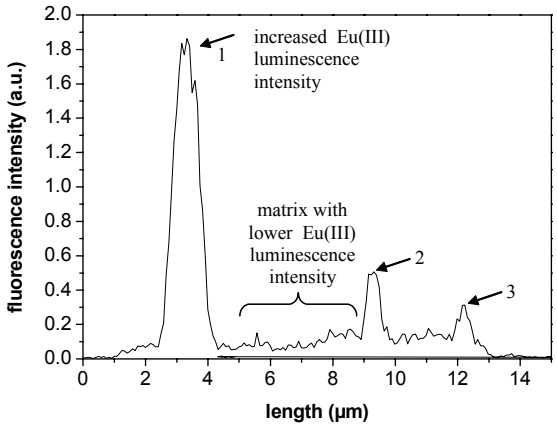

Fig. 5. Line profile of the luminescence intensity in Eu(III)-HA aggregates (dashed line in Fig. 2a; confined patches (1-3) with increased luminescence intensity are marked, see Fig. 1a and text).

Summary

C 1s-NEXAFS spectromicroscopy reveals optically dense zones rich in carboxyl groups surrounded by less absorbing material. The Eu(III) distribution within these zones is mapped by LSLM using laser excitation. In the LSLM micrographs confined patches with increased Eu(III) luminescence are shown to be embedded in a matrix of lower luminescence. The agreement of the morphologies revealed by both methods confirms the Eu(III) induced HA-segregation into fractions of varying chemical functionality and metal ion affinity.

References

[1] G. Buckau, 2005. Physico-Chemical interpretation of complexation/binding capacity or effective humate ligand concentration for An(III) and An(VI) humate complexation. In: E.A. Ghabbour and J. Davies (Editors), Humic Substances: Molecular Details and Applications in Land and Water Conservation. Taylor & Francis, New York, p. 153-165.

[2] V. Neck, M. Altmaier, Th. Fanghänel, , Solubility and Redox Reactions of PuO_2 x H_2O in the presence of oxygen, accepted and to be published in actinides2005 conference proceeding book by The Royal Society of Chemistry (RSC), 2005

[3] H. Nitsche, K. Roberts, R. Xi, T. Prussin, K. Becraft, I.A. Mahamid, H.B. Silber, S.A. Carpenter, R.C. Gatti, Radiochim. Acta, 66, 1994, 3

[4] T.W. Newton, T.W., J.Inorg.Nucl.Chem., 36, 1974, 639-643.

[5] J. Lehmann, Liang, B. Q., Solomon, D., Lerotic, M., Luizao, F., Kinyangi, J., Schäfer, T., Wirick, S. and Jacobsen, C., 2005, Global Biogeochemical Cycles, 19(1): GB1013.

[6] F. Claret, Bauer, A., Schäfer, T., Griffault, L. and Lanson, B., 2002. Clay Clay Min., 50(5): 633-646.

[7] A. Bauer, Rabung, T., Claret, F., Schäfer, T., Buckau, G. and Fanghänel, T., 2005. Appl. Clay Sci., 30: 1-10.

[8] T. Schäfer, Claret, F., Lerotic, M., Buckau, G., Rabung, Th., Bauer, A. and Jacobsen, C., 2005. Source identification and characterization of humic and fulvic acids from Oxfordian argillite and Opalinus Clay. In: E.A. Ghabbour and J. Davies (Editors), Humic Substances: Molecular Details and Applications in Land and Water Conservation. Taylor & Francis, New York, p. 43-62.

[9] F. Claret, Schäfer, T., Rabung, Th., Wolf, M., Bauer, A. and Buckau, G., 2005, Appl. Geochem., 20: 1158-1168.

[10] T. Schäfer, Buckau, G., Artinger, R., Kim, J.I., Geyer, S., Wolf, M., Bleam, W.F., Wirick, S. and Jacobsen, C., 2005, Org. Geochem., 36(4): 567-582.

[11] D. Solomon, Lehmann, J., Kinyangi, J., Liang, B. Q. and Schäfer, T., 2005, Soil Science Society of America Journal, 69(1): 107-119.

[12] C. Jacobsen, S. Williams, E. Anderson, M. T. Browne, C. J. Buckley, D. Kern, J. Kirz, M. Rivers, X. Zhang, Opt. Commun. 86 (1991) 351.

[13] M. Plaschke, J. Rothe, T. Schäfer, M.A. Denecke, K. Dardenne, S. Pompe, K.-H. Heise, Coll. Surf. A 197 (2002) 245.

[14] M. Plaschke, J. Rothe, M.A. Denecke, Th. Fanghänel, J. Electron Spectrosc. Relat. Phenom. 135 (2004) 53.

[15] M. Plaschke, J. Rothe, M. Altmaier, M.A. Denecke, Th. Fanghänel, J. Electron Spectrosc. Relat. Phenom. 148 (2005) 151.

[16] J.-M. Monsallier, F.J. Scherbaum, G. Buckau, J.I. Kim, M.U. Kumke, C.H. Specht, F.H. Frimmel, J. Photochem. Photobiol. A 138 (2001) 55.

5.4 Numerical simulation of the hydro-mechanical behaviour of rock salt around deep excavations

A. Pudewills

Introduction

The excavation of underground repositories leads to the perturbation of the initial lithostatic stress state in the rock mass around the openings, creating micro cracks and degrading the hydro-mechanical properties. For the long-term performance of a repository in rock salt, the evolution of the "Excavation Disturbed Zone" (EDZ) and the hydro-mechanical behavior of this zone represents important issues with respect to the integrity of the geological and technical barriers.

Within the framework of the integrated project NF-PRO funded by the EU, attention focuses on the modelling of hydro-mechanical processes in the near field of disposal drifts in salt and clay formations. In the period under review, a new material model for rock salt that is able to describe the damage of the rock has been implemented into the available finite-element codes. According to this model, the total strain rate is given as the sum of elastic and viscoplastic strain rates. The viscoplastic strain rate is divided into a part without volume changes of the material and a second one taking into account the volume changes due to the damage. In this case, the viscoplastic flow function depends on mean stress, deviatoric stress, and volumetric strain. A preliminary relationship between permeability and the dilatant volumetric strain is employed to calculate the hydraulic properties of the EDZ.

First, some relatively simple analyses of various laboratory transient-creep experiments were performed. In these tests, the volumetric strain (dilatancy) of the samples was measured. The calculations included the calibration of the model parameters and also a first validation of the model by a comparison of numerical results with experimental data from an independent test (i.e. data are not used for parameter fitting). The influence of different material parameters on the numerical results was studied as well. In a next step, the capability of the model to simulate the development of EDZ near a 37 years old gallery in rock salt [1] was studied. The numerical results were compared with in situ measured closure rates, stresses, and rock salt permeability.

Validation of the constitutive model

The applied viscoplastic material model for rock salt damage is based on the mathematical formulation proposed by Hein, 1991 [2] for granular materials such as crushed salt and was already implemented into finite element codes MAUS and ADINA. In order to verify this material model and to demonstrate the applicability of the model to describe the volumetric strain of rock salt, a number of different laboratory tests were investigated numerically.

For example, a transient creep test conducted on a rock salt sample from the WIPP site (Waste Isolation Pilot Plant, New Mexico, USA) [3] for which the volumetric creep strain rates are available was selected for the numerical studies.

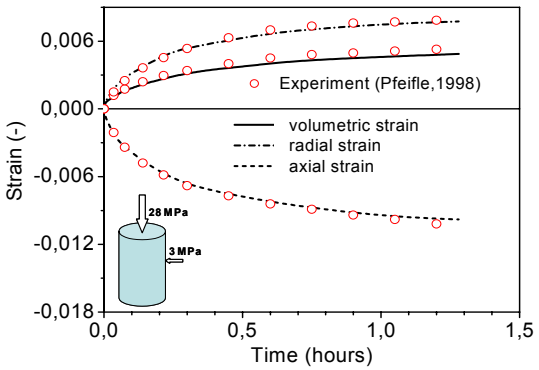

Fig. 1 Comparison between measured creep strains and calculation results

The cylindrical sample was subjected to an axial compression of 28 MPa and a lateral confining pressure of 3 MPa. The creep test lasted 1.2 hours. Figure 1 shows the calculated development of axial, radial, and volumetric strains compared with the experimental data. As evident from this figure, the calculation predicts the dilatant volumetric creep strain of the sample quite well. The calculated permeability values for the sample are in the ranges of in-situ permeabilities of rock salt measured in the near field of a large excavation in the Asse mine [4].

The influence of different material parameters on the numerical results was also analyzed. A detailed discussion of those results is presented in ref. [5].

Modelling of the EDZ around a gallery in rock salt

To illustrate the capability of the material model and the codes used, the long-term evolution of the EDZ around a 37 years old gallery in a rock salt formation was analyzed. The circular gallery with a radius of 1.5 m is located at 700 m depth from the surface in the Sondershausen salt mine. The convergence rates, the radial stress, and permeability distribution after 37 years were measured in situ and are given in reference [1].

To perform the numerical analyses a 2D model was used, assuming plane strain conditions. The radial convergences of the gallery calculated for three sets of model parameters are presented in Figure 2. The measured and calculated closure rates after 37 years are also given in this Figure.

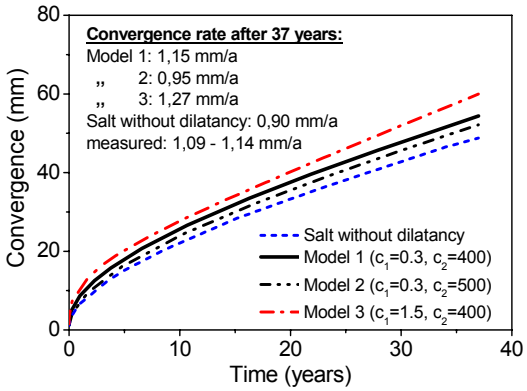

Fig. 2 Gallery convergence computed for different model parameters and the measured andcalculated closure rates 37 years after excavation

Two preliminary relations between permeability and the volumetric strain given in references [4] and [3] are used to calculate the permeability of the rock salt around the gallery. The comparison of the calculated permeability and in situ measured by [1] is presented in Figure 3. The numerical prediction of "Model 1" agrees quite well with the measurement near the gallery surface, but it seems to overestimate the permeability at a distance larger than 0.5 m.
The measured minimal stresses around the gallery and calculated minimal (radial) stresses are shown in Figure 4. The good agreement between the model calculation and the measured data confirms that the current model can predict stress distribution around the gallery with an acceptable accuracy.

Conclusions

A constitutive model for rock salt that permits to describe the development and evolution of the EDZ around the excavations has been implemented in the available numerical codes. Several laboratory experiments have been analyzed numerically to gain confidence into the proposed model.

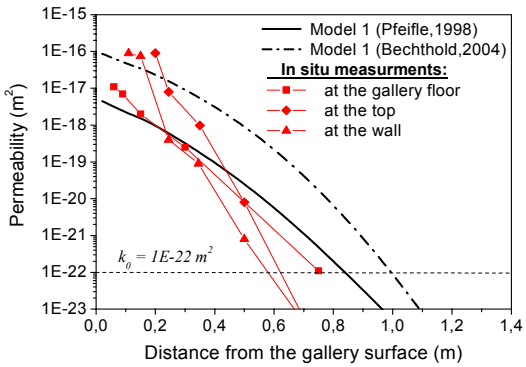

Fig. 3 Comparison of the calculated and measured permeability distribution 37 years after excavation

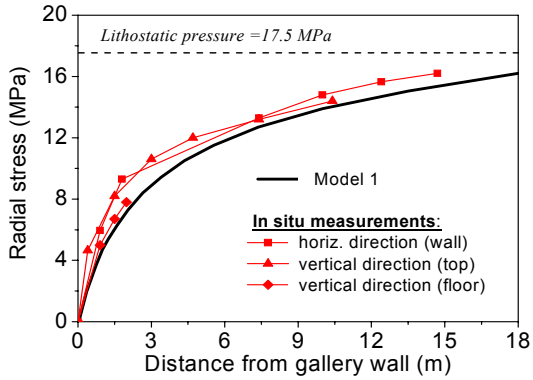

Fig. 4 Comparison of the calculated and measured permeability distribution 37 years after excavation

At the moment, the calibration of the model parameters is limited by the low number of reliable triaxial transient creep tests. Further numerical simulations of long-term creep tests will be required to perform an overall evaluation of the proposed constitutive model.

Nevertheless, the ability of this model to predict the damage zone around a gallery has been tested. The comparison of numerical results and in-situ measurements indicates that the implemented constitutive model with material parameters fitted to laboratory data works accurately and efficiently.

References

[1] F. Häfner, et al., Abschlußbericht zum BMBF- Forschungsvorhaben, IfBF der TU-Bergakademie Freiberg, 2001.
[2] H.J. Hein, Ein Stoffgesetz zur Beschreibung des thermomechanischen Verhaltens von Salzgranulat, Dissertation, RWTH Aachen, 1991.
[3] T.W. Pfeifle et al., Int. J. of Rock Mech. & Min. Sci., vol. 35: 4-5, Paper No. 42, Conference Ref.: USA-324-1, 1998.
[4] W. Bechthold, et al., Backfilling and sealing of underground repositories for radioactive waste in salt, (Bambus-II project), Final report, EUR-20621-EN, Brussels, 2004.
[5] A. Pudewills, Numerical Modelling of the long-term Evolution of EDZ: Development of material models, implementation in finite-element codes, and validation, FZKA-7185, 2005.

5.5 Geochemically based safety assessment

B. Kienzler, E. Korthaus, J. Lützenkirchen, V. Metz

Introduction

The main task of a geotechnical barrier system in a nuclear waste repository is to impede groundwater access to the nuclear waste. However, intrusion of groundwater into the disposal rooms cannot be excluded in the long term. In such a scenario, surrounding rocks, backfill materials, technical barriers and radioactive waste forms interact with the groundwater. Performance assessment (PA) and safety analysis for a radioactive waste repository need to consider the chemical properties of host rock, technical barrier materials, waste forms and intruding solutions. While conventional PA approaches mainly rely on reaction rates and transport processes, they often neglect the complex processes which influence the geochemical environment. Nevertheless, it is clear that chemical reactions affect the performance of all barriers and thus the release of radionuclides (RN), their sorption behaviour and the formation of secondary solid phases. To be able to deal with geochemical aspects in PA, the quasi closed system (QCS) approach was developed [1-4]. This concept can be used to determine source terms and to optimize thee barrier system in an underground repository.

Effective near-field barrier systems significantly reduce groundwater flow and equilibrium in the system can be achieved so that mobile concentrations of actinides will largely depend on the solubility of relevant solid phases, whereas concentrations of more soluble elements such as Cs, Sr or I are correlated with the degradation of the waste forms. Thermodynamic equilibrium calculations are related to redox conditions and solution composition in the system considered. Additional to pure solubility, sorption phenomena, aqueous complexation, (heterogeneous) redox reactions and the formation of colloids have to be taken into account for the determination of a RN source term. Release and migration of the dose determining actinides depend on their complex behaviour in the relevant geochemical environment of the multi-barrier system. Chemical interactions among the emplaced materials, i.e. non-radioactive compounds (such as metals, glass and cement from the waste forms and containers), backfill and sealing materials (such as bentonite, concrete or $MgO/Mg(OH)_2$-rich solids), the host rock and (potentially) intruding solutions ultimately control the geochemical environment and thereby the release or retention of RN. Aspects of the geochemically based safety assessment will be illustrated for the Asse salt mine.

Quasi-closed system approach

Many safety analyses neglect individual chemical reactions of RNs, which causes large uncertainties in performance assessment (PA). Variations of RN concentrations (solubilities) and sorption coefficients (Kd) due to variations of geochemical parameters such as pH, pCO_2 or redox conditions are not explicitly considered in PA codes. By application of the QCS approach, state of the art geochemistry can be included into PA: Data and results obtained in "closed" laboratory systems are applied to an "open" waste repository system for geological time scales.

The QCS, as considered for an emplacement cavern in rock salt, is schematically shown in Figure 1. A general prerequisite for the applicability of QCS is slow and limited mass transport (i.e. restricted exchange with the surrounding environment). This implies the achievement of a local thermodynamic equilibrium in an emplacement cavern or a section of a disposal gallery, respectively. Chemical processes can be sufficiently well described by thermodynamic equilibrium calculations, as long as the equilibrium state is achieved sufficiently fast compared to the rate of the exchange processes with the surrounding open system. Thus, the residence time of the solutions has to exceed by far the characteristic reaction time of the considered chemical processes

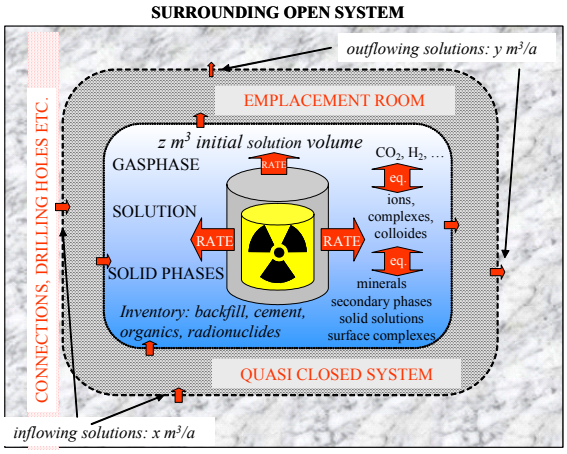

Fig. 1 Sketch of the QCS applied to an emplacement room in a LLW disposal.

To assess the applicability and the limitations of the QCS approach e.g. to an emplacement cavern, a certain exchange of fluids with the

surrounding environment is assumed. The assumed exchange may be approximated by detailed hydrodynamic models (based on the expected driving forces in the system such as rock-convergence and gas-production). The effects of the estimated extra fluid volumes, which react with the cavern inventories, are evaluated by geochemical calculations, in which the mass ratios of reactive components and volumes of solutions are varied.

Radioactive waste forms are generally not considered thermodynamically stable. Relevant reactions among solutes, gases and solid (including secondary) phases are included in the equilibrium calculations presented in the following, so that reliable results are obtained. The QCS approach is applicable to a constant ratio of solid mass to solution volume, as well as to changing mass to volume ratios. The latter condition is relevant to any repository in rock salt, because convergence processes result in squeezing-out of solutions and thereby increasing the mass to volume ratio.

To assess the applicability and the limitations of the QCS approach e.g. to a disposal room, a certain exchange of fluids from the surrounding environment is assumed. The overall exchange may be approximated by detailed hydrodynamic models (based on the expected driving forces in the system such as rock-convergence and gas-production). The effects of these calculated additional fluid volumes which react with the cavern inventories are evaluated by geochemical calculations. The calculations consider variations of mass ratios of reactive components and solution volumes. In the near-field of the radioactive wastes dissolution/precipitation and sorption processes occur simultaneously in the presence of solutions. Our proposed QCS approach includes the evaluation of RN solubilities and sorption processes.

Geochemical modeling tools: The QCS approach for source term evaluation applies geochemical models, which provide information on the expected compositions of solids, solutions and gases. For the present application, the high ionic strength of saturated salt solution systems requires a code for calculating the geochemical environment and the RN speciation including reaction path modelling under such conditions (e.g. EQ3/6 software package [5]).

Thermodynamic data base: Conclusions drawn from geochemical calculations depend on the quality of the input data. Besides the quantities of all relevant chemical components this includes the thermodynamic data required to calculate chemical equilibria. Consequently, for any geochemical assessment and also for the QCS approach reliable and consistent thermodynamic data are crucial

Thermodynamic data currently recommended by OECD/NEA rely on the “Specific Interaction Theory“ (SIT) for the calculation of activity coefficients [6]. However, the SIT is not applicable to describe saturated brine solutions. For the saturated salt solutions, which are relevant for the systems considered here, the Pitzer model is required [7, 8].

Parameters for this model are available for some relevant systems such as the extended Pitzer-Harvie-Møller-Weare data base (*Na-K-Mg-Ca-H-Cl-SO_4-OH-HCO_3-CO_3-CO_2-H_2O s*ystem) [9], but also for selected RN [10-14], heavy metals and other relevant elements. For systems including cement, aqueous silicate and aluminate species as well as additional solid phases had to be incorporated into the data base. The new data base was validated by comparison modelling to experimental results [15]. Assuming thermodynamic equilibrium between the solution and well defined solid phases (e.g. hydroxides), RN solubilities were calculate with the EQ3NR module of the EQ3/6 software package [5]. Solubility constants of actinides are taken from the NEA-TDB [16-18].

Application

The final closure of the Asse salt mine in Northern Germany is under preparation. Originally, the mine was excavated for rock salt and potash salt production. Subsequently, the mine was used to investigate and demonstrate the safe underground disposal for low and intermediate level radioactive waste. Until 1978, about 126000 drums of solidified waste forms were disposed off. The total radioactive inventory amounts to about 10^{15} Bq of fission and activation products (presently) and a significant amount of α-emitters (e.g. ~100 t U, ~87 t Th and ~12 kg Pu). The waste forms cover cemented $NaNO_3$-bearing concentrates from reprocessing, operational wastes and activated metals from LWRs, as well as scrap metal, demolition wastes and a variety of organic materials. Most of the wastes were solidified by cementation. Thus, about 30000 t of hardened Portland cement is present in the emplacement caverns.

Within the Asse salt dome soluble Mg salts are present in some areas close to emplacement caverns. Leaking of ca. 10 m^3 d^{-1} NaCl-rich brine into the mine is observed for several years now. The leaking is considered in the closure concept of the mine. It is expected that the NaCl-rich brine will get into contact with $MgCl_2$- and $MgSO_4$-rich salts. Dissolution of Mg salt bodies would have serious consequences for the mechanical stability of

the mine. Therefore, one option is to backfill the void space of the salt mine with $Mg(OH)_2$-rich material and deliberately flood the remaining pore volumes with $MgCl_2$–rich brine, which is in chemical equilibrium with both the relevant Mg salts and rock salt. Thus, $MgCl_2$-rich brine will be in contact with the disposed waste forms and chemical reactions among salt solutions and minerals, components of the waste matrix, backfill materials, technical barriers and the RN will occur. Cement corrosion is fast in terms of equilibration time. Degradation of organic waste components by microbes and under consumption of residual oxygen as well as nitrate and sulphate-rich waste components may result in production of carbonate species. These processes affect the geochemical environment and the RN source term and have to be evaluated. Within an ongoing project, the following items are quantified both by geochemical modelling and by various experimental approaches:

- Modeling of the geochemical environment and comparison with results obtained from laboratory studies and experiments performed at the 'waste product scale', i.e long-term leaching (> 20 years) of 200 dm^3 RN-doped cemented waste simulates in salt brines (including the evaluation of the kinetics of the relevant processes).
- Determination of thermodynamic data for modelling the actinide solubility in concentrated electrolyte systems and comparison to experimental data in the complex site-specific solutions.
- Selection and optimization of buffer materials to keep pH and the concentration of CO_3^{2-} within favourable ranges (low solubility of actinides by suppression of hydroxo / carbonato complexes and favouring strong retention of RN to the sorbing solid phases).
- Derivation of a robust source term for PA (specified for all emplacement caverns)
- Demonstration of the applicability of geo-chemical methods and evaluation of their reliability.

Results and Discussion

Geochemical environment: Experimental and modelling results show that in contact with Mg-rich brines, the geochemical milieu is mainly controlled by corrosion of cemented waste forms. The modelling results for cement corrosion in a relevant volume of $MgCl_2$-rich brine indicate that pH is buffered at values around 8.5 for cement/brine ratios, which are typical for the vast majority of the emplacement caverns. For those caverns containing cement/brine ratios above a certain limit, Mg^{2+} quantitatively precipitates as brucite and the pH increases to a value above 10. The reliability of these calculations is confirmed by the results of long-term leaching experiments at the waste product scale (Figure 2). A detailed description of the experimental study is out of scope of the present communication and will be given in a forthcoming publication.
The introduction of backfill materials into the emplacement caverns is supposed to provide compatibility and long-term stability with respect to the waste forms and minerals present in the emplacement caverns. The backfilling moreover should act as a buffer for pH and pCO_2 and lead to a minimization of actinide carbonate complexation.

Optimization of backfill materials: To select backfill/buffer materials and the required amounts a broad variety of potential backfill materials (Portland cement, crushed rock salt, clays, $Mg(OH)_2$-based backfill material, and mixtures of these materials) were considered. Geochemical modeling showed a $Mg(OH)_2$-$MgCl_2$-bearing gel to be the preferential backfill material for maintaining favourable geochemical conditions.

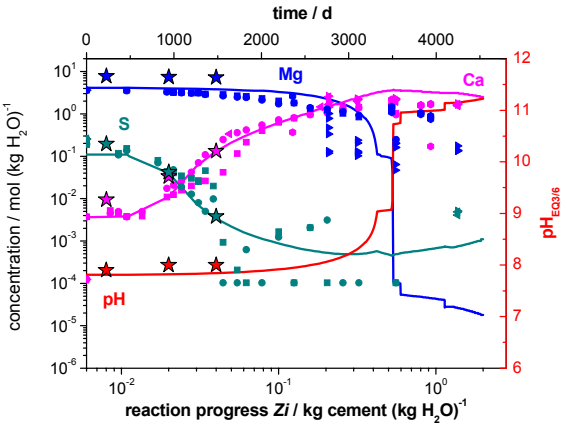

Fig. 2 Comparison of experimental results obtained by waste corrosion experiments performed at waste product (symbols) and laboratory (stars) scales with regard to pH and Ca^{2+}, Mg^{2+} and SO_4^{2-} concentrations with modeling results (lines).

If sufficient amounts of the $Mg(OH)_2$-$MgCl_2$-bearing gel are present in the emplacement caverns, pH will be buffered in an optimum range between 7 and 9 and dissolved inorganic carbon (which potentially forms due to the degradation of organic waste components) will be scavenged. The precipitation of solid carbonate phases and thus the effectiveness of this buffer-material in this respect was corroborated experimentally (see Fig. 3) [19].

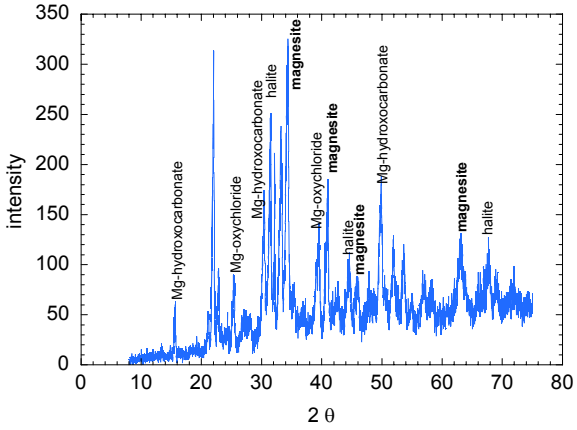

Fig. 3 X-ray diffraction results showing the formation of carbonate bearing solid phases

Using laboratory sorption experiments, the retention properties of the backfill material was further studied with respect to plutonium. In contact with the $Mg(OH)_2$-$MgCl_2$-bearing material the resulting concentration of tetravalent Pu in a carbonate containing system was by several orders of magnitude lower than in absence of the buffer material. Pu(IV) concentrations decreased due to both effects: Scavenging of carbonate and sorption of Pu onto $Mg(OH)_2$-bearing solid phases.

Retention of radionuclides: In the favourable pH range between 7 and 9 actinide solubility is expected to be low. Measured concentrations for uranium in waste product scale corrosion experiments agree well with preliminary calculations as shown in Figure 4.
However, concentrations of other elements (such as Np) may not necessarily be controlled by solubility. In the waste product scale leaching experiments, a Np concentration of $1 \cdot 10^{-10}$ mol dm^{-3} was measured after 9 years, which increased slightly to 4 to $8 \cdot 10^{-10}$ mol dm^{-3} over the following 5 years. The observed Np concentrations are more than one order of magnitude lower than predicted solubilities of known Np(V) and Np(IV) solid phases. The relatively low Np concentration can be explained by Np sorption onto solid phases such as cement corrosion products. Data from laboratory scale experiments in Np(V)/Mg-brine/cement systems (equilibrated for 200 days) exhibit a linear isotherm. Based on the sorption coefficient derived from these batch experiments, Np concentrations in the waste product scale experiment can be estimated ($1.3 \pm 0.3 \cdot 10^{-9}$ mol dm^{-3}). The estimated value is close to the one measured in the waste product scale experiment after 15 years. In this context it is important to note that solubility and sorption are usually difficult to distinguish from macroscopic measurements alone. However, using a solubility limit or a distribution coefficient makes a huge difference for PA. Therefore, it is essential to check for the underlying chemical mechanisms governing radionuclide retention.

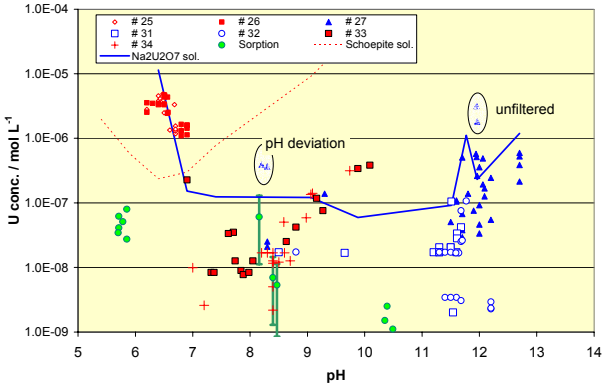

Fig. 4 Comparison of measured U concentrations in waste product scale experiments and preliminarily modelling results.

Robustness of the approach: The robustness of safety analyses depends on the reliability of the individual conceptual sub-models, such as the source term model. By applying the QCS approach to emplacement caverns of the Asse salt mine (based on the knowledge about inventories of chemically relevant constituents) it is shown that RN concentrations will vary in acceptable ranges, if

- pH is in the range $7 \leq pH \leq 9$,
- carbonate concentration $< 10^{-4}$ mol dm^{-3}.

If the exchange of solutions with the system surroundings is limited (as will be demonstrated in the following section) the overall geochemical conditions are expected to be robust and constant over long periods of time. Due to the filling of the void space of the salt mine with $MgCl_2$ brine, the compositions of the solutions inside and outside the emplacement caverns are quite similar. Therefore density driven transport processes are minimized and exchange of solutions will be predominantly driven by advective processes controlled by convergence and gas production.

Exchange of solutions: The geochemical environment calculated based on the QCS approach is the prerequisite for evaluating the effectiveness of the backfill material and the retention of RN in the emplacement caverns. If the extent of exchange of fluids between emplacement rooms and the environment is limited, the initial mass inventories of the major components remain constant in the long term within the system specific uncertainties. If significant exchange of solutions cannot be excluded, the resulting effects need to be

evaluated. In a first step, it has to be proven that the residence time of solutions exceeds the time period needed for approaching equilibrium between solution and solids, especially corroding waste forms [3]. The corrosion of cement in Mg-rich brines is expected to achieve equilibrium after about 15 years [15], whereas residence times of brines within the emplacement caverns are estimated to be in the order of hundreds to thousands of years.

As can be seen in Figure 2, ratios between masses of cement and solution (in units of kg cement (kg $H_2O)^{-1}$) may significantly affect the solution composition. Such changes will affect the radionuclide source term. For caverns having cement/brine ratios above a certain limit, high pH and high Ca-concentrations are expected. Such an emplacement cavern is used to demonstrate the effect of extensive fluid exchange. The effect of continuous exchange with $MgCl_2$-rich brine will finally change the solution's composition in the emplacement cavern completely; Ca will be removed quantitatively from the emplacement cavern. As an example, For such an example, Figure 5 shows that after the initial pore volume has been exchanged by three times with fresh $MgCl_2$-rich brine, about 50% of the total Ca inventory is removed. In Figure 5 the quantity of exchanged volumes of solution (V) is normalized to the initial pore volume V_i.

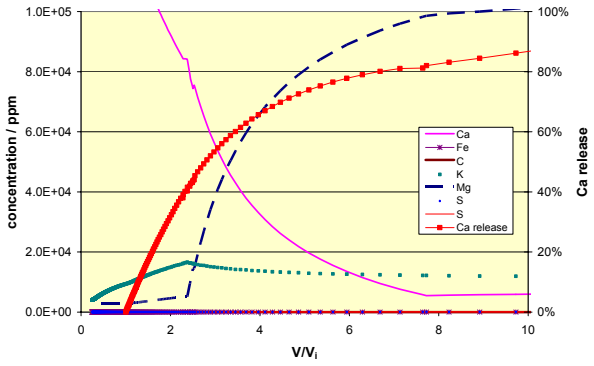

Fig. 5 Simulated concentrations of major ion concentrations and percentage of removed Ca as a function of relative solution exchange V/V_i for a given emplacement cavern.

As a consequence of this exchange process, the composition of the solid phases is changed considerably. Ca-rich corrosion products of the cemented waste forms are dissolved and are no longer available for sorption. Such calculations can be used to evaluate the degree of acceptable solution exchange for each emplacement cavern. In the present model calculations, intrusion of "fresh" $MgCl_2$-rich brine was considered. In reality, exchange is expected to take place between neighbouring emplacement caverns having similar inventories. As a consequence, expected changes are less significant compared to the results shown in Figure 5.

Summary and Conclusions

The presented model results are based on thermodynamic (equilibrium) concepts within a QCS approach. Application of the QCS approach to the studied system is justified because the residence time of solutions exceeds sufficiently the equilibration times for reactions between solutions and relevant solids in the emplacement rooms.

Geochemical modelling of a QCS supports PA by providing consistent solution compositions for equilibrium states, which are relevant for the long periods of time considered in PA. This includes a reliable pH and speciation of matrix components of the solution and gases as well as dissolved trace elements (radionuclides). The approach can also be used for evaluating the effect of exchange processes of gases and solutions with the environment. This is necessary since the exchange may influence the actual geochemical environment, which in turn affects radionuclide concentrations.

Application of QCS to specific host rocks may allow a definition of expected ranges for solution compositions. Thermodynamic data selected in various data bases do not cover highly concentrated salt solutions. For these solutions, only the Pitzer activity coefficient model is reliable. Required parameters for this model are available for some radionuclides and actinides, heavy metals and other relevant elements. Solubility products of well defined solid radionuclide phases are available. However, for many secondary solids, e.g. mixed-phases, solid solutions, or sorbed species, thermodynamic data are missing. Determination of these data requires detailed experimental investigations and process understanding on the molecular scale. As demonstrated in the present study, modelling results for both the geochemical environment and the behaviour of U and Np agreed well with experimental results of long-term leaching experiments of full-scale simulated waste products.

Application of the QCS approach suggests a robust closure concept for Asse salt mine: Backfilling with a $MgCl_2$-rich flooding solution in combination with a $Mg(OH)_2$-rich material yield long-term stability of the geochemical environment with favourable pH-values and sufficiently low carbonate concentrations resulting in low actinide concentrations.

Confidence in the results of PA by the authorities and the public is decisive. Comparison of computed results to

independently determined experimental data - especially from long-term experiments – creates confidence and demonstrates the applicability and the reliability of this geochemical approach.

Acknowledgement

This work is part of experimental studies and site-specific model calculations for the Asse research mine, FB Asse, GSF-Forschungszentrum für Umwelt und Gesundheit.

References

[1] R. Köster, G. Rudolph, Nucl. Techn. 96, 1991, 192.
[2] B. Kienzler, V. Metz, Status of source term modeling for radioactive wastes in Germany, presented at The International High-Level Radioactive Waste Management Conference, Las Vegas, 2001.
[3] V. Metz, W. Schüßler, B. Kienzler, T. Fanghänel, Radiochim. Acta, 92, 2004, 819.
[4] B. Kienzler, V. Metz, J. Lützenkirchen, E. Korthaus, T. Fanghänel, The quasi closed system approach: a geochemically based concept for performance assessment" presented at DisTec 2004, Internat.Conf. on Radioactive Waste Disposal, Berlin, April 26-28, 2004.
[5] T. J. Wolery, EQ3/6, A software package for geochemical modelingof aqueous systems: Package overview and installation guide (Version 7.0), UCRL-MA-110662 PT 1, 1992.
[6] L. Ciavatta, Ann. Chim. (Rome), 70, 1980, 551.
[7] K. S. Pitzer, in Activity coefficients in electrolyte solutions, vol. 2, R. M. Pytkowicz, Ed.: CRC Press, Boca Raton Fl., 1979, 157-208.
[8] K. S. Pitzer, Activity coefficients in electrolyte solutions, 2nd. ed. Boca Raton, Fl., USA: CRC Press, Inc., 1991.
[9] C. E. Harvie, N. Moller, J. H. Weare, Geochim. Cosmochim. Acta, 48, 1984, 723-751.
[10] T. Könnecke, V. Neck, T. Fanghänel, J. I. Kim, J. Sol. Chem., 26, 1997, 561.
[11] T. Fanghänel, V. Neck, J. I. Kim, Radiochim. Acta, 69, 1995, 169.
[12] T. Fanghänel, T. Könnecke, H. Weger, P. Paviet-Hartmann, V. Neck, J. I. Kim, J. Sol. Chem., 28, 1999 447.
[13] T. Fanghänel, V. Neck, Pure Appl. Chem., 74, 2002, 1895.
[14] V. Neck, J. I. Kim, Radiochim. Acta, 89, 2001, 1.
[15] B. Kienzler, P. Vejmelka, H.-J. Herbert, H. Meyer, C. Altenhein-Haese, Nucl. Techn., 129, 2000, 101.
[16] I. Grenthe, J. Fuger, R. J. M. Konings, R. J. Lemire, A. B. Muller, C. Nguyen-Trunc, H. Wanner, Chemical Thermodynamics of Uranium: North Holland Publisher, 1992.
[17] R. Guillaumont, T. Fanghänel, J. Fuger, I. Grenthe, V. Neck, D. A. Palmer, M. H. Rand, F. J. Mompean, M. Illemassene, C. Domenech Orti, K. Ben-Said, Update on the Chemical Thermodynamics of Uranium, Neptunium, Plutonium, Americium and Technetium: Elsevier Science, 2003.
[18] R. J. Silva, G. Bidoglio, M. H. Rand, P. B. Robouch, H. Wanner, I. Puigdomenech, Chemical Thermodynamics of Americium: Elsevier Publisher, 1995.
[19] V. Metz, W. Schüßler, P. Vejmelka, J. Lützenkirchen, B. Kienzler, Radionuclide source term for the Asse salt mine – geochemical assessment for the use of magnesium(II) based backfill material, presented at The 9th International Conference on Radioactive Waste Management and Environmental Remediation, Oxford, UK, 2003.

6. Development of speciation methods: Speciation of actinides at trace concentrations

The application of sensitive speciation techniques is crucial for the elucidation of radionuclide reactions on a molecular level. INE made a lot of efforts in the past and will continue this strategy in the future to further develop advanced tools for the characterization of radionuclide species. From 2005 on, INE operates an X-Ray beamline at the Karlsruhe synchrotron source ANKA where radioactive samples containing activities up to 10^6 times the limit of exemption can be analysed. Existing sensitive laser spectroscopic techniques are improved and new methods are introduced as e.g. the surface sensitive sum frequency vibrational spectroscopy. As colloidal radionuclide species still represent an uncertainty for nuclear waste performance assessment, respective analytical techniques as the laser-induced breakdown detection (LIBD) and the field flow fractionation (FFF) are applied and continuously developed. Theoretical methods as quantum chemical calculations start contributing to a more profound understanding of radionuclide binding states, provide complementary structural insight and help to interpret spectroscopic data. Applications to relevant INE research areas are reported for the first time.

6.1 The INE-Beamline for Actinide Research at ANKA

B. Brendebach, K. Dardenne, M.A. Denecke, J. Rothe

Introduction

INE has constructed and commissioned a beamline dedicated to actinide research [1] at the FZK synchrotron source ANKA. Official operation of the INE-Beamline commenced on October 1st, 2005. There is presently a growing demand for synchrotron facilities, where the infrastructure, safety equipment, and expertise are available for performing research on radioactive samples. One great advantage of the INE-Beamline is that the ANKA accelerator and INE's active laboratories are both located within the same FZK site. This symbiosis has numerous advantages including profiting from the existing infrastructure, backed by decades of know-how. Samples can be prepared, characterized, and analyzed using the spectroscopic, analytical, microscopic, and structural methods available at INE's active laboratories before being transported to ANKA and investigated using synchrotron based methods at the INE-Beamline. The time-span between sample preparation and experiment is relatively short, which allows investigations of dynamic systems within a time-frame of hours. The samples are also retrievable, so that sample characterization in INE laboratories following the experiments at the INE-Beamline is possible. In addition, hazards associated with transporting radioactive samples to and from INE and nearby ANKA are minimized and the administrative requirements associated with such transports simplified.

Beamline design considerations

Because actinide speciation associated with nuclear disposal concerns is manifold, the major aim in the INE-Beamline design was to ensure variability, i.e., provide a multi-purpose station, where a number of methods are possible, including standard, surface sensitive and spatially resolved methods.

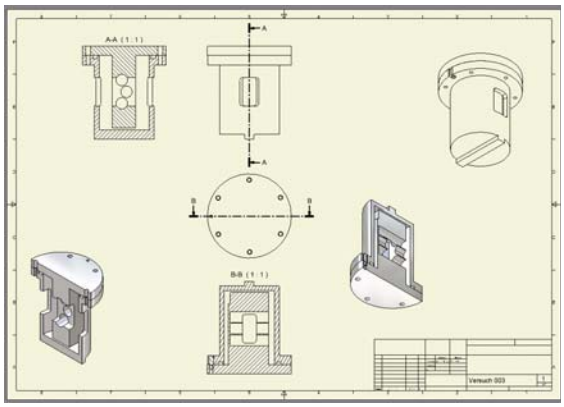

Fig. 1 Blue print of the standard transmission sample holder. Lid diameter = 90 mm. The design example is for wet paste or liquid samples sealed in 2 ml vials (design by G. Herrmann, INE workshop).

The design is optimized for spectroscopic X-ray methods, X-ray absorption fine structure (XAFS) and X-ray fluorescence (XRF). First tests of combined XAFS and X-ray diffraction (XRD) are planned for 2006. Because many reactions of actinides in the hydro- and geosphere are at interfaces and junctions, emphasis at the INE-Beamline is being placed

onsurface sensitive techniques based on grazing incidence (GI) geometry such as GI-XAFS, X-ray reflectivity and total external reflection X-ray fluorescence analysis (TXRF). In addition, a micro-focus option will be available after a planned future upgrade to offer spatially resolved measurements. This will allow chemical state imaging (μ-XAFS), elemental mapping (μ-XRF), and identification of phases (μ-XRD). The combination of X-ray methods with other techniques, e.g., laser based methods, will be possible at the beamline.

Investigation of samples with activities up to 10^6 times the limit of exemption of nuclides not suited as nuclear fuel are possible. This amount of activity allows experiments on samples containing, e.g., more than 25 mg long-lived nuclides 237-Np, 242-Pu, 243-Am, or 248-Cm. The necessary infrastructure and safety equipment is available at the INE-Beamline for active experiments. The experimental section of the radiation hutches is equipped with a special ventilation / filter system, specially sealed chicanes, easily decontaminated surfaces, and a personnel lock room with a hand-foot monitor for entry and exit. During the experiments, the samples themselves are contained within two independent levels of containment. A standard sample containment is available. However, the requirement of two independent levels of containment, without predetermined container geometry or specified types or designs, ensures highest flexibility. The sample primary containment depends on the sample properties (solid, liquid or wet paste) and the secondary containment is the sample holder itself. The first containment is typically a sealed sample cuvette, vial, or plastic bag. The second containment is a mechanically stable container having sealed windows for beam entrance, transmitted beam and fluorescent beam, into which a sample or a number of samples are mounted. The standard containment/sample holder for transmission experiments is shown in Fig. 1. The cylinder is placed onto a motorized stage allowing remote-controlled sample changing and positioning relative to the incident beam. The windows are made of low-Z material, e.g., Kapton® or polycarbonate. Special sample containers for non-standard geometries (e.g., for GI-XAFS) are available or can be easily adapted to the experimental requirements. A special protocol for working with radioactive samples at the INE-Beamline exists and must be adhered to.

Optics and experimental station

The INE-Beamline layout is given in Fig. 2. The INE-Beamline design is optimized for X-ray spectroscopic investigations using photon energies from the K-edge of S (2472 eV) to the Rh K-edge (23220 eV). This range covers key energy regions of interest for investigations of actinides (L3-edges ~16 – 20 keV) and lanthanides, as actinide homologues and for comparative studies (L-edges ~5.5 – 11 keV). The thickness of the Be window separating the beamline vacuum from the first mirror and ring vacuum is the determinant factor for the lower energy limit. Presently the Be window is 100 μm thick. The upper energy is limited by both the Rh coating on the mirrors and the characteristic energy of the ANKA ring. The monochromator at the INE-Beamline is a Lemonnier type double-crystal X-ray monochromator (DCM), built at the Universität Bonn, Physikalisches Institut. INE designed and constructed the DCM first crystal copper cooling block and second crystal piezo actuator adjustment for detuning and feedback control to maintain a constant content of

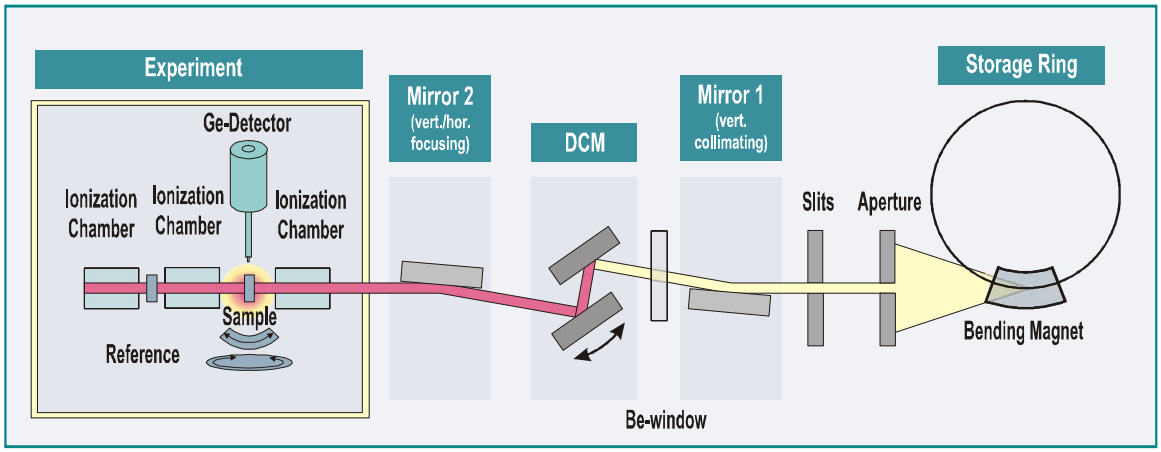

Fig. 2 INE-Beamline layout installed at ANKA port 3.2.5. The experimental hutch marked with a rectangular box is operated as controlled area, where experiments on radioactive samples are allowed.

harmonic radiation. The pressure inside the DCM vacuum housing is ~10^{-6} mbar and the housing is only 380 mm in diameter, allowing fast changes of crystals, without long pumping times. Four pairs of crystals are presently available, Si(111), Si(311), Ge(220), and Ge(422). The DCM can also accommodate multi-layer mirrors for wide energy band-pass experiments, e.g., for XRF analysis measurements requiring higher flux.

The INE-Beamline optics includes collimating and focusing Rh coated silicon mirrors for a sub-mm beam dimension at the sample position. The synchrotron radiation beam is vertically collimated through the cylindrical mirror (Mirror 1) up-stream from the DCM. Down-stream from the DCM, the beam is focused horizontally and vertically by a toroidal mirror (Mirror 2). Mirror 2 is suspended hanging so that the beam is reflected down from its surface, in order to allow studies of liquid films. The beam focus location is in the experimental hutch at a distance of ~24 m from the bending magnet source. There is a beam-shutter between the experimental and optics hutches so that work can be performed in the experimental hutch without having to turn off the beam in the optics hutch, thereby keeping optical elements under a constant heat load. The distance between Mirror 2 and the beam focus is as nearly the same distance from the source to Mirror 2, thereby minimizing source point image aberration. In order to enable spatially resolved studies with a µ-focused incident beam, an upgrade is planned to install an auxiliary µ-focusing optic such as a polycapillary, an elliptical monocapillary, or new planar compound refractive lenses (CRL) fabricated by the Institut für Mikrostrukturtechnik (IMT) at FZK [2]. The focal length of monocapillaries and CRLs can be a number of centimeters, which is an advantage for working with radioactive samples, where their containment limits the working distance between focusing optics and sample. Capillaries have the advantage for spectroscopy in that they are achromatic. No achromatic CRL is yet available, although design studies for achromatic planar CRLs are presently being conducted at IMT.

The optical tabletop in the experimental hutch is a 1.2 × 3 m^2 breadboard, large enough to accommodate almost any experimental set-up. Three ionization chambers (HASYLAB Design, "IONIKA") and a LEGe five pixel fluorescence detector (Canberra) are available for recording XAFS spectra in transmission and fluorescence mode. The grazing incidence equipment (HUBER Diffraktionstechnik GmbH) available at the beamline consists of two goniometer cradles with a common center of rotation (step-size = 0.0001°), a z-stage (step-size = 40 nm) and a rotation stage (step-size = 0.0001°), as well as two micrometer-adjustable vertical slits. The goniometer cradles are for adjusting the relative incident angle of the impinging beam onto the sample surface, the z-stage for vertical height adjustment, and the rotational stage for selecting the sample surface orientation relative to the synchrotron beam polarization vector during polarization dependent measurements. There is a special chamber available at the beamline for performing spectroscopy measurements at lower energies.

Beamtime request

The INE-Beamline and INE active laboratories are one of the pooled facilities of the EU European Network of Excellence for Actinide Science (ACTINET) and access to the beamline is possible via this avenue. A portion of annual beamtime at the INE-Beamline (30%) is available via the standard ANKA facility proposal procedure (for detailed information see [3]). ACTINET users are prompted to also submit a proposal to the ANKA facility for their beamtime. Experiments are also possible through cooperation with INE. INE-Beamline scientists are to be contacted prior to proposal submittal to ensure feasibility of any experiment involving radioactivity (contact persons can be found in [4]). INE provides a radiation protection officer during active measurements who is responsible for all radioactive substances.

XAFS investigations performed during the commissioning phase

The first transport of radioactive samples to the INE-Beamline and subsequent X-ray absorption measurements were performed with americium (243-Am) containing samples on February 17, 2005. Examples of on-going in-house research projects performed during the commissioning phase of the INE-Beamline include [5]:

XAFS investigation of the formation and structure of Zr(IV) colloids (first peer-reviewed report of a comprehensive sample series measured at the INE-Beamline [6]), XAFS investigation of Am(III) incorporation into secondary minerals calcite and iron oxy/hydroxide (HFO), interaction of U(VI) and Th(IV) with silica and aluminosilicate colloids, Pu L3-XAFS investigation of colloidal Pu(IV)-fulvate species, Am L3-EXAFS of Am(III) complexed with partitioning relevant ligands, and Cm L3-XAFS investigation of Cm(III) hydration in highly acidic aqueous solutions (Fig. 3).

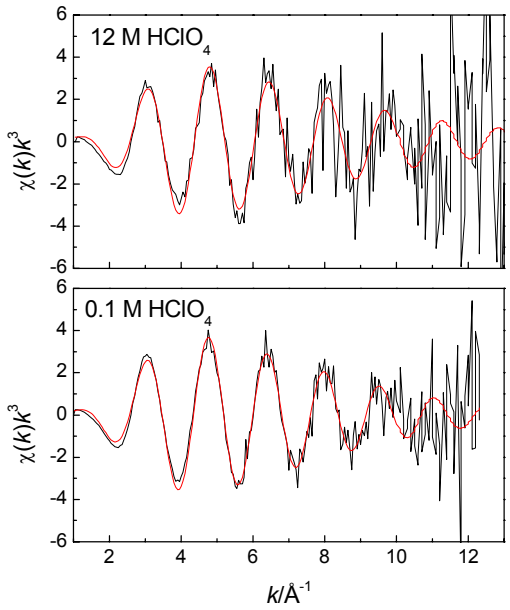

Fig. 3 Cm L3-EXAFS and least-squares fit results for the hydration shell of 10 mM Cm^{3+} in aqueous 12 M $HClO_4$ (top) and 0.1M $HClO_4$ (bottom).

Cooperations

The following groups have been involved in experiments at the INE-Beamline in 2005:

- Universität Bonn, Physikalisches Institut
- Universität Mainz, Kernchemie
- TU München, Radiochemie
- Institute for Transuranium Elements (ITU)
- FZK-INT, FZK-IMT, FZK-ISS
- CEA Cadarache (ACTINET User)
- Ecole Nationale Supérieure de Chimie de Paris (ENSCP), Applied Solid State Chemistry
- Institut de Recherches Subatomiques, Strasbourg
- PSI-LES, Villigen, Switzerland
- University of Manchester (ACTINET User)
- University of Cyprus, Department of Chemistry (ACTINET User)

Acknowledgements

Cooperation with FZK-ISS, especially the computing group headed by W. Mexner, is acknowledged with gratitude. Part of the beamline development is a contractual cooperation between FZK-INE and Universität Bonn, Physikalisches Institut.

References

[1] M.A. Denecke, J. Rothe, K. Dardenne, H. Blank, J. Hormes, Physika Scripta T115, 1001 (2005).
[2] V. Nazmov, E. Reznikova, A. Somogyi, J. Mohr, V. Saile, *Planar sets of cross X-ray refractive lenses from SU-8 polymer*, Proceedings of SPIE 5539, 235-242 (2004).
[3] http://ankaweb.fzk.de/
[4] http://ankaweb.fzk.de/instrumentation_at_anka/beamlines.php?id=9&field=7
[5] see ANKA Annual Report 2005 and projects reported herein for further details
[6] H.-R. Cho, C. Walther, J. Rothe, V. Neck, M.A. Denecke, K. Dardenne, T. Fanghänel, Anal. Bioanal. Chem. 383, 28-40 (2005).

6.2 Laser spectroscopy

S. Büchner, H.R. Cho, M. Flörsheimer, R. Götz, W. Hauser, R. Klenze, K. Kruse, P. Lindqvist-Reis, C. Walther

Introduction

The investigation of radionuclides at trace concentration level requires highly sensitive techniques tailored to the respective application. Since commercially available instruments very often cannot serve our purposes, a substantial part of the R&D program is devoted to methodological developments. In the following, recent advances of three spectroscopic methods which now are in routine use in the INE are presented.

Investigation of Cm^{3+}- groundstate splitting by Σ-Δ-excitation laser-fluorescence-excitation spectroscopy

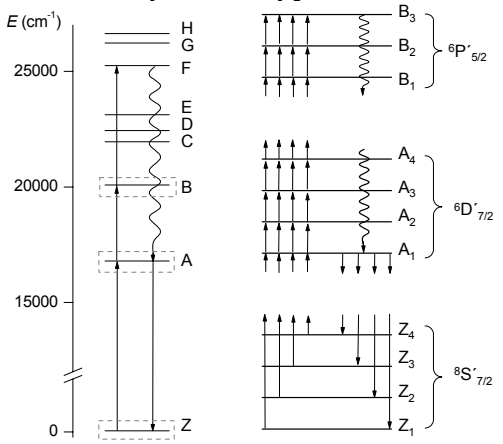

Fig. 1 Free ion energy levels of the Cm^{3+} $5f^7$ configuration (left) and crystal field splitting of the $^{8}\mathbf{S}'_{7/2}$ ground state ($Z_{1\text{-}4}$) and the two excited state levels $^{6}\mathbf{D}'_{7/2}$ ($A_{1\text{-}4}$) and $^{6}\mathbf{P}'_{5/2}$ ($B_{1\text{-}3}$).

Time-resolved laser-fluorescence-spectroscopy (TRLFS) is a powerful and widely used tool for probing the local chemical environment of various luminescent metal ions. Within the actinide series, Cm^{3+} is especially well suited for such studies due to high cross-sections, large band gaps and relatively simple spectroscopic structure of the f-intra band transitions. Excitation of the F- or G-level (Fig.1,left) causes a non-radiative relaxation to the $^{6}\mathbf{D}'_{7/2}$ state (A-band) followed by fluorescence emission to the $^{8}\mathbf{S}'_{7/2}$ ground state (Z-band). This approach combines the sensitivity of the $^{6}\mathbf{D}'_{7/2}$ state with respect to chemical surrounding (energy and lifetime) with the high absorption cross section of the F-band (analytical LOD ~$5 \cdot 10^{-12}$ M for $Cm^{3+}_{(aq)}$). The F-excitation is unspecific, i.e. if Cm^{3+} ions are present in more than one non-equivalent sites, the resulting emission signal comprises the superposition of all sites.

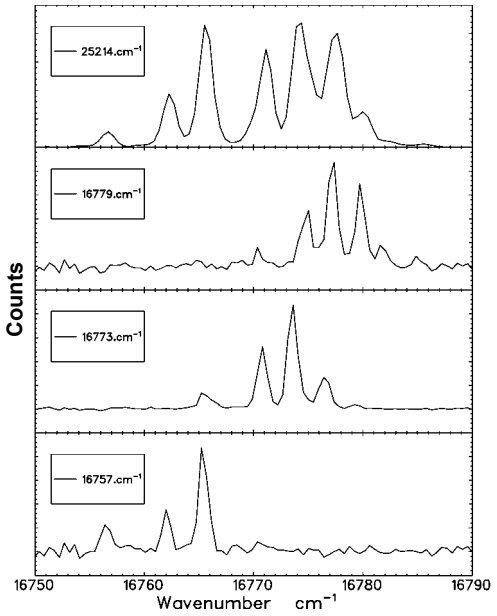

Fig. 2 $^{6}\mathbf{D}'_{7/2} \rightarrow {}^{8}\mathbf{S}'_{7/2}$ Emission spectra of $[Cm^{3+}:Y(H_2O)_9](BrO_3)_3$ at different excitation energies.

It is, however, possible to investigate only one site at a time by exciting directly from the $^{8}\mathbf{S}'_{7/2}$ ground-state (Z) to the $^{6}\mathbf{D}'_{7/2}$ state, and observing the emission of the $^{6}\mathbf{D}'_{7/2}$ state after a time delay appropriate for discrimination of the excitation light. This is illustrated in Fig.2 for $[Cm^{3+}:Y(H_2O)_9](BrO_3)_3$. Seven broad peaks with additional structure are observed after F-band excitation (top) at low temperature (10K).

A-band excitation at three selected energies (below) reveals three different emission spectra, each of which with four peaks, suggesting the presence of at least three non-equivalent sites. The peak width at A-band excitation is further reduced (spectrometer resolution 1.7 cm^{-1}), which clearly proves that the F-band spectrum is composed of even more non-resolved lines.

The four peaks of each individual site reflect the ground state splitting of the Cm^{3+} ion due to the crystal field of its host [1]. While this effect was studied extensively for different Cm^{3+}-doped unhydrous solids, no analog investigations on the electronic structure of Cm^{3+} in crystalline hydrates or solvates were reported, a surprising fact considering the significance of such basic knowledge on the

interpretation of TRLFS data. The crystal field caused by water as a ligand was assumed to be small and the ground state splitting of hydrated Cm^{3+} assumed to be of the order of 2 cm^{-1}[2].

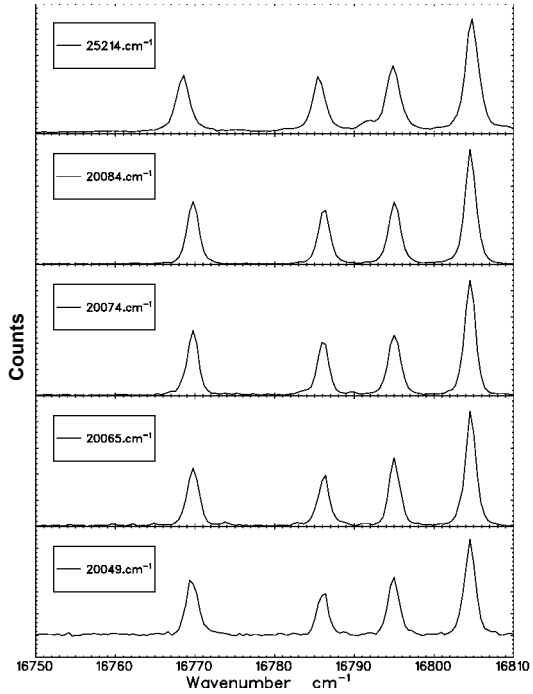

Fig. 3 Emission spectra of [Cm^{3+}: $Y(H_2O)_8]Cl_3$·15-crown-5 at different excitation energies [3].

However, eightfold coordinate $[Cm(H_2O)_8]^{3+}$ doped $Y(H_2O)_8Cl_3$·15-crown-5 shows a much larger ground state splitting [3].

In contrast to the bromate system discussed above, the emission spectrum of [Cm: $Y(H_2O)_8]Cl_3$·15-crown-5 does not change for different excitation wavelengths (Fig.3). This is clear evidence that Cm^{3+} is present in only one site and that the four lines are due to the electronic transitions between the lowest crystal-field levels of the excited state $^6D'_{7/2}$ (A1) and the four crystal field levels of the ground state $^8S'_{7/2}$ (Z_{1-4}).
The same spectral lines are observed in the excitation spectra, where the excitation laser is scanned and the intensity of fluorescence serves as a measure of the absorption cross section. Four peaks are observed at the same positions as for emission (Fig.4, top), however, the relative intensity of the lines is different. Since the sample is at low temperature (10K) the higher crystal field levels of the ground state are only weakly populated (Boltzmann distribution) and the absorption is therefore weak. The emission, in contrast, is not affected by the population of the ground state but only depends on the transition strength from the respective excited state to the ground state.

A second excitation spectrum is shown in Fig.4 (bottom). Cm^{3+} is excited to the $^6P'_{5/2}$ (B_1) state. The P-state decays rapidly to the D-state by energy transfer to the water ligands, and $^6D'_{7/2}$ $^8S'_{7/2}$ emission is observed. Four emission lines are clearly visible and the relative positions match those of the emission spectra (Fig.3) and the emission spectrum of Fig.4 (top).

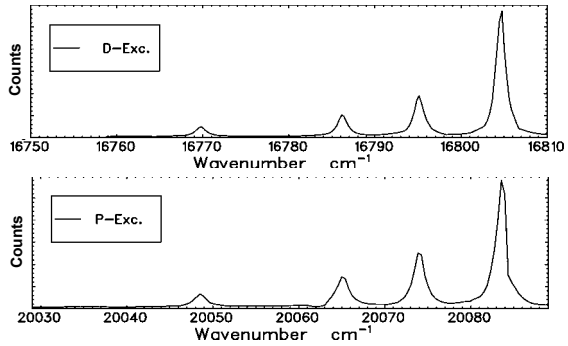

Fig. 4 Excitation spectra of [Cm^{3+}: $Y(H_2O)_8]Cl_3$15-crown-5. $^8S'_{7/2}$ - $^6D'_{7/2}$ transition (top) and $^8S'_{7/2}$ - $^6P'_{5/2}$ (bottom) [3].

The observed ground state splitting of ~ 35cm^{-1} which is comparably large as that of Cm^{3+} in ThO_2 [4] hints at a strong crystal field caused by the short mean Cm-O distance (2.46Å) in conjunction with the distorted bicapped coordination geometry.

Conclusion

Excitation-spectroscopy is a valuable tool for investigating metal coordination chemistry. Recent investigations extended the application successfully to Am and Eu in solid matrices and Cm-fulvate and humate complexes in solution.

A new fibre connected high-temperature optical detection cell for time-resolved laser-fluorescence spectroscopy

Most investigations using time-resolved laser-fluorescence spectroscopy have been performed at room temperature e.g. to study the complexation of Cm^{3+} in different solutions or for Cm^{3+} incorporated in solids (see above). But concepts for the deep disposal of high-level radioactive waste contain maximum temperatures of ~ 200°C in a repository. A pioneering study on the hydration of the Cm^{3+} aquaion has been published in 2005 [5]. A new high temperature optical detection cell has been developed for the determination of spectroscopic data at elevated temperatures ≤ 200°C.

The cell (Fig. 5) is designed as a flow-through detection cell with 1.5 mL sample volume and

4 optical silica windows, one at each side. It is fabricated from TiPd. For heating and temperature control, two electrical heaters with thermocouples are fixed to the upper and lower part of the cell (Fig. 5). All fittings, tubings, valves outside the hot region, are made from standard PEEK material. Syringes are used for draining or filling the sample volume. After filling and closing the respective valves, the cell may be heated up to 200°C (closed system).

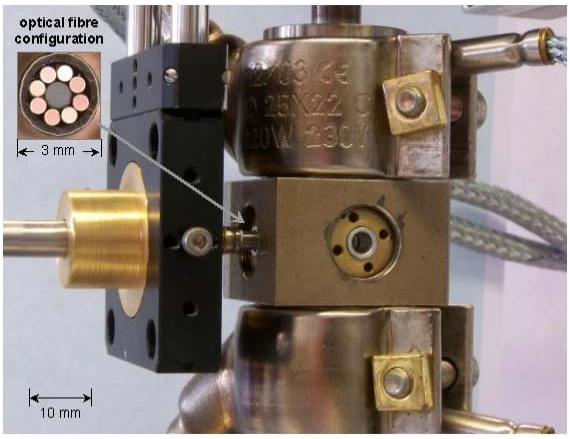

Fig. 5 High-temperature detection cell

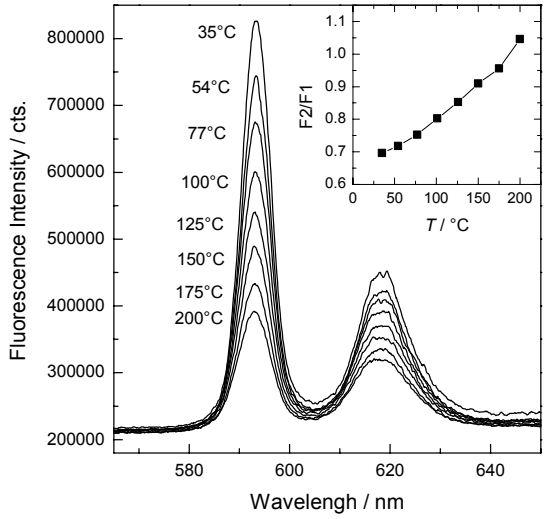

Fig. 6 Fluorescence spectra showing the $^7F_1$ and $^7F_2$ bands of Eu^{3+} (aq) (10^{-5} M Eu^{3+} in 0.1 M $HClO_4$, λ(exc) = 394 nm); The inset shows integrated (baseline corrected) $^7F_2/^7F_1$ ratios.

The laser pulses are transmitted into the detection cell in a radioactivity controlled laboratory by a 20 m optical fiber. Fig. 5 shows the fiber configuration (Optrode) directly at the cell window. Here, eight fibers for fluorescence transmission are arranged around the central excitation fiber. (The fluorescence fibers go back 20 m to the spectrometer in an inactive laser laboratory.)

In 2005, a series of TRLFS experiments using dilute (~ 1–10 μM) Eu^{3+} aqueous solutions for system optimization have been performed. An example for such a variable-temperature experiment is shown in Fig. 6. With increasing temperature from 35 to 200 °C the fluorescence intensity decreases noticeably. The intensity of the $^7F_1$ band decreases somewhat more with temperature than the hypersensitive $^7F_2$ band does. This is reflected by the increase of the $^7F_2/^7F_1$ ratio with increasing temperature (Fig 6, inset). Also, the fluorescence lifetime decreases slightly with temperature; that is, from about 106 to 95 μs when moving from 35 to 200 °C.

TRLFS investigations on the complexation of Cm^{3+} with selected ligands at elevated temperatures will be performed in 2006.

Vibrational Sum Frequency Spectroscopy

The adsorption of radionuclides at the mineral surfaces of a given aquifer is an important process which leads to the retention of the contaminants. That means that their transport by the ground water is suppressed or slowed down. For the reliable long-term modelling of metal ion migration, the adsorption/ desorption properties and the reactivity of the mineral surfaces must be understood at the molecular level.

The interaction of a mineral with an electrolyte is controlled by the surface functional species. We use sapphire (α-Al_2O_3) as a model mineral for natural clay minerals supposed to contain as well >Al-OH surface functional groups and analogous iron oxide phases. An example for surface >Al-OH groups is given in the middle formula of Fig. 7. The most basic and most important reaction of the surface functional species is their protonation and deprotonation which occur as a reaction of pH variations in solution. As a result, the surface properties change dramatically, for example the interaction capability with actinide and lanthanide ions. Although the protonation and deprotonation equilibria are so important, the corresponding stability constants are not definitely known for most mineral surfaces because it is difficult to obtain in situ chemical analytical information with interface selectivity under natural aquatic conditions.

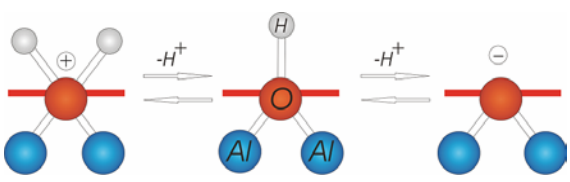

Fig. 7. Scheme of sapphire/water interface, protonation and deprotonation of aluminol species

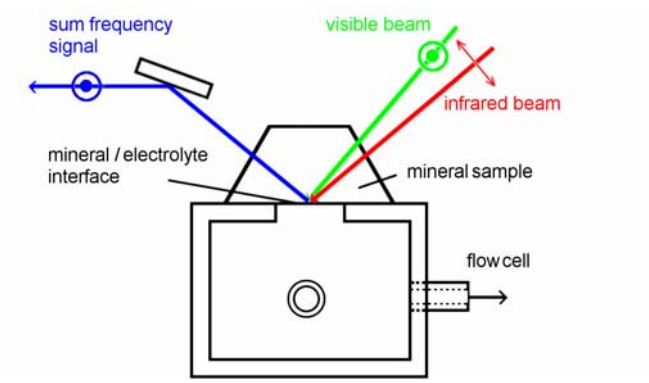

Fig. 8. Scheme of the sum frequency experiment, top view. The polarizer orientations indicated here have been selected for the measurement of the spectrum given in Fig. 9.

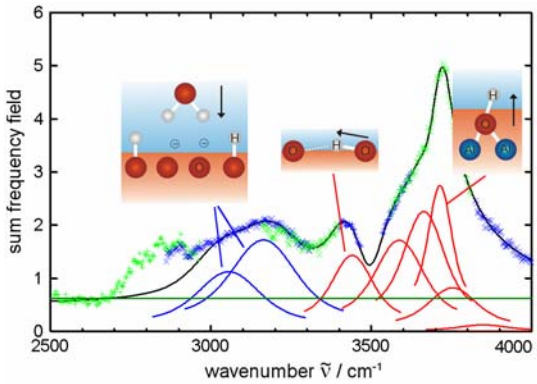

Fig. 9. Sum frequency spectrum of the sapphire (001) surface under water at pH 12 together with the result of deconvolution and interpretation. The arrows indicate the dipoles of the OH species

We have, however, shown in a systematic study of sapphire single crystal surfaces that sum frequency spectroscopy provides this information. A scheme of the experiment is given in Fig. 8. A surface of the mineral sample is in contact with the electrolyte. The interface is then illuminated with intense light from two lasers at frequencies ω_1 and ω_2. Due to the high intensities, photons from the two beams can couple to the sample at the same time in order to generate photons at the sum frequency $\omega_{SF} = \omega_1 + \omega_2$. An SF signal [6] can always be generated at a surface or an interface. In the bulk of media which exhibit certain point groups, however, SF generation is symmetry forbidden. In particular centrosymmetric matter such as the bulk of a liquid does not provide SF light in the electric dipole approximation. Also, no signal originates from the bulk of, for example, a sapphire crystal (point group $\bar{3}m$). As a result, we can obtain SF light selectively from the interface between sapphire and water.

Fig. 9 gives the OH stretch region of the SF spectrum obtained from a sapphire (001)/electrolyte interface at pH 12 (ionic strength *I* = 50 mM, NaCl). In the non linear optical experiment, we consider the field of the generated SF light as the signal. The deconvolution of the spectrum leads to the magnitudes of the contributing bands (red and blue lines in Fig 9) and to their phases indicated in Fig 9 for the resonance maxima. This phase information, which cannot be obtained in the corresponding linear optical experiment, provides information on the absolute orientation of the molecular dipoles which are responsible for the generation of the signal.

The two blue bands in Fig 9. are due to the polar ordered water film near the mineral surface which is well known from various aquatic interfaces [7]. At high pH, our spectrum shows that the water dipoles point into the direction of the mineral surface (phase φ = 0°). This is consistent with a negative surface charge which we expect at high pH.

Additionally we observe a surprisingly large number of additional bands (red curves in Fig. 9) which are due to different aluminol species and to specifically bound water molecules. We could identify two species so far. Analyzing the polarization and the magnitude of their bands as a function of the incident polarizations, we obtained the axial orientations of their OH dipoles. The result is given in Fig 9. The dipole orientation and the spectral band positions agree well with molecular dynamics calculations [8].

Upon reduction of the pH we expect an inversion of the water dipoles' absolute orientation due to the change of the surface charge from negative to positive sign near the point of zero charge. The dipoles, however, flip twice in the range between pH 6 and pH 4. These phenomena cannot be explained with electrostatic forces but with two types of hydrogen bonds. The interaction is dominated by these hydrogen bonds in a broad range around the point of zero charge.

Conclusions

The nonlinear optical technique allows to obtain a picture of the mineral/water interfaces at molecular level with a surprising richness of details.

References

[1]G. K. Liu, J. V. Beitz, and J. Huang, Journal of Chemical Physics 99, 3304 (1993).
[2]W. T. Carnal and K. Rajnak, J. Chem. Phys. 63, 3510 (1975).
[3] P. Lindqvist-Reis, C. Walther, R. Klenze, Th. Fanghänel, J. Phys. Chem. B, 110 (2006), 5279-85.
[4]P. Thouvenot, S. Hubert, and N. M. Edelstein, Phys.Rev.B 50, 9715 (1994).
[5] P. Lindqvist-Reis, R. Klenze, G. Schubert, Th. Fanghänel, J. Phys. Chem. B, 109 (2005), 3077-83.
[6]Y. R. Shen, Surface Properties Probed by Second-harmonic and Sum Frequency Generation, Nature, 337, 2004, 519-525.
[7]G. L. Richmond, Molecular Bonding and Interactions at Aqueous Surfaces as Probed by Vibrational Sum Frequency Spectroscopy, Chem. Rev. 102**,** 2002, 2693-2724.
[8]K. C. Hass, W. F. Schneider, A. Curioni, W. Andreoni, First-principles Molecular Dynamics Simulations of H_2O on alpha-Al_2O_3 (0001), J. Phys. Chem. B 104, 2000, 5527-5540.

6.3 Colloid characterization methods

M. Bouby, S. Büchner, H.R. Cho, M.A. Denecke, H. Geckeis, R. Götz, W. Hauser, J. Rothe, C. Walther

Introduction

Formation of colloidal species is known to contribute to radionuclide mobilization and can play a significant role for the radionuclide release during nuclear waste form dissolution. Development of sensitive analytical techniques is required to allow for the detection and characterization of colloids in solution even at trace concentrations. Various arrangements for ultra-trace analysis of colloids by laser-induced breakdown detection (LIBD) have been set up at INE during the last years and are continuously developed. A mobile LIBD has been assembled to gain insight into the colloid provenance in natural groundwater of different origin and geochemistry. Different sampling techniques have been investigated to avoid analytical artifacts. Solubility studies on tetravalent actinides and their chemical homologues have been performed by LIBD to determine the onset of precipitation via formation of colloidal species. The elucidation of the nature of those colloids or polynuclear species has been the aim of recent studies on Zr colloid characterization by LIBD and EXAFS. A further technique which is applied to colloid characterization is the flow-field flow fractionation combined with various detection techniques. An appropriate calibration method has been developed in order to quantify element signals in AsFlFFF-ICP-MS fractograms.

Characterization of natural groundwater colloids with a mobile LIBD system

Motivation

The aim of this study is to improve the experimental procedure for the colloid analysis by LIBD and to determine the amount of background colloids as a function of groundwater geochemistry under unperturbed in-situ conditions with a minimum of possible sampling interferences. Natural colloid concentrations are analyzed in granite groundwater taken from a series of boreholes at the Äspö underground laboratory (Sweden), at Grimsel Test Site (Switzerland) and from sedimentary groundwater at Ruprechtov (Czech Republic).

Experimental

A mobile system for the laser-induced breakdown detection (LIBD) combined with a geo-monitoring unit for pH, Eh, electrical conductivity, and oxygen content detection is applied. The LIBD method has previously been described. The main advantage compared to conventional methods is a several order of magnitude higher sensitivity, especially for colloids < 200 nm (detection limit for 20 nm colloids in the low-ppt range). The whole arrangement, including an ultra-pure water processing unit is installed in a van for *in-situ* measurements at site. An optical high pressure flow-through detection cell is used. Colloids are detected under hydrostatic groundwater pressures up to ~ 40 bar without contact to atmosphere oxygen.

Fig. 1 The mobile LIBD detection system in the Äspö tunnel (not referred to in text)

Additionally, a system for remote groundwater sampling completes the experimental configuration. Pressurized steel cylinders with remotely operated valves can be lowered by a cable winch into deep vertical boreholes. Groundwater samples are taken with these cylinders when a direct connection between mobile LIBD and groundwater, e.g. in deep boreholes drilled from above ground is not possible (Ruprechtov). After sampling, the cylinders are in-line connected with the LIBD and the geo-monitoring unit for the detection of colloids and geo-chemical parameters, such as pH, Eh, O_2-content, electrical conductivity. The investigations are completed with groundwater chemical analysis by ICP-MS, ICP-AES, IC. Colloids > 50 nm are filtered from some groundwater samples with track etched polycarbonate filters. The remaining colloids on the filters are characterized by scanning electron microscopy and EDX.

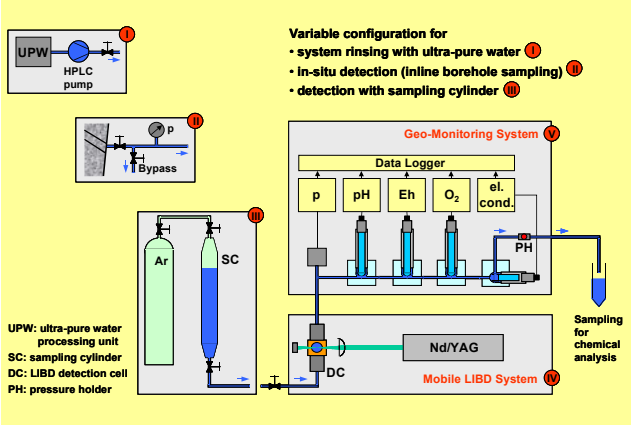

Fig. 2 Sampling and detection configuration (not referred to in text)

Results

Earlier colloid studies claimed the existence of a significant correlation of colloid concentrations in ground water with the salinity (ionic strength) of the ground water [1,2]. Recent LIBD results of in-situ investigations at Äspö confirm low colloid concentrations (< 0.1 µg/l) for groundwater with chloride contents ≥ 4 g/l. For two different groundwater with chloride concentrations > 10 g/l, the colloid concentrations were close to the LIBD detection limit of the LIBD arrangement under given conditions at ~ 10 ng/l.

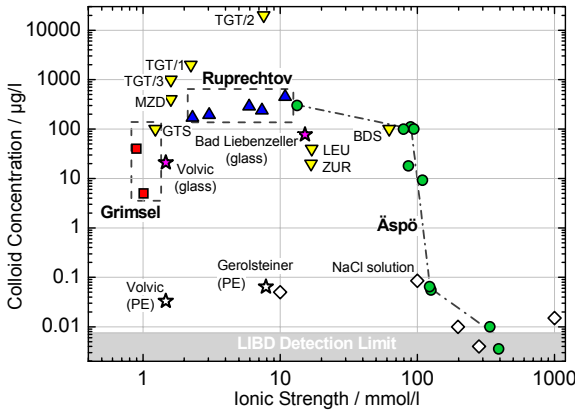

Fig. 3 Comparison of colloid concentration in different types of natural ground water, mineral water and synthetic NaCl-solution versus ionic strenth (△ Ruprechtov; □ Grimsel CRR tunnel; O Äspö tunnel; ☆ mineral water; ◇ NaCl solution ; ▽ Data from [3]: TGT: transit gas tunnel, MZD: Menzenschwand, GTS: Grimsel test site, BDS: Bad Säckingen, LEU: Leuggern, ZUR: Zurzach)

A comprehensive representation of colloid concentrations in different water samples as determined by LIBD plotted versus the respective ionic strength is given in Fig. 3. The trend observed in figure 3 demonstrates the destabilization of colloid dispersions at increasing ionic strength in a given groundwater.

The broad bandwidth of detected colloid concentrations in groundwater of ionic strength < 10 mmol/l (Grimsel, Ruprechtov) suggests that other parameters besides geochemistry as e.g. mechanical forces, groundwater flow or chemical disequilibria may control the actual colloid concentrations. At ionic strengths > 10 mmol/l the upper limit for the colloid concentration may now be governed by colloid stability and thus by the ionic strength of the groundwater. Notably for groundwater samples from Äspö and simulated NaCl solutions a clear dependency of the maximum colloid concentrations with the salinity of the groundwater is found.

Investigation of Zr(IV)-hydroxide solubility with LIBD and EXAFS

Zr(IV) gained increasing attention in recent literature as homologue of Pu(IV), due to its similar hydrolysis and colloid formation [4,5]. In addition, Zr is an important material in reactor technology and a fission product of high yield and long lifetime (^{93}Zr). In the present work, the solubility of $Zr(OH)_4$ (am) in 0.5M HCl/NaCl solution is determined. Conventional solubility data are obtained by measuring the equilibrium amount of solvated species in the presence of a precipitate starting from undersaturation. In the present case, a different approach is chosen, similar to a previous study with Th(IV) [6]. In the acidic range, the "$Zr(OH)_4$ (am)"-solubility decreases with increasing pH. When the pH is increased until the solubility limit is exceeded, some fraction of the Zr will precipitate. However, precipitation is difficult to observe at low concentration. Prior to precipitation, oligomers or colloids form in the solution which remain suspended by Brownian motion due to their small size (<100nm) and detection of these particles by laser induced breakdown detection (LIBD) [7,8] is a very sensitive method for solubility measurements. From a concentrated stock solution ([Zr] = $5 \cdot 10^{-3}$ M in 0.5 M HCl), 12 starting solutions are prepared below the solubility limit at Zr concentrations between 10^{-3} M and $2.5 \cdot 10^{-8}$ M, at 1<pH<3 and constant ionic strength I=0.5 M (addition of NaCl). pH is increased very slowly by coulometric titration (< $3 \cdot 10^{-9}$ mol OH^- s^{-1}) while current control, pH detection and LIBD measurements are fully automated and operate remote-controlled continuously up to several weeks. The pH is increased by predefined steps (≤ 0.1 pH units) and after a 30 minute equilibration time the particle size distribution (PSD) is measured by LIBD [9].

Close to the expected solubility limit, the pH is increased very slowly by reducing the electric current down to 10μA.

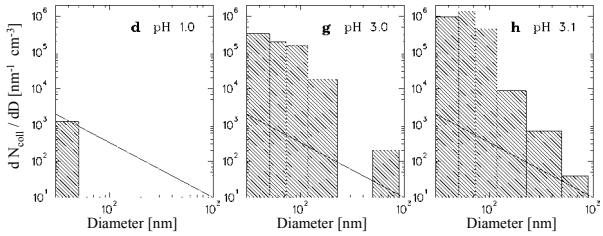

Fig. 4 Colloid number density as function of size of the titration series at [Zr]=1.07·10^{-3} M measured by LIBD.

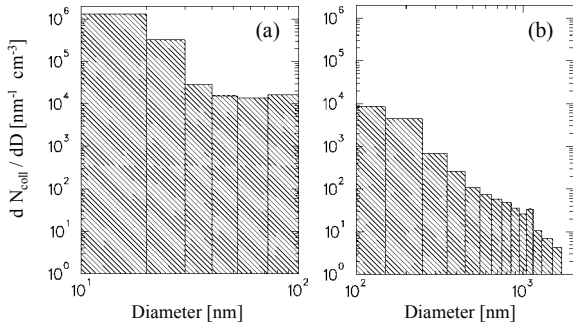

Fig. 5 The PSD from (a) LIBD measurement and (b) SPC measurement at [Zr] = 3.5·10^{-7} M and pH 6.5.

Fig. 4 shows the measurement at [Zr]=1mM. When the pH of the colloid free starting solution (Fig.4, left) increases, colloids form spontaneously at pH 3.0 (Fig.4, center) and with higher pH, number and size of colloids increase (Fig.4, right). By combining LIBD and static light scattering (single particle counter) the size distribution of the colloids is measured over an extended range from 50nm to 2μm (Fig.5).

The onset of colloid formation is plotted as a function of Zr concentration in Fig.6 (▲). In order to calculate the solubility product, hydrolysis has to be taken into account. The first hydrolysis constant for the complex $ZrOH^{3+}$ is known from potentiometric studies [10] and the other formation constants of $Zr(OH)_n^{(4-n)+}$ ($n = 2-6$) are estimated by using the semi-empirical ligand repulsion model [11]. Based on the assumption that colloids form from mononuclear species, which is most likely valid for low concentrations, the calculated solubility product, $\log K_{sp}^{o}$, is 53.1 ± 0.6. The data of the present work is in qualitative agreement with a similar method using light scattering for detection (x from [4]). Deviations at low concentration are due to the low sensitivity of light scattering, as the authors state themselves. The data of Kovalenko (+, from [4]) and Ekberg (◇) [5] deviate by six orders of magnitude because they describe the solubility of microcrystalline ZrO_2 and not of amorphous hydroxide.

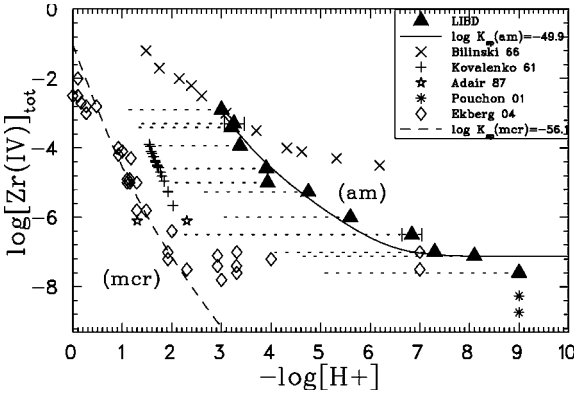

Fig. 6 Solubility of Zr(IV) and literature data. Triangles (▲) depict the onsets of colloid formation determined by LIBD. The solubility product is obtained to be log K^{O}_{sp} = -53.1 ± 0.6 extrapolated to zero ionic strength.

In order to characterize the structure of the colloids and polynuclear species, several solutions of millimolar concentration were investigated by EXAFS [12]. At high concentrations and very acidic conditions ([Zr] = 1·10^{-2} M, pH= 0.3) the EXAFS spectra can be well described by the presence of Zr-tetramers ($[Zr_4(OH)_8(H_2O)_{16}]^{8+}$), well in line with X-ray and neutron scattering experiments [113,14]. It is hence likely that under these conditions colloids form from tetrameric building blocks. At [Zr] = 1·10^{-3} M no Zr-Zr interaction is found for pH < 2 which indicates that monomeric Zr-species dominate under these conditions. As the solubility limit is approached close to pH 3, oligomers form and with increasing pH the disorder in the Zr-O coordination shell increases. Since the EXAFS spectra cannot be explained with any of the known modifications of zirconiumdioxide solid (tetragonal, monoclinic, orthorhombic) the disorder hints at the simultaneous presences of several similar Zr-species, which might be built from oligomers such as the tetramer, pentamer, octamer and bigger units, which are known for many decades to form in highly concentrated (10-1000 mM) Zr solutions [15]. The direct quantification of the oligomeric species is presently being undertaken by means of electrospray mass spectrometry.

Asymmetric Flow Field-Flow Fractionation (AsFlFFF) coupled to ICP-MS: development of an on-line quantification method

The AsFlFFF combined with an ICPMass-Spectrometer, provides information on colloid size distribution and the inorganic element composition of different colloid size fractions [16,17]. This technique is applied to gain insight into the dynamics of colloid behaviour and metal ion/radionuclide - colloid interaction processes especially at metal/radionuclide trace concentrations as they are expected under natural groundwater conditions (i.e: ~10^{-9} mol/L range). Previous experiments revealed considerable flow fluctuations during a fractionation run making a quantitative assessment difficult. Therefore, a method for the on-line element quantification in ICP-MS-fractograms has now been developed in order to overcome those problems and to correct for daily system sensitivity variations [18]. The method is based on the measurement of the constant ICP-MS intensity ratios for an internal standard (Rh-103) and the elements of interest (Al, Mg, U, Th…)(intensity: counts per second; cps). Rh is added to a 6 % nitric acid solution which is delivered at a constant flow rate and mixed via a T-piece with the AsFlFFF channel effluent before it enters the ICP-MS nebulizer. Calibration factors R_{an} are determined for each element by relating intensity ratios of the analyte to the Rh-103 intensity for a given metal ion concentration. R_{an} for the elements under investigation is found to remain constant within < 4.4 % uncertainty irrespective of the channel outflow rate. The application of this calibration factor allows the conversion of fractograms based on raw data (cps) into mass versus elution time fractograms (see figure 7). The system has been used to study the kinetics of radionuclide/metal ion – colloid interaction over longer time periods where metal concentrations can be determined independent of the analysis time and the system status (see separate contribution within this issue). Figure 7 shows an example for the fractionation of a bentonite colloid dispersion 5 months or 17 months after its preparation before any correction (A) and after calibration by using Rh as an internal standard (B). A slow colloid agglomeration process is clearly evidenced in the fractograms. Calculated peak area and colloid masses, respectively, are consistent after calibration, even though the date of analysis and system status concerning ICP-MS sensitivity and flow conditions in the channel were different for both runs. In general, the reproducibility for the colloid mass determination varies by less than 6 % for replicate measurements of the same sample and the uncertainties for measured average sizes as determined from the peak position of the main fraction are below 5 %.

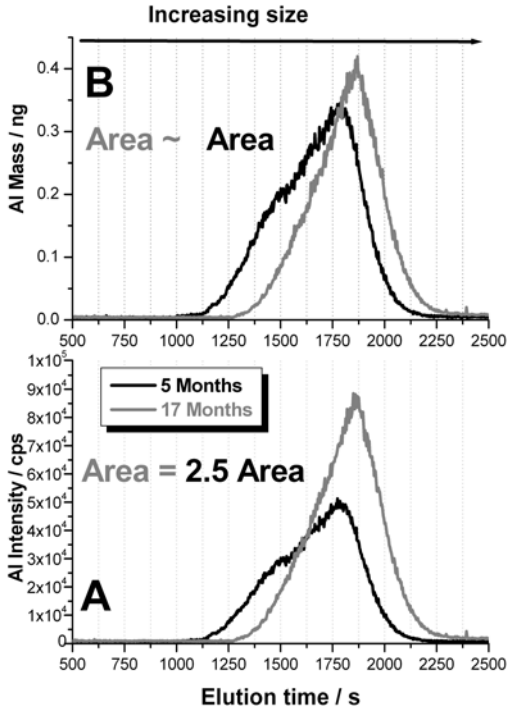

Fig. 7 Corrected (B) and uncorrected (A) fractograms for a 20 $mg.L^{-1}$ bentonite colloid dispersion prepared in natural Grimsel groundwater; Al is analysed as a indicator element for the bentonite colloids.

References

[1] Degueldre, C., Triay, I., Kim, J.I., Vilks, P., Laaksoharju, M., Miekeley, N., Ground water colloid properties: a global approach, Appl. Geochem. 15 (2000) 1043-1051

[2] Hauser, W., Geckeis, H., Götz, R., In situ determination of natural ground water colloids in granite shear zones along the Äspö HRL Tunnel by LIBD, 27th Int. Conf. on Scientific Basis for Nuclear Waste Management, Kalmar, S, June 15- 18, 2003

[3] Degueldre, C., Grauer, R., Laube, A., Oess, A., Silby, H., Colloid properties in granitite ground water systems. II. Stability and transport study, Appl. Geochem. 11 (1996) 697-710

[4] E. Curti and C. Degueldre. Radiochim. Acta 90(9-11), 801-804 (2002).

[5] C. Ekberg, G. Kallvenius, Y. Albinsson, and P. L. Brown. J. Solution Chem. 33(1), 47-79 (2004).

[6] T. Bundschuh, R. Knopp, R. Müller, J.I. Kim, V. Neck, and Th.Fanghänel. Radiochim. Acta 88, 625-629 (2000).

[7] T. Kitamori, K. Yokose, M. Sakagami, and T. Sawada. Japanese J. Appl. Phys. 28(7), 1195-1198 (1989).

[8] F.J. Scherbaum, R. Knopp, and J.I. Kim. Appl. Phys. B 63,299-306 (1996).
[9] C. Walther, H.R. Cho, and Th. Fanghänel. Appl. Phys. Lett.85(26), 6329-6331 (2004).
[10] C. Ekberg, P. Brown, J. Comarmond, and Y. Albinsson. On the Hydrolysis of Tetravalent Metal Ions. In Mat. Res. Soc. Symp. 663 1091-1099 (2001).
[11] V. Neck and J. I. Kim. Radiochim. Acta 88(9-11), 815-822 (2000).
[12] A. Singhal, L. M. Toth, J. S. Lin, and K. Affholter. J. Am. Chem. Soc.118(46),11529-11534 (1996).
[13] H. R. Cho, C. Walther, J. Rothe, V. Neck, M. A. Denecke, K. Dardenne, and T. Fanghänel, Anal. Bioanal. Chem. 383, 28 (2005).
[14] C. Hagfeldt, V. Kessler, and I. Persson. Dalton. Trans. (14), 2142-2151 (2004).
[15] W. Blumenthal, *The chemical behaviour of Zirconium*, D.van Nostrand Company, Princeton 1958
[16] H. Geckeis, T. Ngo Manh, M. Bouby, J.I. Kim, Coll.&Surf. A, 217(2003), 101-108
[17] M. Bouby, H. Geckeis, T. Ngo-Manh, J.I. Yun, K. Dardenne, T. Schäfer, C. Walther, J.I. Kim, J. Chrom. A, 1040 (2004), 97-104
[18] M. Bouby, H. Geckeis, Anal. Chim. Acta, to be submitted.

6.4 Computational Chemistry

B. Schimmelpfennig, M. Patzschke, R. Polly

Introduction
Computational chemistry was established as a new research area at INE a few years ago. The goal is to corroborate the experimental results achieved at INE by a theoretical basis and to provide additional data, which can often not be obtained from experiment directly. The work is focussed on compounds of actinides. Sound quantum chemical calculations for these very heavy elements became feasible only very recently.

Computational Chemistry aims to describe chemical compounds and their various properties, such as structure, thermodynamic data, vibrational or optical spectra by approximately solving the quantum mechanical equations of the system with as few experimental data as input as possible.

The complicated set of coupled differential equations in many dimensions is difficult to solve and even approximate solutions require the use of huge computer power and state-of-the-art software. The effects of surrounding media such as solvents or a crystal can be treated at an approximate level only. For heavy elements such as lanthanides and actinides the high density of low lying states with coupled open-shells and the strong relativistic effects must be treated in an adequate manner. For these problems computational methods have been developed and implemented over the last decade. A critical analysis of the approximations employed, either by benchmarking against reliable experimental reference data or highly accurate theoretical data is still mandatory and the choice of the methods not trivial.

For our purposes, the use of Effective-Core Potentials (ECPs), which reduce the number of explicitly treated electrons and include relativistic effects by parameterisation, has shown to be a useful tool. ECPs have been employed for all calculations of lanthanide and actinide compounds. The treatment of solvent effects is currently limited to the use of continuum models, but will be extended to approaches which treat the surrounding waters explicitly at an approximate level.

Software Development:
The TURBOMOLE software package has been extended at INE to handle actinide compounds. This software is used at different levels of theory such as Density-Functional Theory (DFT) and post-Hartree-Fock methods like Møller-Plesset Perturbation Theory (MP2) and Coupled-Cluster Theory (CC2) combined with the Resolution-of-the-Identity (RI) technique, which allows the treatment of large systems.

Spin-orbit interaction is strong in open-shell actinide compounds and can not be neglected especially when describing electronically excited states. We collaborate with INT (Institut für Nanotechnologie) and the University of Karlsruhe on the development of two-component methods. This will allow treating spin-orbit effects not only as a perturbation but including them from the beginning of the calculations. The use of the RI-technique will make it possible to apply this method to large systems.

Results

Extraction Ligands
The efficient separation of trivalent actinides from trivalent lanthanides in HAW solution is mandatory for transmutation of minor actinides. The design of selective ligands for liquid-liquid extraction is a demanding task because of the similar chemical behaviour trivalent actinides and lanthanides. The extraction ligand BTP (Alkylated 2,6-ditriazinylpyridine) developed at INE, was the first ligand showing excellent separation factors. Previous EXAFS and TRLFS studies provided no sound explanation for this result. Identical structures and metal-nitrogen bond distances of 255 pm were found for BTP complexes of both Cm(III) and Eu(III).

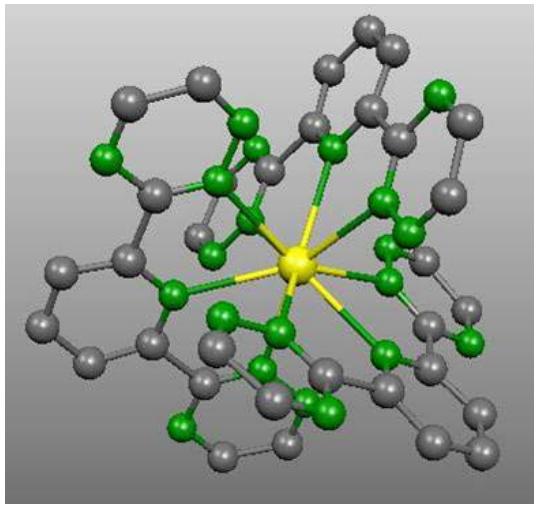

Fig. 1: DFT calculation on the Cm(III)BTP_3 complex (hydrogens omitted)

DFT calculations were performed by TURBOMOLE to optimise the structure of several M(III)BTP_3 complexes, testing various functionals. The calculations proved a nine-coordinated structure with high D_3 symmetry to be lowest in energy (see Fig. 1). The calculated metal-nitrogen bond distances for Eu(III) and Cm(III) agree within 1 pm at all levels of theory investigated. The deviation from EXAFS data for these distances varied strongly depending on the functional employed, in some case by more than 10 pm. In order to get theoretical reference data RI-MP2 calculations were carried out for the complexes using a large-core Effective Core Potential (ECP) for Eu(III), where the open 4-f-shell is included in the parameterised potential. These calculations gave Eu-N bond distances in quantitative agreement with the EXAFS data. Recently, the group of Prof. Dolg (Cologne University) developed ECPs with the 5f-shell in the core for the actinides. As the 5f-shell is less compact than the 4f-shell in the lanthanides, the approximation is less accurate, and calculations at the RI-MP2 level overestimate the Cm-N bond distance by 3-4 pm. This overestimation can also be found at the DFT-level when comparing calculations with the explicit treatment of the 5f-shell and with the 5f-shell in core. Taking this systematic effect into account, the structural parameters for the Cm(III)BTP_3 complex at the RI-MP2 level are in full agreement with experiments [1].

The calculation revealed further details on other properties of the complexes, such as the vibrational frequencies and the torsion of the ligands and the structure of the ligands, which have not been determined experimentally.

It was suggested that the difference in extraction behavior for Eu(III) / Gd(III) and Cm(III) is due to a difference in covalency of the metal-nitrogen bond. For the BTP complexes of Gd(III) and Cm(III) DFT-calculations with explicit f-functions were carried out at the optimised structure of the Gd(III) complex. As shown in Fig.2, the calculated difference in electron density between both complexes is so small that a significant contribution for different covalence character to the binding energy can be ruled out.

This is in full agreement with theoretical investtigations of the difference in metal-ligand binding when comparing BTP and Ter-Pyridine (Terpy), the latter to be known as a non-selective ligand. The calculations gave a small energy difference of only 20kJ / mol which is close to the numerical accuracy of the calculations.

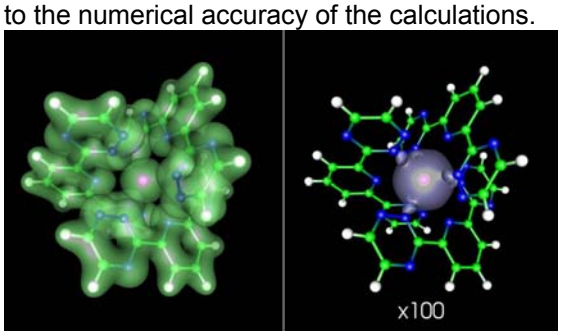

Fig. 2 Total density and scaled density difference for Gd(III)BTP_3 and Cm(III)BTP_3

C(1s) NEXAFS-Spectra of Benzoic-acid derivatives

STXM has been used previously to characterize colloidal natural humic substances by spatial resolved C(1s) NEXAFS spectra. For

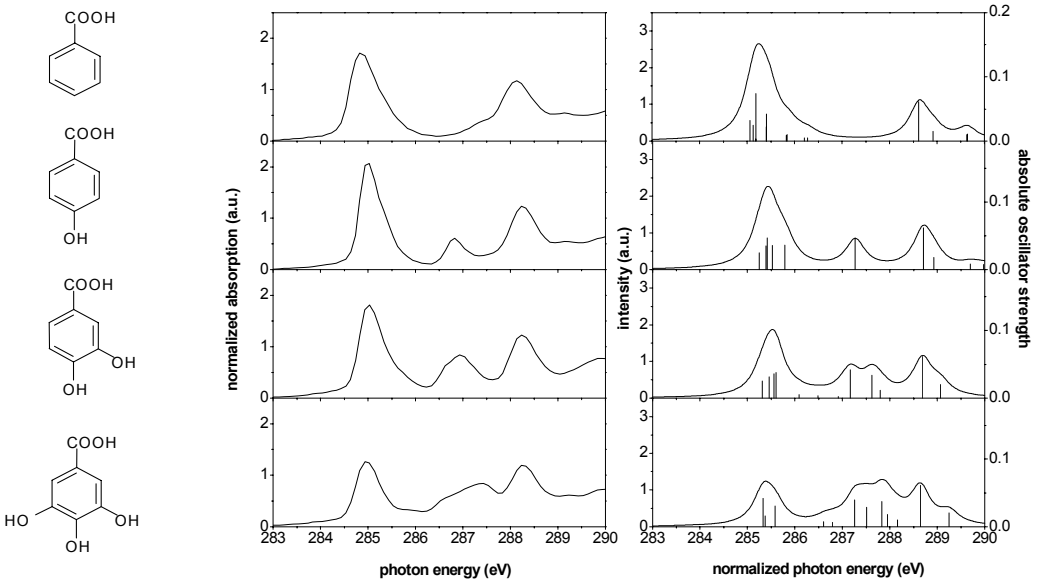

Fig. 3 Experimental (left) and calculated C(1s) NEXAFS spectra of Benzoic acid and its derivatives

the assignment of the various functional groups derivatives of benzoic acid have been measured as reference compounds. However, the interpretation of the experimental spectra is not straight-forward as different peaks cannot always be resolved. Additionally, the number of contributing excitations into the various π^* orbitals and the relative intensities to be expected can not be deduced from experiment. In collaboration with the University of Heidelberg, ab initio calculations at the ADC(2) level, which is a diagrammatic perturbation theory, were performed on the C(1s) $\rightarrow\pi^*$ excitations in various benzoic acid derivates and compared with the experimental data [2].

The calculated peak positions, which are shifted systematically by 2 eV relative to experiment, and the calculated intensities are in excellent agreement with the experimental data (see Fig.3). This study clearly shows the power of combined theoretical / experimental studies for a deeper understanding of the underlying processes by giving a further interpretation of experimental data. Additional joint studies of NEXAFS spectra are planned for systems with metal complexation.

Coordination of Cm(III) in aqueous solution

Temperature dependent time-resolved laser fluorescence studies of Cm(III) in aqueous solution by Lindqvist-Reis et al. [3] were interpretted as an equilibrium between eight- and nine-coordination with an entropy driven increase of the eight-coordination for increasing temperature. We carried out quantum-chemical calculations with either nine waters in the first coordination shell or eight waters in the first and one in the second coordination shell as a model for the coordination in solution (see Fig. 4). Our calculations fully support the interpretation of the experimental data with respect to the coordination numbers. They also show that Density Functional Theory combined with a polarizable continuum model (COSMO) for long-range solvent effects is sufficient to describe the structure of the complexes, but strongly overestimates the binding energy in the eight-coordinated complex with an additional water in the second hydration sphere. Single-point calculations with RI-MP2 were carried out at the optimised DFT structures and are in excellent agreement with the experimental ΔH value [3], whereas ΔS can be reproduced only qualitatively at the DFT-level. The errors in the ΔS calculations can be attributed to the low-frequency twisting modes of the water molecules. These low-lying modes and their population are not well described with the harmonic oscillator approximation used to calculate thermodynamic data.

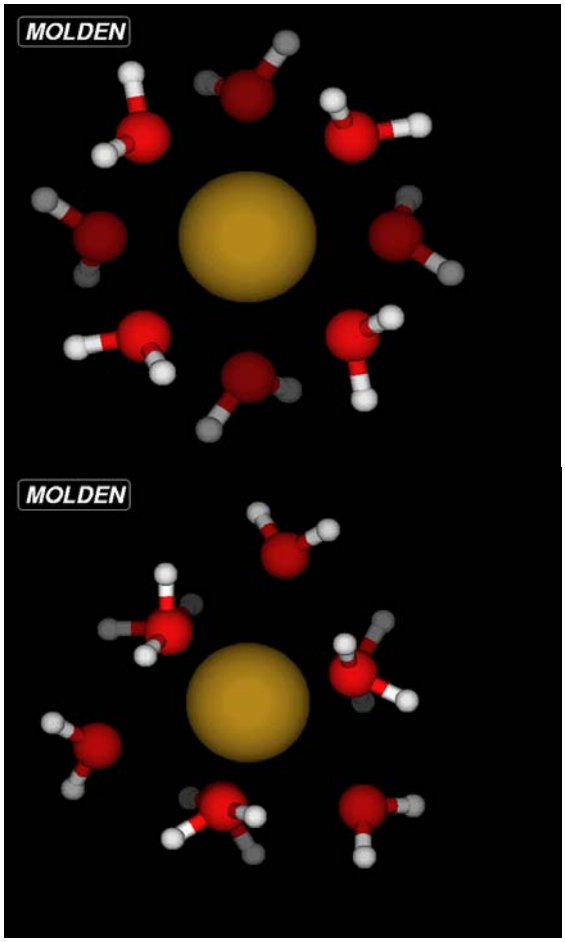

Fig. 4 Calculated coordination geometries for the first hydration sphere of the Cm^{3+} aquo ion. Top: 8-fold hydration (squared antiprism, S_8); bottom: 9-fold hydration (tri-capped trigonal prism, D_3)

Mineral-water interfaces

Reactions at the mineral-water interface play an important role for the radionuclide retention in the near and far field of a nuclear repository. As a model mineral phase, single crystals of α-Al_2O_3 (sapphire) with selected orientations have been studied by various experimental methods. For an accompanying theoretical study, small clusters of Al_2O_3 and their interaction with water have been investigated as a first model of the sapphire water interface. Emphasis is on the calculation of O-H and Al-O vibrations at the interface to be compared with results from non-linear infra-red spectroscopy performed at INE. For these small systems, calculations with the highest possible accuracy were carried out and can be used as reference data for subsequent calculations of larger systems, where the employed highly accurate methods become too demanding. Structural parameters and binding energies to water were obtained. Further calculations including long-range solvent effects are in progress.

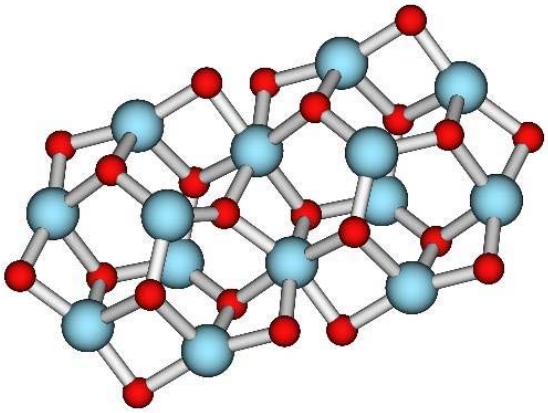

Fig. 5 $Al_{14}O_{22}$ Cluster as a first model for the sapphire/water interface reactions

As an alternative approach, slab-models with periodic boundary conditions will be studied in collaboration with the Universities in Lille (France) and Stockholm (Sweden) within ACTINET. We expect the combination and comparison of these approaches to help us finding an appropriate description of the surface-water interface and in a later step of the sorption of trivalent lanthanides and actinides on mineral surfaces.

Collaborations

Several projects at INE require support from theory and this task cannot be performed by the quantum chemistry group at INE alone. Therefore, projects are carried out in collaboration with neighbour institutes namely the INT and the computational chemistry groups in Heidelberg (Prof. Schirmer) and Karlsruhe (Prof. Klopper). International collaborations/cooperations exist within the European NoE ACTINET. Long-term collaborations have been established with V. Vallet (Lille), U. Wahlgren and I. Grenthe (Stockholm).

The Theoretical Userlab (ThUL)

The INE coordinates the promotion of theoretical / computational approaches in the European NoE ACTINET. Activities are the organisation of Workshops (first in October 2005 at FZK) and Schools (first in May 2006 Lille/France). The main goal is to foster communication between the theoretical and the experimental communities of actinide research. The financial support from ACTINET is mainly used to reimburse young participants. Additionally, ThUL supports the development of state-of-the-art software which is relevant for computational actinide chemistry or physics. A second workshop is in preparation for October 2006 with the topic “Interface Reactions”, again we aim for a balanced mixture of overview talks from both, theory and experiment. A poster session will also be included.

References

[1] M.A. Denecke, A. Rossberg, P.J. Panak, M. Weigl, B. Schimmelpfennig, A.Geist, Characterization and Comparison of Cm(III) and Eu(III)Complexed with 2,6-Di(5,6-dipropyl-1,2,4-triazin-3-yl)pyridine Using EXAFS,TRFLS,and Quantum-Chemical Methods, Inorg. Chem. 2005 , 44, 8418-8425

[2] I. Baldea, B.Schimmelpfennig, M.Plaschke, J. Rothe, J.Schirnmer,A.B: Trofimov and Th. Fanghänel, C 1s Near Edge X-ray Absorption Fine Structure (NEXAFS) of substituted benzoic acids – a theoretical and experimental study, J. Elec. Spec.(submitted)

[3] P. Lindqvist-Reis, R.Klenze, G.Schubert, Th. Fanghänel, Hydration of Cm^{3+} in Aqueous Solution from 20 to 200 (degree) C. A Time-Resolved Laser Fluorescence Spectroscopy Study, J. Phys. Chem. B 2005, 109, 3077-3083

7. Separation of long-lived minor actinides

7.1 Separation of Minor Actinides

A. Geist, M. Weigl, M.A. Denecke, P.J. Panak,B. Schimmelpfennig, U. Müllich, K. Gompper

Introduction

The separation of plutonium and the minor actinides (neptunium, Np; americium, Am; curium, Cm) from spent nuclear fuels and their subsequent transmutation by nuclear fission in advanced reactors could significantly reduce the radiotoxicity of the highly active waste to be stored in a final repository [1]. This is the so-called *Partitioning & Transmutation* strategy [2]. In this context, we study aspects of two separation processes based on liquid-liquid extraction:

1. The DIAMEX process, which is the co-extraction of Am, Cm, and the lanthanides from the PUREX raffinate solution.

2. The SANEX process, involving separation of Am and Cm from the chemically similar lanthanides, from the DIAMEX product solution.

Whereas the DIAMEX process can be considered mature, the SANEX process is still under development, owing primarily to the fact that SANEX extracting agents developed so far all have their shortcomings.

The separation chemistry involved in the SANEX process is not understood from a fundamental point of view: Why do nitrogen (N)-donor extractants preferentially extract trivalent Am and Cm over the lanthanides, in spite of their chemical similarity? Using EXAFS (extended X-ray absorption fine structure) and TRLFS (time-resolved laser fluorescence spectroscopy), we have started to look for answers to this open question.
Furthermore, we have developed and tested miniature hollow fibre modules (HFM) as phase contactors for liquid-liquid extraction [3]. Two so-called HFM micro-plants have been built and tested with such HFM. One of them will be used for tests with actual hot fuel solutions, in collaboration with the Institute for Transuranium Elements (ITU).

This research is carried out within the EC Integrated Project, EUROPART [4], and a joint INE-CEA/Grenoble ACTINET project [5], which was recently launched.

EXAFS Studies

Alkylated 2,6-ditriazinylpyridines (BTP, Fig. 1) have been developed at INE [6] as highly selective SANEX extractants. Their development is considered a major breakthrough in the challenging field of actinide(III)-lanthanide separation. Improved SANEX extractants such as $CyMe_4$-BTBP (see "New SANEX Extractants" below) are a continuation of this development. We use BTPs to study and elucidate the selectivity of N-donor SANEX extractants for trivalent actinides over the lanthanides.

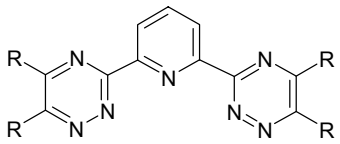

Fig. 1 Alkylated 2,6-ditriazinylpyridines (BTP).

In a report comparing uranium(III), lanthanum(III), and cerium(III) complexed with BTP, U(III)-N bonds were found significantly shorter than La(III)-N and Ce(III)-N bonds [7]. This was attributed to a more covalent character for actinide(III)-N bonds (and thus "stronger") than lanthanide(III)-N bonds and proposed to be an explanation for the observed selectivity. However, in contrast to Am(III) and Cm(III), U(III) is not of practical interest in the Partitioning & Transmutation strategy. Thus, we study the complexes that form with BTP and Am(III), Cm(III), and a lanthanide with a similar cation radius, europium(III), in organic solution.

In a previous EXAFS study [8], the structures of Cm(III) and Eu(III) complexed with 2,6-di(5,6-dipropyl-1,2,4-triazin-3-yl)pyridine (n-Pr-BTP) have been identified. The complexes were prepared by extracting the metal nitrates from nitrate solution, and L3 EXAFS spectra were recorded from the separated organic solution containing the metal complexes.

Three BTP molecules coordinate Cm(III) or Eu(III) via three N atoms each, to give the $[M(BTP)_3](NO_3)_3$ complexes (Fig. 2; nitrate ions are present for charge neutralization but not involved directly in coordination). Both metals have identical complex structures; identical metal ion-nitrogen bond lengths within experimental error are found for both Cm and Eu (Table 1). Quantum-chemical calculations performed at different levels of theory confirm the experimental results. These results do not support shorter actinide(III)-N bond lengths (and assumed associated higher bond

covalency) compared to lanthanide(III)-N bonds as the reason for the unique selectivities of N-donor SANEX ligands.

In a similar manner, Am(III) complexed with n-Pr-BTP is investigated at the INE-Beamline [9]. Again, a structure identical to those of $[Cm(BTP)_3](NO_3)_3$ and $[Eu(BTP)_3](NO_3)_3$ complexes (Table 1), without any significant differences in bond lengths is observed [10,11].

Sample	Shell	*N*	*R* [Å]
$Am(BTP)_3$	1	9	2.56 (0.01)
	2	18	3.42(0.02)
	3	18	4.79 (0.19)
	4	9	5.27 (0.21)
$Cm(BTP)_3$	1	9	2.568 (0.007)
	2	18	3.431 (0.009)
	3	18	4.81 (0.03)
	4	9	5.30 (0.04)
$Eu(BTP)_3$	1	9	2.559 (0.008)
	2	18	3.42 (0.01)
	3	18	4.82 (0.02)
	4	9	5.30 (0.03)

Table 1 Coordination numbers (*N*; held constant at the given value) and bond lengths (*R*) determined from four-shell fits to the L3 EXAFS of the BTP complexes studied [8,10,11].

We conclude that BTP's high selectivity for trivalent actinides over lanthanides is not structural in origin.

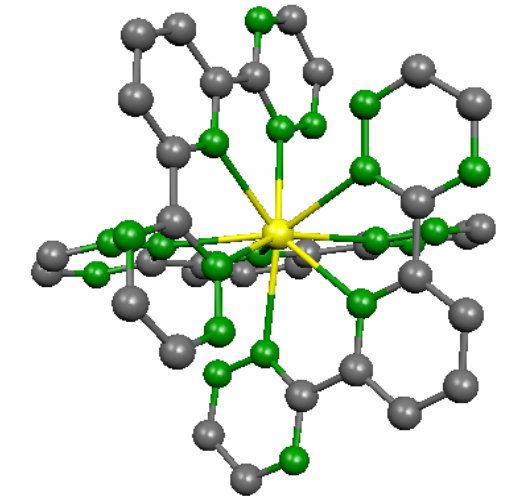

Fig. 2 Coordination structure of the $[M(III)(BTP)_3]^{3+}$ complexes. Yellow = M(III) (Am, Cm, or Eu); green = nitrogen; gray = carbon. Hydrogen atoms and alkyl moieties not shown.

Recently we measured Am and Eu complexed with $CyMe_4$-BTBP (cf. "New SANEX Extractants" below) in organic solution at the INE-Beamline. A preliminary evaluation of the Am complex EXAFS shows that two BTBP molecules coordinate the metal ion via four N atoms each. This is in accordance with the stoichiometry as determined by slope analysis (see below).

TRLFS Studies

The Cm and Eu complexes are also studied by TRLFS [8]. Cm(III) or Eu(III) are complexed with n-Pr-BTP in n-octanol, at varying ligand-to-metal ion concentrations ratios, [L]/[M], and their fluorescence emission (luminescence) spectra recorded.

In the case of Cm, the emission spectra do not change for 8 < [L]/[M] < 620, meaning that only one species is present in the [L]/[M] range studied. This is supported by the observation of the same emission spectra lifetimes throughout the [L]/[M] range. The single species present is the $[Cm(BTP)_3]^{3+}$ complex, as identified by EXAFS (cf. above).

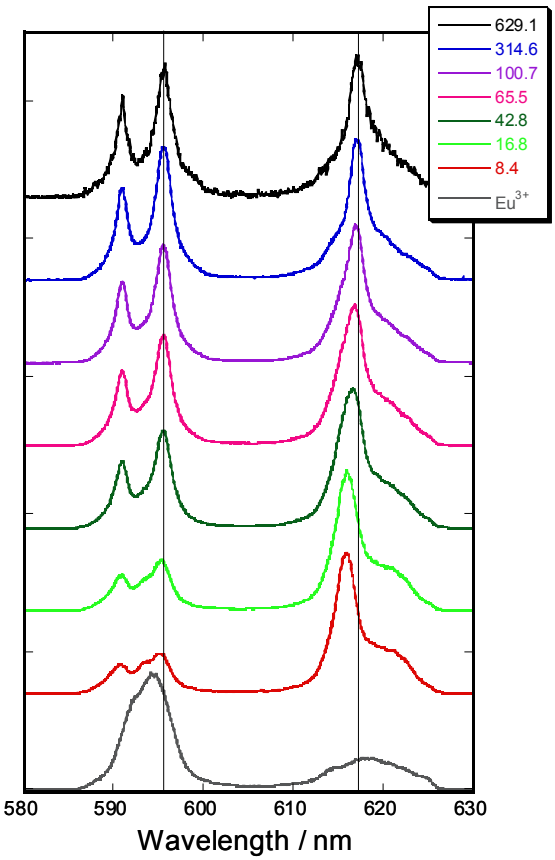

Fig. 3 Europium fluorescence spectra with varying [L]/[M] (given in the legend; [Eu(III)] = $1.2 \cdot 10^{-5}$ M) for complexation of Eu(III) with n-Pr-BTP in n-octanol.

In contrast, the Eu emission spectra change with varying [L]/[M], meaning that at least two species form (Fig. 3). The spectrum at high [L]/[M] corresponds to the $[Eu(BTP)_3]^{3+}$ complex identified by EXAFS. As determined from lifetime measurements, the spectrum at low [L]/[M] corresponds to the 1:1 complex, $[Eu(BTP)]^{3+}$. The 1:2 complex does not form.

This study shows that the $[Eu(BTP)_3]^{3+}$ complex, which is relevant for liquid-liquid extraction, forms only at higher [L]/[M] than the respective Cm complex, $[Cm(BTP)_3]^{3+}$. These differences in the formation of the $[M(BTP)_3]^{3+}$ complexes lies either in the kinetics of formation or in their stability constants and are in accordance with the trend of BTP's selectivity in liquid-liquid extraction.

New SANEX Extractants

Although many N-donor SANEX extracting agents have been synthesised and tested during previous EC projects, NEWPART [12] and PARTNEW [13], none of them fulfilled all process requirements, such as stability, reversibility of extraction, reasonably fast kinetics.

In search of improved extracting agents 6,6'-bis(5,5,8,8-tetramethyl-5,6,7,8-tetrahydro-benzo[1,2,4]triazin-3-yl)-[2,2']bipyridine ($CyMe_4$-BTBP, Fig. 4) has been synthesised at Reading University (UK),. Much of the assessment of its extraction performance has been performed at INE [14]. The most important results are given below.

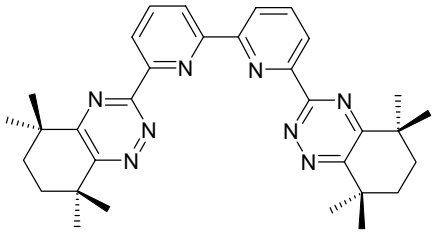

Fig. 4 6,6'-bis(5,5,8,8-tetramethyl-5,6,7,8-tetra-hydro-benzo[1,2,4]triazin-3-yl)-[2,2']bipyridine ($CyMe_4$-BTBP).

$CyMe_4$-BTBP extracts Am and Cm, e.g., from 1 M nitric acid, with high separation factors (SF) over Eu ($SF_{Am/Eu}$ = 120; Fig. 5). It is also possible to separate Am and Cm from all the lanthanides. $SF_{Am/lanthanide}$ values decrease from 1500 (lanthanum) to 50 (dysprosium), increasing again to 500 (lutetium), across the rare earth series. Stripping is thermodynamically possible with dilute nitric acid (Fig. 5).

From slope analysis of distribution data, extraction is identified to proceed by solvation of the metal nitrates, according to:

$$M^{3+} + 3\ NO_3^- + 2\ BTBP_{org} = M(NO_3)_3 \cdot 2BTBP_{org}$$

Process Development

Following the first successful spiked DIAMEX test in a HFM micro-plant [15], several improvements to the process flow-sheet have been tested.

Tests whether the acid scrubbing section can be omitted have been made. Omitting this section means that only three instead of four HFM would be required. However, the mass balances dramatically deteriorate in these tests, probably due to oxalate precipitation.

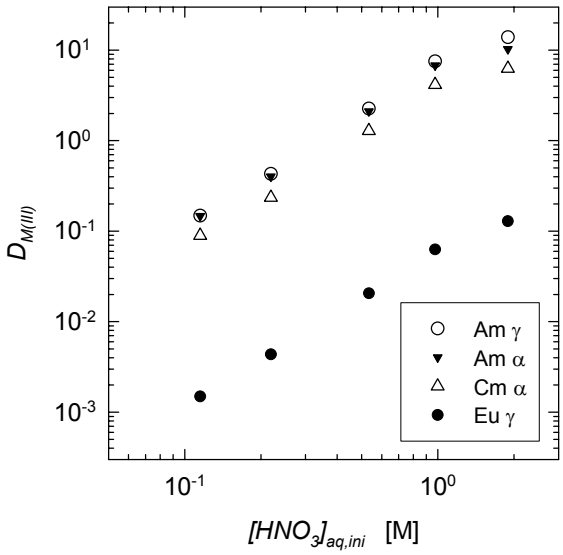

Fig. 5 Extraction of Am(III), Cm(III), and Eu(III) from HNO_3 into 10 mM $CyMe_4$-BTBP + 0.25 M N,N'-dimethyl-N,N'-dioctyl-2-(2-hexyloxy-ethyl)-malonamide in n-octanol, distribution ratios (*D*) as a function of initial nitric acid concentration.

Further flow-sheet modifications, as suggested by computer-code calculations, have been tested: Reducing the flow-rates, increasing the nitric acid concentration of the acid scrubbing solution, using a combined HFM for the fission product scrubbing and acid scrubbing sections, using a longer stripping HFM.

In the most recent spiked test, both Am and Cm are found to be extracted to ≥ 99.9% from a simulated PUREX raffinate. Back-extraction efficiency is 99.9%. Very low concentrations of non-lanthanide fission products are found in the product solution. The experimental results are in very good agreement with computer-code calculations.

The second HFM micro-plant to be used for hot tests (see Fig. 6) has been transferred to the ITU and three successful cold DIAMEX tests carried out in collaboration with ITU. Experimental results from the two micro-plants are in good agreement.

The final goal is to perform a hot DIAMEX-SANEX cycle in the HFM micro-plant, producing a pure Am-Cm product solution from a PUREX raffinate.

Fig. 6 The HFM micro-plant to be used for hot tests at ITU.

Conclusions

The research on minor actinide separation covers aspects from fundamental studies contributing to understanding the selectivites of N-donor extracting agents for trivalent actinides to process development.

For the first time, structural investigations on trivalent minor actinides (americium, curium) complexed with BTP are performed and compared with the respective europium complex. Although no structural differences as a possible explanation of BTP's selectivity are found, significant differences in the formation of the $[M(BTP)_3]^{3+}$ complexes are responsible for BTP's selectivity in liquid-liquid extraction.

Successful cold and spiked DIAMEX processes are performad in two HFM micro-plannt setups, one of them dedicated to future hot experiments. Both americium and curium are extracted to ≥ 99.9% from simulated PUREX raffinate.

Financial support from the Commission of the European Community is acknowledged (contract FI6W-CT-2003-508854).

References

[1] J. Magill, V. Berthou, D. Haas, J. Galy, R. Schenkel, H.-W. Wiese, G. Heusener, Nucl. Energy 2003, 42 (5), 263-277.

[2] Actinide and fission product partitioning and transmutation, status and assessment report. OECD-NEA (1999).

[3] A. Geist, M. Weigl, K. Gompper, Radiochim. Acta 2005, 93, 197-202.

[4] "EUROpean research programme for the PARTitioning of minor actinides from high active wastes issuing the reprocessing of spent nuclear fuels" (contract no. FI6W-CT-2003-508854).

[5] "Performance and coordination structure of N-donor extracting agents for partitioning of trivalent actinides from lanthanides".

[6] Z. Kolarik, U. Müllich, F. Gassner, Solvent Extr. Ion Exch. 1999, 17 (5), 1155-1170.

[7] J.-C. Berthet, Y. Miquel, P.B. Iveson, M. Nierlich, P. Thuéry, C. Madic, M. Ephritikhine, Dalton Trans. 2002, 3265-3272.

[8] M.A. Denecke, A. Rossberg, P.J. Panak, M. Weigl, B. Schimmelpfennig, A. Geist, Inorg. Chem. 2005, 44 (23), 8418-8425.

[9] M.A. Denecke, J. Rothe, K. Dardenne, T. Fanghänel, H. Blank, H. Modrow, J. Hormes, Physika Scripta 2005, T115, 1001–1003.

[10] M.A. Denecke, A. Geist, M. Weigl, P.J. Panak, B. Schimmelpfennig, ANKA Annual Report 2005, S. 86-87. Forschungszentrum Karlsruhe GmbH.

[11] A. Geist, M.A. Denecke, P.J. Panak, M. Weigl, B. Schimmelpfennig, K. Gompper, Nachrichten – Forschungszentrum Karlsruhe 2005, 37 (4), 191-196.

[12] C. Madic, M.J. Hudson, J.-O. Liljenzin, J.-P. Glatz, R. Nannicini, A. Facchini, Z. Kolarik, R. Odoj, New partitioning techniques for minor actinides. EUR 19149 (2000).

[13] C. Madic, F. Testard, M.J. Hudson, J.-O. Liljenzin, B. Christiansen, M. Ferrando, A. Facchini, A. Geist, G. Modolo, A. Gonzales-Espartero, J. De Mendoza, PARTNEW – new solvent extraction processes for minor actinides. CEA-R-6066 (2004).

[14] A. Geist, C. Hill, G. Modolo, M.R.S. Foreman, M. Weigl, K. Gompper, M.J. Hudson, C. Madic, (submitted).

[15] A. Geist, M. Weigl, K. Gompper, A continuous DIAMEX process in a hollow fibre module micro-plant. Proc. Internat. Solvent Extraction Conf. (ISEC 2005), Beijing, China, September 19-23, 2005, 659-664.

8. Vitrification of High-level radioactive liquid waste

8.1 Commissioning of Process Systems of VEK

W. Grünewald, J. Knobloch, W. Metzger, W. Tobie, G. Roth, K.H. Weiß, H. Braun, S. Weisenburger

Forschungszentrum Karlsruhe, Institut für Nukleare Entsorgung (INE), P.O.Box 3640, 76021 Karlsruhe

J. Fleisch, M. Weishaupt

Wiederaufarbeitungsanlage Karlsruhe (WAK), VEK-Projekt Hermann-von-Helmholtz-Platz 1, 76344 Eggenstein-Leopoldshafen

Abstract

The high level liquid waste vitrification plant VEK (Verglasungseinrichtung Karlsruhe) located at the site of Forschungszentrum Karlsruhe is now in the commissioning phase. Hot operation of the facility is scheduled for late 2006. In 2005 the Institut für Nukleare Entsorgung (INE) of Forschungszentrum Karlsruhe has been involved in functional test of major process systems. The basis of the tests has been detailed functional test programs and test instructions for each system in the years 2003/2005 and supplied by the VEK-management to the experts of the licensing authority for approval. In the following the work done in 2005 by INE is described and an outlook is given for further commissioning in 2006. It includes a short description of the planned cold test operation of VEK by which HLLW simulant will be vitrified and approximately 27 glass canisters produced.

Introduction

Towards the end of the year 2006 the high-level liquid waste vitrification plant VEK located at the site of Forschungszentrum Karlsruhe is scheduled to be put into radioactive operation [1]. The process technology of the facility is based on the liquid fed ceramic-lined waste glass melter (LFCM). It has been developed during the last three decades by the Institut für Nukleare Entsorgung (INE) of FZK [2,3] and first time applied at the PAMELA plant in Mol/Belgium at the former EUROCHEMIC site [4]. By the LFCM technique the high level liquid waste (HLLW) is continuously fed into the melter. On top of the molten glass pool a cold cap is formed. It consists of a layer of evaporating liquid and below a layer of dried/calcined material which contacts the molten glass pool being at temperatures of 1150-1200°C. When the material in the lower area of the cold cap achieves 700°C the glass formers begin to react with the waste oxides, and with increasing temperature the waste glass is formed.

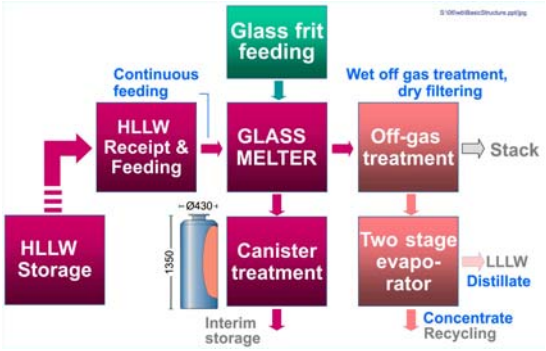

Fig. 1: Simplified flow sheet of the vitrification plant

A very simplified scheme of the process is given in Fig. 1. Basically the process consists of a receipt system for HLLW, a melter feeding system for glass formers and HLLW, a glass melting system, a melter offgas cleaning system and a glass canister handling area in which glass canister cooling, canister lid welding and canister decontamination takes place.

The VEK-project has been started in 1996. Construction and major installations of the plant took place from 1999 until 2004. In 2005 the focus has been directed to the commissioning of the entire plant including the start of the functional tests of the process systems. An outside view of the process building is given in Fig. 2.

In early 2005 INE overtook from VEK-management the task to lead and perform the portion of the VEK commissioning work related to the process systems. The work carried out so far in 2005 will be the subject of the following description. The several systems of VEK including the process systems are given in table 1. The systems INE is involved in commissioning are

indicated on the right column of this table. The major process systems cover the HAWC receipt system, the vitrification system, and melter offgas treatment. Other process systems comprise the can handling system, the MLLW evaporation, the plant ventilation, the tank ventilation, electrotechnical equipment, water supplies, as well as the system for pressurized air, steam and supply of chemicals.

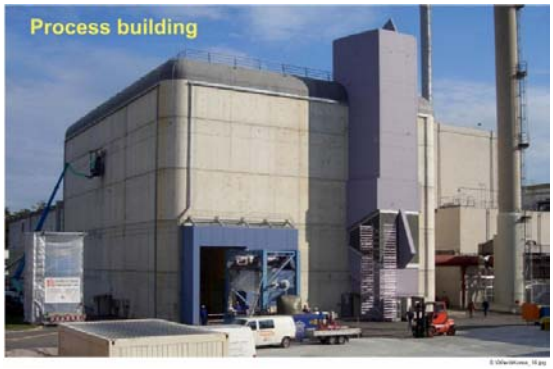

Fig. 2: Outside view of the VEK process building

Table 1: Systems of VEK facility

Code	System	Commissioning with INE involvement
800	Vitrification plant	
810	Outdoor facilities	
820	Process building	
840	Process systems	
841	HAWC receipt system	•
842	Vitrification system	•
843	Can handling system	•
844	Can buffer store	
845	MLLW evaporation	•
847	Tank ventilation system	•
848	Melter offgas treatment wet	•
849	Melter offgas treatment dry	•
850	Auxiliary systems	
851	Plant ventilation	
852	Electrotechnical equipment	
853	Fresh water supply	•
854	Cooling-/Cold water	•
856	Pressurized air system	•
857	Steam/Condensate system	•
859	Supply of chemicals	•
866	Sampling system	•
871	Mobile radiation protection	
872	Fixed radiation protection	
873	Fire protection	
876	Process control system	
879	Plant security equipment	
882	Collection of secondary liquid waste	•
884	Solid waste management	
885	Glass can lock and transport	

Commissioning of the process systems

The commissioning of the process systems as indicated in table 1 comprises the following main steps for each system:

- Function tests of its single items
  (mechanical valves, control valves, air pressure reducer etc.)
- Function tests of its components
  (e.g. for the vitrification system 842 the function tests of the feeding vessel, the glass frit feeding device, the melter, and the mean frequency generator)
- Start up programs for selected systems
  (receipt system 841, vitrification system 842, offgas system 848/849)
- Final test during cold test operation
  (while VEK is vitrifying HLLW simulant)

Function tests of single items of a system

In 2005 function tests of the single items of each of the process systems have been performed by or under the lead of INE. The results have been documented in function test check protocols. As for example for the vitrification system 842 the tests of single items included hand- and pneumatically operated valves, magnetic valves, hand- and pneumatically operated control valves, and reducers for pressurized air. All systems of the VEK vitrification plant together possess nearly 2000 such single items. Most of them are installed in the valve galleries.

Function tests of system components

For the function test of each system an approved functional test instruction program has been used. Within these programs the steps of the tests to be carried out are described in detail for each component. It describes the aims of the tests, the pre-conditions, the test basis, the test means and finally the detailed instructions for performing the test.

Function tests of components of the systems have been one of the major work in 2005. They included components of the core systems of the VEK plant (e.g. receipt tanks, feeding vessel, dust scrubber, condenser, jet scrubber, NO_X-column), but not yet the melter.

The feeding vessel of the vitrification system 842 is representative of these types of components which had been tested in 2005. Its function test can be taken as fairly typical for the others. The functional test instruction of the feeding vessel covered the following in detail:

- Establishing the volume vs. level curve of the feeding vessel
- Testing of the homogenisation device of the vessel
- Testing of devices for level/density measurements including tests of the limits (e.g. warnings high/low)
- Checking of the procedure to empty the vessel

- Measurement of feed rate curve of feeding air lift
- Testing of temperature measurement devices
- Testing of deco-equipment of the vessel

The tests have been carried out with water as the liquid and documented in check protocols. The function tests of the HLLW receipt tanks included additionally the test of the two-stage airlift systems (performing batch transfers of HLLW into the feeding vessel), and the test of the water cooling system of each receipt tank. The function tests of components of the offgas line included additionally the tests of the circulation of the scrub solutions.

The function test of the glass frit feeding device as a key equipment of the vitrification system 842 has also been carried out in 2005. A major focus was the check whether the glass frit feeding device works reliable via the process control system 876 of VEK. The simplified scheme of the glass frit feeding device is shown in Fig. 3. Its task is to transfer glass frit batchwise into the melter. A batch transfer is started when the pregiven lower level in the feeding vessel is achieved due to continuous feeding of HLLW from the feeding vessel into the melter by the feeding airlift. The lower level signal generated by the feeding vessel activates both, the HLLW batch transfer from receipt tank to feeding vessel by the two-stage airlift system, and the glass frit feeding device to start another glass frit batch transfer cycle. The function tests of the glass frit feeding device included the check of the following automatic steps of the control chain:

1. Opening of the pneumatically operated air lock 5 and then air lock 4 to transfer the glass frit present in the transfer vessel into the melter by gravity and closing of the air lock 4 first and then air lock 5.
2. Switch on of conveyer chute for continuous transfer of glass frit from bunker into weighing vessel 1 and switch it off when target weight of glass frit has achieved in weighing vessel 1
3. Opening of pneumatically operated lock valve 1 that the glass frit from weighing vessel 1 falls by gravity into weighing vessel 2 and closing of lock valve 1
4. Control weighing of the frit in weighing vessel 2 (weight difference to weighing vessel 1 must be less than a pregiven value)
5. Opening of pneumatically operated lock valve 3 and then lock valve 2 that the glass falls by gravity into transfer vessel and closing of lock valve 2 and then lock valve 3.
6. Automatic stop of the cycle

To assure the correct function of the glass frit feeding device is of particular importance because the waste glass loading and thus other melt- and quality properties of the glass are directly related to the correct function of the glass frit feeding system.

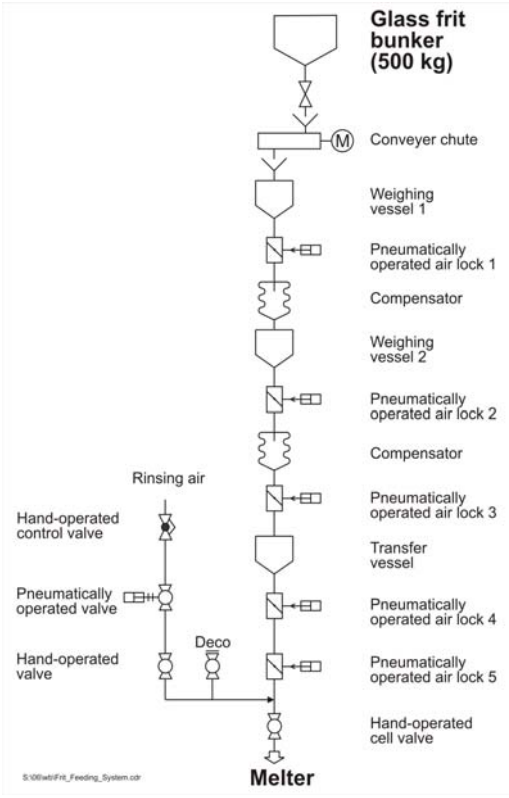

Fig. 3: Simplified scheme of glass frit feeding device

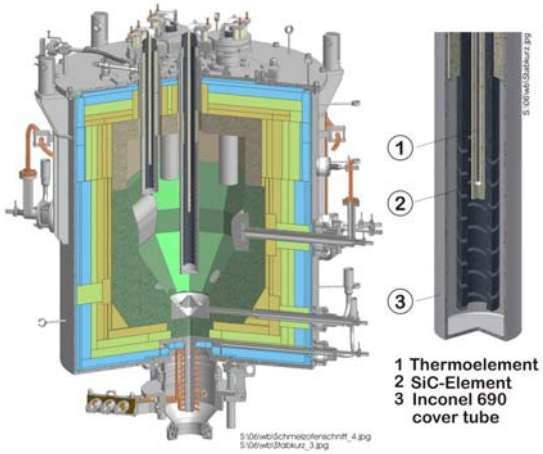

Fig. 4: Heating up of the internal melter structure by an external heat source (five SiC-heating elements encased in INCONEL 690 protection tubes including a thermocouple)

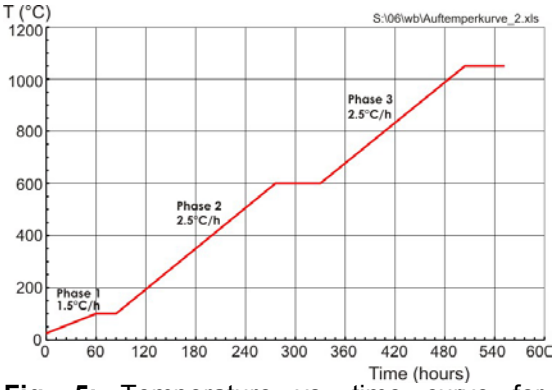

Fig. 5: Temperature vs. time curve for heating up of the inner melter structure

The functional test of the waste glass melter is foreseen in 2006. It requires a special program starting with the heat up of the internal melter structure by an external heat source. The melter needs a special function test program because most key functions of it are associated with the presence of molten glass in the glass tank. Because glass is an electrical insulating material at ambient temperature, the empty melt tank must be first heated to temperatures of approximately 1000°C. A typical heating up vs. time curve of the melter is shown in Fig. 5. Then start glass must be filled into the melter. At increasing temperatures of the start glass above 800°C the start glass becomes gradually el. conductive and thus suitable for Joule-heating. Heating up is done by SiC-heating elements encased in INCONEL 690 protecting tubes. They are placed inside the melter as illustrated in Fig. 4. Heating up is performed slowly in order to avoid undesired thermally induced stresses inside the thick-walled ceramic refractories of the glass tank. When the temperatures of the melter interior have reached about 1000°C, the heating devices are removed from the melter and start glass is batchwise put into the glass tank via the glass frit feeding system, every hour about 10-30 kg. When the Joule heating can be applied the temperature in the melter is adjusted to about 900°C.

Key functions of the melter include, besides glass heating by releasing Joule-heat between the power electrodes, also glass pouring, glass level detection and maintaining several mbars underpressure in the melter at a reasonable low air-inleakage rate of about 10-20 Nm^3/h. These last three functions are tested during the starting up program of selected systems.

Starting up program of selected systems

Whereas the majority of the process systems require successful functional tests only to be ready for cold test operation, the core process systems need another additional step of commissioning, i.e. a starting up program.

Within the starting up program all components of a system are operated simultaneously. Thus the correct operational interactions between components are checked. In particular the correct communication of them with the central VEK process control system must be demonstrated. The starting up programs will be carried out in 2006. The detailed descriptions of the starting up programs have been prepared by INE in the years 2004/2005. The systems which are to pass a starting up program are the HAWC-receipt system 841, the vitrification system 842, and the melter offgas cleaning systems 848/849.

HLLW receipt system 841

The starting up program for the HLLW receipt system 841 includes:

- Filling of the receipt tanks with demineralised water
- Start up of the water cooling circuit, the agitation air, and the level measurement devices
- Testing of overtaking evaporator concentrate from evaporator system 845 (i.e. demineralized water from concentrate tank of the evaporator system)
- Sampling tests using sampling system 866
- Finally functional coupling of the receipt system 841 (i.e. the two-stage airlift system) with the vitrification system 842 (i.e. to the feeding vessel and to the glass frit feeding device)

Vitrification system 842

The starting up program for the vitrification system includes particularly demonstration of key functions of the melter as described before. Regarding glass heating, the el. power data are monitored and compared with the design data. As to test the glass pouring, the glass pool must be heated to approximately 1150°C under the condition of continuous water feeding and batchwise feeding of start glass into the melter via the water-cooled feed- and glass frit inlet tube. These pouring tests are carried out in connection with phase 3 of the start up program for the melter offgas system (see below). By feeding of water and start glass into the melter and adjustment of the water flow rate a “cold cap” of evaporating water and melting start glass is formed across the major surface of the glass pool. It keeps the temperature of the melter plenum and thus the upper melter structure below the desired

range of about 500°C. Start glass feeding into the melter via the glass frit feeding system serves also for replacing the glass mass poured for testing. Tests of the glass pouring system uses start glass melt because its viscosity vs. temperature curve is similar to the waste glass product and thus suitable for this purpose. The normal glass frit is not suitable because its viscosity is too high.

Melter offgas system 848/849

The starting up program to be carried out for the melter offgas system 848/849 is divided into three phases. Before, all components of the offgas system 848/849 are first prepared to be ready for operation. This includes for the wet offgas line 848 filling of the components with demineralised water, set up the valves associated with the components to the right position, and filling of the circulation pumps of the jet scrubber and NO_X-Absorber with demineralised water. Additionally preparation of the dust scrubber entrance with a variable free cross section device is carried out. For the dry offgas line 849 the preparation includes selection of one of the parallel filter lines to be used, selection of the offgas blower to be used (1 of 3), set up of valves to the right position and preparation of the el. circuits for the offgas heaters. Afterwards the three phases of the start up program are carried out.

- Phase 1
  In phase 1 the offgas blower is put into operation and the air flow rate through the offgas system is adjusted to approximately 40 Nm^3/h. The further steps include to put the offgas heaters in the dry offgas line as well as the gas cooler before the blower into operation. The scrub solution circuits of the dust scrubber, jet scrubber and NO_X-columns are started up followed by adjustment to the parameters gained as preliminary values from former functional test program. Further tests in phase 1 include the switch from the dry filter line to the parallel one. Also switch of the circulation pumps in the wet offgas system to the redundant ones are carried out.
- Phase 2
  In phase 2 the offgas system is connected to the melter via the offgas pipe melter-dust scrubber. In this phase the glass melter is kept at idling conditions, i.e. the glass pool is at about 900°C. Adjustment of the offgas blower to an underpressure in the melter of ≤ 2 mbars is done followed by monitoring and documentation of the operational parameters of each component and the pressure drop across the entire offgas line. Furthermore switching of the circulation pumps for the jet scrubber and NO_X-absorber scrub solution circuits and of the dry filter line to the parallel one are performed again under particular monitoring of the melter underpressure.
- Phase 3
  In phase 3 the offgas system will be operated under conditions of melter feeding with demineralised water and start glass to allow the key function tests of the melter as outlined above. Under these conditions and heating up the pool to 1150°C all tests of phase 2 are repeated under particular observation of the underpressure in the melter. The complete data set will be documented and used as preliminary operation parameters for the later cold test operation.

Cold test operation

Objective of cold test operation foreseen for the second half of 2006 is to show the correct function of the entire plant and its systems under normal operation conditions. For the cold test operation, 15 m^3 of HLLW simulant will be vitrified and the resulting simulated waste glass poured into 27 stainless steel canisters each having a glass capacity of 400 kg. The chemical composition of the HLLW simulant is given in table 2 and compared with that of the radioactive HLLW. During cold test operation sampling will take place according to the analytical plan worked out for the hot operation. Also the canister lid welding and the entire canister handling will be demonstrated.

The chemical composition of the HLLW simulant will be as similar as possible to that of the radioactive HLLW. Radioactive samples have recently been taken from the HLLW storage tanks and analysed. Only the noble metals ruthenium, rhodium and palladium as well as the actinides and technetium will be replaced by other elements. The continuous cold test operation will last about 68 days. Operation will take place in a manner similar to the later hot operation. It includes to establish a control area and operation of the plant according to the operation manual for each system. The operation manuals for the major process systems 841, 842 and 848 have been worked out by INE in the years 2004/05 and supplied by the VEK-management to the expert organisation TÜV for approval.

The HLLW-simulant will be procured from company VWR International/Leuven, Belgium. It will be delivered in batches of several m^3 by tank track. By special tanks

with a capacity of about 1 m^3 the HLLW-simulant will be transferred into the receipt tanks 841 BB 01 and 841 BB 02 of the HLLW receipt system through the chemical supply system 859 of VEK.

Table 2: Chemical composition of the HLLW-simulant in terms of oxide residue compared to the HLLW

1.8.2005	Radioactive HLLW			HLLW-Simulant		
Oxide residue	Element	Oxide		Element	Oxide	
	g/l	g/l	Wt.%	g/l	g/l	Wt.%
SeO2	0,09	0,13	0,11	0,09	0,13	0,11
Rb2O	0,42	0,46	0,38	0,42	0,46	0,38
SrO	1,11	1,32	1,09	1,11	1,32	1,09
Y2O3	0,82	1,04	0,86	0,82	1,04	0,86
ZrO2	4,01	5,41	4,48	4,01	5,42	4,48
MoO3	4,38	6,57	5,44	4,38	6,57	5,44
TcO2	1,11	1,65	1,36	–	– [1]	– [1]
RuO2	3,82	5,03	4,16	–	– [2]	– [2]
Rh2O3	0,89	1,09	0,90	–	– [3]	– [3]
PdO	2,00	2,30	1,91	–	– [4]	– [4]
Ag2O	0,20	0,21	0,17	0,20	0,21	0,17
CdO	0,12	0,14	0,11	0,12	0,14	0,11
SnO2	0,09	0,12	0,10	0,09	0,12	0,10
Sb2O3	0,02	0,02	0,02	0,02	0,02	0,02
TeO2	0,80	1,00	0,82	0,80	1,00	0,82
Cs2O	3,57	3,79	3,13	3,57	3,79	3,13
BaO	3,41	3,80	3,15	3,41	3,81	3,15
La2O3	2,32	2,72	2,25	11,88	13,93	11,52
CeO2	4,38	5,38	4,45	4,38	5,38	4,45
Pr2O3	2,04	2,38	1,97	2,04	2,38	1,97
Nd2O3	7,23	8,44	6,98	7,24	8,44	6,98
Pm2O3	0,00	0,01	0,00	0,00	0,01	0,00
Sm2O3	1,58	1,83	1,52	1,58	1,83	1,52
Eu2O3	0,20	0,23	0,19	0,20	0,23	0,19
Gd2O3	0,61	0,70	0,58	0,61	0,70	0,58
UO2	8,21	9,68	8,01	–	– [5]	– [5]
Np2O3	0,54	0,60	0,49	–	– [6]	– [6]
PuO2	0,25	0,29	0,24	–	– [7]	– [7]
Am2O3	0,56	0,61	0,51	–	– [8]	– [8]
CmO2	0,02	0,03	0,02	–	– [9]	– [9]
Cr2O3	2,03	2,96	2,45	2,03	2,96	2,45
MnO2	0,32	0,50	0,42	4,54	7,18	5,94
Fe2O3	7,63	10,90	9,02	7,63	10,91	9,02
CoO	–	–	–	0,86	1,09	0,90
NiO	1,58	2,02	1,67	3,39	4,32	3,57
CuO	0,03	0,04	0,03	0,03	0,04	0,03
ZnO	0,02	0,03	0,02	0,02	0,03	0,02
PbO	0,01	0,01	0,01	0,01	0,01	0,01
Na2O	24,08	32,45	26,85	24,08	32,46	26,85
MgO	0,59	0,98	0,81	0,59	0,98	0,81
Al2O3	0,08	0,16	0,13	0,08	0,16	0,13
K2O	0,31	0,38	0,31	0,31	0,38	0,31
CaO	0,51	0,71	0,59	0,51	0,71	0,59
F	0,07	0,07	0,06	0,07	0,07	0,06
Cl	0,05	0,05	0,04	–	–	–
P2O5	1,15	2,63	2,17	1,15	2,63	2,17
Sum		120,85	100,0		120,89	100,0
Density g/cm^3				1.20-1.30	–	–
HNO_3 mol/l				2.5	–	–

L:\HAWC-Simulat\Kalttestbetrieb VEK_DaSa(LÜA050801)INE1.xls\Tabelle7(3)

1) TcO_2 replaced by MnO_2
2) RuO_2 replaced by MnO_2
3) Rh2O3 replaced by CoO
4) PdO replaced by NiO
5) UO_2 replaced by La_2O_3
6) Np_2O_3 replaced by La_2O_3
7) PuO_2 replaced by La_2O_3
8) Am_2O_3 replaced by La_2O_3
9) CmO_2 replaced by La_2O_3

Outlook

After successful demonstration of the process systems by cold test operation commissioning of the process systems will be continued within the final step, i.e. the hot test. During the hot test approximately 2 m^3 diluted HLLW will be vitrified consisting of a mix of HLLW simulant as used in the cold test operation, and about 1 Vol.% of actual HLLW.

The hot test operation of the process systems will be of particular importance before the plant will be put into active operation. During active operation the plant will vitrify the HLLW stored at the site and producing approximately 130 glass canisters (430 mm in dia, 1335 mm height, appr. 400 kg glass each) for intermediate storage and later final disposal.

References

[1] G. Roth, S. Weisenburger, J. Fleisch, M. Weishaupt, Proceeding of GLOBAL 2005, Tsukuba, Japan, Oct 9-13, 2005, Paper No. 296

[2] S. Weisenburger, IEEE Transaction on Industry Application, Vol. IA-18, No. 1, Jan/Febr. 1982, 73-82

[3] G. Roth, S. Weisenburger, Verglasungstechnologie des Forschungs-zentrums Karlsruhe für hochradioaktive flüssige Abfälle, in Radioaktivität und Kernenergie, Forschungszentrum Karlsruhe, 103-116 (2001), ISBN 3-92-3704-26-7

[4] G. Höhlein, E. Tittmann, S. Weisenburger, H. Wiese, Waste Management' 86, Vol. 2, Tucson AZ (USA), University of Arizona, 1986, 413-420

9. List of Publications

Papers in Peer Reviewed Journals

ABBASI, A.; LINQUIST-REIS, P.; ERIKSSON, L.; SANDSTRÖM, D.; LIDIN, S.; PERSSON, I. SANDSTRÖM, M.;
Highly hydrated cations: Deficiency, mobility, and coordination of water in crystalline nonahydrated scandium(III), yttrium(III), and lanthanoid(III) trifluoromethanesulfonates.
Chemistry - a European Journal, 11(2005), 4065-77

ALONSO, U.; MISSANA, T.; GECKEIS, H.; GARCIA-GUTIERREZ, M.; TURRERO, M.J.; MÖRI, A.; SCHÄFER, TH.; PATELLI, A.; RIGATO, V.;
Role of inorganic colloids generated in a high-level deep geological repository for the migration of radionuclides: Open questions
Journal of Iberian Geology, 32 (2005), 79-94

ALTMAIER, M.; NECK, V.; MÜLLER, R.; FANGHÄNEL, T.;
Solubility of $ThO_2.xH_2O$(am) in carbonate solution and the formation of
ternary Th(IV) hydroxide-carbonate complexes.
Radiochimica Acta, 93(2005), 83-92

BAMBAUER, H.U.; BERNOTAT, W.; BREIT, U.; KROLL, H.;
Perthitic alkali feldspar as indicator mineral in the Central Swiss Alps. Dip and extension of the surface of the microcline/sanidine transition isograd.
European Journal of Mineralogy, 17(2005), 69-80

BAUER,A.; RABUNG,T.: CLARET,F.; SCHÄFER,T.; BUCKAU,G.; FANGHÄNEL,T.;
Influence of temperature on sorption of europium onto smectite: The role of organic contaminants
Applied clay science 30 (2005), 1-10

BRADBURY, M.H.; BAEYENS B.; GECKEIS, H.; RABUNG, T.;
Sorption of Eu(III)/Cm(III) on Ca- montmorillonite and Na-illite, Part 2: Surface complexation modeling,
Geochimica et Cosmochimica Acta., 69, 2005, 5403-5412

CHO, H.; WALTHER, C.; ROTHE, J.; NECK, V.; DENECKE, M.A.; DARDENNE, K.; FANGHÄNEL, T.;
Combined LIBD and XAFS investigation of the formation and structure of Zr(IV) colloids.
Analytical and Bioanalytical Chemistry 383 (2005), 28-40

CLARET, F.; SCHÄFER, T.; RABUNG, T.; WOLF, M.; BAUER, A.; BUCKAU, G.
Differences in properties and Cm(III) complexation behavior of isolated humic and fulvic acid derived from Opalinus clay and Callovo-Oxfordian argillite.
Applied Geochemistry, 20 (2005), 1158-68

DEGUELDRE, C.; DARDENNE, K.;
Analysis of zirconia films by grazing incidence X-ray absorption fine structure spectroscopy.
Nuclear Instruments and Methods B, 238 (2005), 323-28

DENECKE, M. A.; BOSBACH, D.; DARDENNE, K.; LINDVIST-REIS, P.; ROTHE, J.; YIN, R.;
Polarization Dependent Grazing Inzidence XAFS Measurements of Uranyl Cation Sorption onto Mineral Surfaces
Physika Scripta, T115 (2005), 877-881,

DENECKE, M. A.; DARDENNE, K.; MARQUARDT, C. M.;
Np(IV)/Np(V) valence determinations from Np L3 edge XANES/EXAFS
Talanta, 65(4) (2005), 1008-1014

DENECKE, M.A.; JANSSENS, K.; PROOST, K.; ROTHE, J.; NOSECK, U.;
Confocal micrometer-scale X-ray fluorescence and X-ray absorption fine structure studies of uranium speciation in a tertiary sediment from a waste disposal natural analogue site.
Environmental Science and Technology, 39 (2005), 2049-58

DENECKE, M. A.; ROSSBERG, A.; PANAK, P.J.; WEIGL, M.; SCHIMMELPFENNIG, B.; GEIST, A.;
Characterization and Comparison of Cm(III) and Eu(III) Complexed with 2,6-Di(5,6-dipropyl-1,2,4-triazin-3-yl)pyridine Using EXAFS, TRFLS, and Quantum-Chemical Methods
Inorganic Chemistry, 44(23) (2005), 8418-8425

DENECKE, M. A.; ROTHE, J.; DARDENNE, K.; BLANK, H.; HORMES, J.;
The INE Beamline for Actinide Research at ANKA
Physica Scripta, T115 (2005), 1001-1003

FROMAGER, E.; VALLET, V.; SCHIMMELPFENNIG, B.; MACAK, P.; PRIVALOV, T.; WAHLGREN, U.;
Spin-Orbit Effects in Electron Transfer in Neptunyl(VI)-Neptunyl(V) Complexes in Solution
Journal of Physical Chemistry A, 109 (2005), 4957-4960

FOREMAN, M.R.S.; HUDSON, M.J.; GEIST, A.; MADIC, C.; WEIGL, M.;
An Investigation into the Extraction of Americium(III), Lanthanides and D-Block Metals by 6,6'-Bis-(5,6-dipentyl-[1,2,4]triazin-3-yl)-[2,2']bipyridinyl (C5-BTBP)
Solvent Extraction and Ion Exchange, 23(5) (2005), 645-662

GAILLARD, C.; BILLARD, I.; CHAUMONT, C.; MEKKI, S.; QUADI, A.; DENECKE, M.A.; et al.
Europium (III) and its halides in anhydrous room temperature imidazolium based Ionic liquids
Inorganic Chemistry, 44 (2005), 8355-8367

GEIST, A.; WEIGL, M.; GOMPPER, K.;
Small-scale Actinide(III) Partitioning Processes in Miniature Hollow Fibre Modules
Radiochimica Acta, 93 (2005), 197-202

GLAUS, M.A.; BAEYENS, B.; LAUBER, M.; RABUNG, T.; VAN LOON, L.R.;
Influence of water-extractable organic matter from Opalinus Clay on the sorption and speciation of Ni(II), Eu(III) and Th(IV).
Applied Geochemistry, 20 (2005), 443-51

GREATHOUSE,J.; STELLALEVINSOHN, H.; DENECKE, M.A.; BAUER, A.; PABALAN, R.;
Uranyl surface complexes in an mixed-charge montmorillonite
Clays and Clay minerals, 53(3) (2005), 278-286

HANSEN, K.; HERLERT, A.; SCHWEIKHARD, L.; VOGEL, M.; WALTHER, C.;
The dissociation energy of V_{13}+ and the consequences for radiative cooling.
European Physical Journal D, 34 (2005), 67-71

KELM, M.; BOHNERT, E.;
Gamma radiolysis of NaCl brine: Effect of dissolved radiolysis gases on the radiolytic yield of long-lived products
Journal of Nuclear Materials, 346 (2005), 1 - 4

KIM, M.A.; PANAK, P.J.; YUN, J.I.; PRIEMYSHEV, A.; KIM, J.I.;
Interaction of actinides(III) with aluminosilicate colloids in 'statu nascendi'. Part III. Colloid formation from monosilanol and polysilanol.
Colloids and Surfaces A, 254(2005) S.137-45

KÖHLER, S.J.; BOSBACH, D.; OELKERS, E.H.;
Do clay mineral dissolution rates reach steady state?
Geochimica et Cosmochimica Acta, 69 (2005), 1997-2006

KRETZSCHMAR, R.; SCHÄFER, T., 2005.
Metal retention and transport on colloidal particles in the environment.
Elements, 1(4) (2005), 205-210.

KUNZE, S.;
Entwicklung von Fußbodenbeschichtungen und -belägen seit den Anfängen der Kerntechnik
Atomwirtschaft (ATW), 50 (2005), 260-262

LANTENOIS,S.; LANSON, B.; MULLER, F.; BAUER, A.; JULLIEN, M.; PLANÇON, A.;
Experimental study of smectite interaction with metal Fe at low temperature:1. Smectite destabilization
Clays and Clay Minerals, 53(6) (2005), 597-612

LÉON, A.; SCHILD, D.; FICHTNER, M.;
Chemical state of Ti in sodium alanate doped with $TiCl_3$ using X-ray photoelectron spectroscopy.
J. Alloys Compd., 404-406 (2005), 766-770

LEHMANN, J.; LIANG, B.Q.; SOLOMON, D.; LEROTIC, M.; LUIZAO, F.; KINYANGI, J.; SCHÄFER, T.; WIRICK, S.; JACOBSEN, C.;
Near-edge X-ray absorption fine structure (NEXAFS) spectroscopy for mapping nano-scale distribution of organic carbon forms in soil: Application to black carbon particles.
Global Geochemical Cycles, 19 (2005), GB1013

LINDQUIST-REIS, P.; KLENZE, R.; SCHUBERT, G.; FANGHÄNEL, T.;
Hydration of Cm^{3+} in aqueous solution from 20 to 2000 ^{o}C. A time-resolved laser fluorescence spectroscopy study.
Journal of Physical Chemistry B, 109 (2005), 3077-83

LOIDA, A.; METZ, V.; KIENZLER, B.; GECKEIS,H.;
Radionuclide release from high burnup spent fuel during corrosion in salt brine in the presence of hydrogen overpressure
Journal of Nuclear Materials, 346 (2005), 24-31

LÜTZENKIRCHEN, J.;
On derivatives of surface charge curves of minerals
Journal of Colloids and Interfaces Sciences, 290 (2005), 489-497

MACAK, P.; FROMAGER, E.; PRIVALOV, T.; SCHIMMELPFENNIG, B.; GRENTHE, I.; WAHLGREN, U.;
Electron Transfer in Neptunyl(VI)-Neptunyl(V) Complexes in Solution.
Journal of Physical Chemistry A, 109 (2005), 4950-56

MAY, A.J.; VALEEV, E.; POLLY, R.; MANBY, F.R.;
Analysis of the errors in explicitly correlated electronic structure theory.
Physical Chemistry and Chemical Physics, 7 (2005), 2710-13

METZ, V.; AMRAM, K.; GANOR, J.;
Stoichiometry of smectite dissolution reaction
Geochimica Cosmochimica Acta, 69 (2005), 1755-1772

METZ V.; RAANAN H.; PIEPER H.; BOSBACH D.; GANOR J.;
Towards the establishment of a reliable proxy for the reactive surface area of smectite.
Geochimica et Cosmochimica Acta, 69 (2005), 2581-2591

PANAK, P.J.; KIM, M.A.; KLENZE, R.; KIM, J.I.; FANGHÄNEL, T.;
Complexation of Cm(III) with aqueous silicic acid.
Radiochimica Acta, 93 (2005), 133-139

PLASCHKE, M.; ROTHE, J.; ALTMAIER, M.; DENECKE, M.A.; FANGHÄNEL, T.;
Near edge X-ray absorption fine structure (NEXAFS) of model compounds for the humic acid/actinide ion interaction.
Journal of Electron Spectroscopy and Related Phenomena, 148 (2005), 151-57

RABUNG, T.; PIERRET, M.C.; BAUER, A.; GECKEIS, H.; BRADBURY, M.H.; BAEYENS, B.; Sorption of Eu(III)/Cm(III) on Ca-montmorillonite and Na-illite, Part 1: Batch sorption and Time Resolved Laser Fluorescence Spectroscopy experiments
Geochimica et Cosmochimica Acta, 69 (2005), 5393-5402

SCHÄFER, T.; BUCKAU, G.; ARTINGER, R.; KIM, J.I.; GEYER, S.; WOLF, M.; BLEAM, W.F.; WIRICK, S.; JACOBSEN, C.;
Origin and mobility of fulvic acids in the Gorleben aquifer system: implications from isotopic data and carbon/sulfur XANES.
Organic Geochemistry, 36 (2005), 567-82

SMAILOS, E.; KIENZLER, B.;
Galvanic corrosion between the nuclear waste disposal container material pairs of copper-nickel alloys and carbon steel in salt brines
Corrosion, 61 (2005), 230 - 236

SOLOMON, D.; LEHMANN, J.; KINYANGI, J.; LIANG, B.; SCHÄFER, T.;
Carbon K-Edge NEXAFS and FTIR-ATR spectroscopic investigation of organic carbon speciation in soils.
Soil Science Society of America Journal, 69 (2005), 107-19

WEIGL, M.; DENECKE, M.A.; PANAK, P.J.; GEIST, A., GOMPPER, K.;
EXAFS and time-resolved laser fluorescence spectroscopy (TRLFS) investigations of the structure of Cm(III)/Eu(III) complexed with di(chlorophenyl)dithiophosphinic acid and different synergistic agents
Dalton Trans. (2005), 1281–1286

Reports

BITEA, C.;
Laser-induzierte Breakdown Detektion (LIBD): Quantifizierung der Kolloidbildung vierwertiger Actiniden und Homologen.
Wissenschaftliche Berichte, FZKA-7083 (Februar 2005)
Dissertation, Universität Karlsruhe 2003

BUCKAU, G.; [EDT.]
Humic substances in performance assessment of nuclear waste disposal: actinide and iodine migration in the far-field. Third technical progress report.
Wissenschaftliche Berichte, FZKA-7070 (April 2005)

BRENDEBACH, B.; DARDENNE, K.; DENECKE, M.A.; ROTHE, J.; FANGHÄNEL, T.; BLANK, H.; HORMES, J.; MODROW, H.;
INE-Beamline für Actinidenforschung
FZK-Nachrichten Bericht „ANKA“ 37/4 (2005).

CARBOL, P.; COBOS-SABATE, J.; GLATZ, J-P.; GRAMBOW, B.; KIENZLER, B.; LOIDA, A.; MARTINEZ ESPARZA VALIENTE, A.; METZ, V.; QUIÑONES, J.; RONCHI, C.; RONDINELLA, V.; SPAHIU, K.; WEGEN, D. H.; WISS, T.; edited by: SPAHIU, K.;
The effect of dissolved hydrogen on the dissolution of ^{233}U doped UO_2(s), high burnup spent fuel and MOX fuel.
Deliverable D10 EU contract No. FIKW-CT-2001-20192 SFS, SKB TR-05-09 (2005)

DENECKE, M.A.; JANSSENS, K.; SIMON, R.; NAZMOV, V.;
Ortsaufgelöste µ-XRF Untersuchungen eines uranreichen Sediments in konfokale Geometrie
FZK-Nachrichten Bericht „ANKA“ 37/4 (2005).
GEIST, A.; DENECKE, M.A.; PANAK, P.J. ; WEIGL, M.; SCHIMMELPFENNIG, B.; GOMPPER, K.;
Studien zur Selektivität von Di-triazinyl-pyridinen: EXAFS, TRLFS und quantenchemische Rechnungen
FZK-Nachrichten Bericht „ANKA“ 37/4 (2005).

JOHNSON, L.H.; POINSSOT, C.; FERRY, C.; LOVERA, P.; POULESQUEN, A.; MISERQUE, F.; CORBEL, C.; CAVEDON, J.M.; ANDRIAMBOLOLONA, Z.; WEGEN, D.; CARBOL, P.; GLATZ, J.P.; COBOS-SABATE, J.; SERRANO, D.; RONDINELLA, V.V.; WISS, T.; GRAMBOW, B.; SPAHIU, K.; KELM, M.; METZ, V.; LOIDA, A.; KIENZLER, B.; LUNDSTROM, T.; CHRISTENSEN, H.; JONSSON, M.; DE PABLO, J.; ROVIRA, M.; CLARENS, F.; CASAS, I.; MARTINEZ-ESPARZA, A.; GAGO, J.A.; BRUNO, J.; CERA, E.; MERINO, J.; GONZALEZ DE LA HUEBRA, A.; IGLESIAS, E.; QUINONES, J.; CACHOIR, C.; LEMMENS, K.; MAYER, G.; JEGOU, C.;
Spent fuel evolution under disposal conditions. Synthesis of results from the EU Spent Fuel Stability (SFS) project
Technical Report 04-09 (2005), NAGRA, Wettingen, Switzerland.

KIENZLER, B.; VEJMELKA, P.; RÖMER, J.; SCHILD, D.; MARQUARDT, C.; SCHÄFER, T.; SOBALLA, E.; WALSCHBURGER, C.;
Actinide migration experiment in the ÄSPÖ HRL in Sweden: results for uranium and technetium with core # 7. (Part IV).
Wissenschaftliche Berichte, FZKA-7113 (Mai 2005)

POINSSOT, C.; FERRY, C.; KELM, M.; GRAMBOW, B.; MARTINEZ, A.; JOHNSON, L.; ANDRIAMBOLOLONA, Z.; BRUNO, J.; CACHOIR, C.; CAVEDON, J.M.; CHRISTENSEN, H.; CORBEL, C.; JEGOU, C.; LEMMENS, K.; LOIDA, A.; LOVERA, P.; MISERQUE, F.; DE PABLO, J.; POULESQUEN, A.; QUINONES, J.; RONDINELLA, V.V.; SPAHIU, K.; WEGEN, D.H.;
Spent fuel stability under repository conditions – Final report of the European (SFS) project
CEA-R-6093, Octobre 2005, ISSN 0429 - 3460

PUDEWILLS, A.;
Numerical modelling of the long-term evolution of EDZ. Development of material models, implementation in finite-element codes, and validation.
Wissenschaftliche Berichte, FZKA-7185 (November 2005)

KIENZLER,B.; BAUER,A.; BOSBACH, D.; MARQUARDT, C.; PLASCHKE, M.;
Schutzfunktionen und Wirkungsweise des Multibarrierenkonzept bei der Endlagerung von radioaktiven Abfällen – Zwischenbericht im Auftrag der GNS Essen
FZK-INE Bericht 03/05 (Juni 2005)

KIENZLER,B.; BAUER,A.; BOSBACH, D.; MARQUARDT, C.; PLASCHKE, M.; SCHÄFER,TH.;
Schutzfunktionen und Wirkungsweise des Multibarrierenkonzept bei der Endlagerung von radioaktiven Abfällen – Abschlussbericht im Auftrag der GNS Essen
FZK-INE Bericht 09/05 (Dezember 2005)

Invited oral presentations

ALTMAIER, M.; NECK, V.; FANGHÄNEL, T.;
Solubility and Complex Formation of Uranium and Thorium in Alkaline Solution.
University of Cyprus, Department of Chemistry, Nikosia, Zypern, 20. April 2005.

BUCKAU, G.;
Humic Substances and Performance Assessment of Nuclear Waste Disposal: Some Present Basic Studies
LES Palaver, 8 March 2005,PSI-Paul-Scherrer Institut

DENECKE, M. A.;
Actinide Speciation at INE using Synchrotron Radiation
Johannes-Gutenberg-Universität Mainz, Institut für Kernchemie, 16. Februar 2005, Universität Mainz

DENECKE, M. A.;
Spectroscopic Actinide Speciation for Nuclear Waste Disposal
Plenar-Vortrag, Actinides2005, 4.-8. Juli 2005, Manchester, UK

DENECKE, M. A.;
Confocal µ-XRF and µ-XAFS Studies of an Uranium-Rich Sediment from a Nuclear Waste Disposal Natural Analogue Site
Microscopy & Microanalysis 2005, 31. July-4. August 2005, Honolulu, Hawaii

DENECKE, M. A.;
Comparative EXAFS and TRLFS study of trivalent actinides and Eu(III) complexed with partioning relevant ligands, 27. October 2005, CEA-Grenoble

FLÖRSHEIMER, M.; KRUSE, K.; KLENZE, R.; FANGHÄNEL, T.; KIM, J.-I.;
In situ Speciation of Mineral/Electrolyte Interfaces by Linear and Nonlinear Optical Vibrational Spectroscopy.
10th International Conference on Chemistry and Migration Behaviour of Actinides and Fission Products in the Geosphere (MIGRATION '05), Avignon (France), September 18 – 23, 2005

GECKEIS, H.;
Geochemical aspects of nuclear waste disposal: The role of colloids for actinide migration.
Ruprecht-Karls-Universität Heidelberg, Institut für Umweltgeochemie, 01. Februar 2005

GECKEIS, H.;
Research in actinide geochemistry: Do we need speciation information at the molecular level ?
29th Symposium on the Scientific Basis for Nuclear Waste Management, MRS 2005, Ghent, Belgium, September 12-16, 2005

GECKEIS, H.;
Actinidengeochemie: Von der molekularen Skala zum Felslabor,
GDCH Jahrestagung 2005, Tagung der Fachgruppe Nuklearchemie, Düsseldorf, 11.09.-14.09.2005

GECKEIS, H.; RABUNG, T.; BOUBY, M.;
Actinide interaction with humic matter
1st International Workshop on Organic Matter Modelling-WOMM'05, November, 16.-18., 2005, Toulon (France)

GEIST, A.;
Options for the Treatment of Spent Fuel from Nuclear Power Plants - Partitioning and Transmutation
8th German-American Frontiers of Engineering Symposium
May 4 - May 7, 2005, Potsdam, Germany

NECK, V.; ALTMAIER, M.; FANGHÄNEL, T.;
Solubility and redox reactions of $PuO_2 \cdot xH_2O$(s) in the presence of oxygen.
Int. Conf. Actinides 2005, Manchester, UK, July 4 - 8, 2005.

SCHÄFER, T.; JACOBSEN, C.
Mineral-Organic interaction: It's role in nature
Clay Mineral Society (CMS) Annual meeting workshop "Characterization of Solid-Water Interface Reactions of Metals and Actinides on Clays and Clay Minerals", Burlington VT, USA., 11.06.2005.

WALTHER, C.; FANGHÄNEL, T.; CHO, H.R.; HAUSER, W.; YUN, J.I.;
Spurennachweis und Gr¨oßenbestimmung aquatischer Kolloide mit der Laser-induzierten Breakdown Detektion, Jahrestagung der Gesellschaft deutscher Chemiker, Fachgruppe Analytische Chemie, ANAKON 2005, Regensburg, 15.-18. März 2005

WALTHER, C., M. Fuß, S. KOLTSOV, T. BERGMANN,;
Untersuchung von Actinid-Komplexen mittels ESI-MS, 69. Jahrestagung der Deutschen Physikalischen Gesellschaft, Fachgruppe Massenspektrometrie, Berlin, 4.-9. März 2005

YUN, J.-I.; PANAK, P.J.; KIM, M.A.; KIM, J.I.; FANGHÄNEL, T.;
Interaction of An(IV) with Ln(III)/An(III): Colloid formation and stabilization
Johannes-Gutenberg-Universität Mainz, Institut für Kernchemie, Mainz, 19. Januar 2005

Presentations at conferences, workshops

ALTMAIER, M.; NECK, V.; FANGHÄNEL, T.;
Ion interaction (SIT) coefficients for the Th^{4+} ion derived from trace activity coefficients in $NaClO_4$, $NaNO_3$ and NaCl solution.
10^{th} Int. Conf. on the Chemistry and Migration Behaviour of Actinides and Fission Products in the Geosphere, Avignon, France, Sept. 2005.

ALTMAIER, M.; NECK, V.; MÜLLER, R.; FANGHÄNEL, T.;
Solubility of U(VI) and formation of $CaU_2O_7 \cdot 3H_2O$(cr) in alkaline $CaCl_2$ solutions.
10^{th} Int. Conf. on the Chemistry and Migration Behaviour of Actinides and Fission Products in the Geosphere, Avignon, France, Sept. 2005.

ALTMAIER, M.; NECK, V.; MÜLLER, R.; FANGHÄNEL, T.;
Löslichkeit von Uran(VI) und Bildung von $CaU_2O_7 \cdot 3H_2O$(cr) in alkalischer $CaCl_2$-Lösung.
GdCH-Jahrestagung, Düsseldorf, Sept. 2005.

ARMBRUSTER, M.K.; WEIGEND, F.; SCHIMMELPFENNIG, B.; KLOPPER, W.;
A two-component RI-Hartree-Fock with a meanfield spin-orbit-operator in the one-centre approximation: Theory and first results.
Relativistic Effects in Heavy Elements (REHE 2005), Wolfsburg, Mülheim, April 6-10, 2005 (Poster)

BOUBY, M.; GECKEIS, H.; SCHÄFER, T.; MIHAI, S.; FANGHÄNEL, T.;
Interaction of Eu, Th and U with Bentonite Colloids in presence of Humic Acid: A Flow-Field Flow Fractionation study
10th International Conference on Chemistry and Migration Behavior of Actinides and Fission Products in the Geosphere (Migration '05) Avignon, France, Sept. 18 - 23, 2005

BOUBY, M.; GECKEIS, H.; RABUNG, T., FANGHÄNEL, T.;
Metal-induced humic acid agglomeration and its influence on actinide-humic-colloid dynamics
10th International Conference on Chemistry and Migration Behavior of Actinides and Fission Products in the Geosphere (Migration '05) Avignon, France, Sept. 18 - 23, 2005

BOUBY, M.; GECKEIS, H.; FANGHÄNEL, T.;
Interaction of radionuclides with aquatic colloids
First AQUANET Conference, Birmingham, 8th November 2005

BOUBY, M.; GECKEIS, H.; SCHÄFER, T.; MIHAI, S.; FANGHÄNEL, T.;
Bentonite colloids influence on radionuclide migration
FUNMIG annual workshop, 28. Nov. - 1. Dec. 2005, Saclay, France

CHO, H.R; WALTHER,C; ROTHE,J.; DENECKE,M; NECK, V; FANGHÄNEL,TH.;
Solubility of Zr(IV) oxide/hydroxide with LIBD and EXAFS,
Jahrestagung der Gesellschaft deutscher Chemiker, Fachgruppe Nuklearchemie, Düsseldorf, 11.-14. September 2005

CHO, H.R.; MARQUARDT, C.M.; NECK, V.; SEIBERT, A.; WALTHER, C.; YUN, J.I.; FANGHÄNEL, T.;
Redox behavior of plutonium(IV) in acidic solutions, ACTINIDES 2005, Intenational Conference, Manchester, UK, 4.-8. July 2005

CHO, H.R.; BITEA, C.; MARQUARDT, C.M.; NECK, V.; SEIBERT, A.; WALTHER, C.; YUN, J.I.; FANGHÄNEL, T.;
Hydrolysis of Pu(IV) studied by measurements of the Pu(IV)/Pu(II) redox equilibrium combined with spectroscopy, MIGRATION 2005 Chemistry and migration behaviour of actinides and fission products in the geosphere, Avignon, France, 18.-23. September 2005

CLARET, F.; KUMKE, M.; RABUNG, T.; STUMPF, T.; KLENZE, R.; KIM, J.I.; FANGHÄNEL, T.; BUCKAU, G.;
Photodynamic Processes in Cm(III) Humic and Fulvic Acid Complexes
10th International Conference on Chemistry and Migration Behavior of Actinides and Fission Products in the Geosphere (Migration '05) Avignon, France, Sept. 18 - 23, 2005

CLARET, F.; SCHÄFER, T.; RABUNG, T.; WOLF, M.; BAUER, A.; BUCKAU, G.
Clay organic matter as a potential humic source under alkaline perturbations.
Clays in Natural and Engineered Barriers for Radioactive Waste Confinement : 2nd Internat.Meeting, Tours, F, March 14-18, 2005.

DENECKE, M. A.;
Grazing incidence (GI) XAFS measurements of metal cation sorption onto mineral surfaces
Status seminar of the Helmholtz Virtual Institute Functional Properties of Aquatic Interfaces, Karlsruhe, 28. February 2005

DENECKE, M. A.;
Examples of the use of X-ray absorption spectroscopy in Geochemistry / Mineralogy
Seminar “Synchrotron X-ray and IR methods in the Geosciences at ANKA”, Karlsruhe, 24.October 2005 - 25.10.2005

DENECKE, M. A.;
Introduction to ANKA and the INE-Beamline
ITU 3rd Summer School on Basic Actinide Research 2005, Karlsruhe, June 2005

DENECKE, M. A.;
XAFS / INE-Beamline an der ANKA
25 Jahre INE – Jubiläumsveranstaltung, Forschungszentrum Karlsruhe, 17. Juni 2005

DENECKE, M. A.;
A new confocal µ-XRF set-up for measuring 3D elemental distributions with spatial resolution on the micrometer scale
1st Annual Workshop Proceedings 6th EC FP - FUNMIG IP, Saclay, France, 27. November-1. December 2005.

FANGHÄNEL, T.; ROTH, G.;
Die Verglasung von hochradioaktiven Flüssigabfällen- ein Weg zu mehr Sicherheit in der nuklearen Entsorgung, Vortrag Statuskoklloqium nuklearer Stillegungsprojekte im Forschungszentrum Karlsruhe, 6. Dezember 2005, Forschungszentrum Karlsruhe (FTU)

FLEISCH, J.; ROTH, G.; TOBIE, W.; WEISHAUPT, M.;
Verglasungsanlage VEK - Funktionsprüfungen und Schritte der Inbetriebnahme bis zur Aufnahme des aktiven Verglasungsbetriebs.
Jahrestagung Kerntechnik 2005, Nürnberg, 10.-12.Mai 2005
Berlin : INFORUM GmbH, 2005 S.258-61 CD-ROM

FLÖRSHEIMER, M.; KRUSE, K.; KLENZE, R.; FANGHÄNEL, T.;
Speziation der funktionellen Gruppen von Mineraloberflächen.
Status seminar of the Helmholtz Virtual Institute Functional Properties of Aquatic Interfaces, Karlsruhe, February 28, 2005

FLÖRSHEIMER, M.; KRUSE, K.; KLENZE, R.; FANGHÄNEL, T.; KIM, J.-I.;
Infrared Sum Frequency Spectroscopy to Study the Speciation of Surface Functional Groups.
ACTINET Meeting Spectroscopy and Quantum Chemistry Applied to Surface Reactions on Aluminium Oxy-Hydroxides, Karlsruhe, April 12, 2005

FLÖRSHEIMER, M.; KRUSE, K.; KLENZE, R.; FANGHÄNEL, T.;
Observing the Chemical Composition and the Point of Zero Charge of Mineral Surfaces in situ under Water by Nonlinear Optics.
15th Annual Goldschmidt Conference 2005, Moscow, Idaho (USA), Mai 20 – 25, 2005

FLÖRSHEIMER, M.; KRUSE, K.; KLENZE, R.; FANGHÄNEL, T.;
Reaktionen von Actiniden an der Mineral/Grundwasser Grenzfläche: Einblicke in die molekulare Dimension.
ITC-WGT Workshop Molekulare Interaktionen an Grenzflächen, Karlsruhe, July 7, 2005

FLÖRSHEIMER, M.; KRUSE, K.; KLENZE, R.; FANGHÄNEL, T.;
Wechselwirkung von Metalloxid- und Silikat-Oberflächen mit Elektrolyten.
Status seminar of the Helmhotz Virtual Institute Functional Properties of Aquatic Interfaces, Karlsruhe, September 2, 2005

FLÖRSHEIMER, M.; KRUSE, K.; KLENZE, R.; FANGHÄNEL, T.; KIM, J.-I.;
In situ Speciation of the Functional Groups at Mineral/Electrolyte Interfaces by Sum Frequency Vibrational Spectroscopy.
10th International Conference on Chemistry and Migration Behaviour of Actinides and Fission Products in the Geosphere (MIGRATION '05), Avignon (France), September 18 – 23, 2005

FLÖRSHEIMER, M.; KRUSE, K.; KLENZE, R.; FANGHÄNEL, T.; KIM, J.-I.;
In situ Speciation of the Functional Groups at Mineral/Electrolyte Interfaces by Sum Frequency Vibrational Spectroscopy.
2nd INE – CEA/SECR Meeting, Karlsruhe, October 18 - 19, 2005

GECKEIS, H.; SCHÄFER, T.; HAUSER, W.; RABUNG, T.; PUDEWILLS, A.;
Kolloidgetragener Radionuklidtransport in geklüftetem Gestein,
BMWA Fachgespräch: Radionuklidmigration – aktueller Stand in der Endlagersicherheitsforschung 26.-27.04.2005, Karlsruhe

GECKEIS, H.;
- (Geo-) chemical behaviour of radionuclides
- Colloid influence on radionuclide migration
FUNMIG Course on the Fundamentals of Radionuclide Migration, 07.-11. November 2005, Barcelona, Spain

GEIST, A.; MALMBECK, R.; SERRANO-PURROY, D.; WEIGL, M.; GOMPPER, K.; GLATZ, J.-P.;
Separation of Minor Actinides with Nitrogen Containing Extractants
Workshop "Future Nuclear Systems and Fuel Cycles", Karlsruhe, 1.-2. September 2005

GEIST, A.; WEIGL, M.; GOMPPER, K.;
A continuous DIAMEX Process in a hollow fibre module microplant
International Solvent Extraction Conference (ISEC 2005): „Solvent Extraction for Sustainable Development" Peking, China, 19-23 September 2005

GOMPPER, K.; GEIST, A.; MODOLO, G.; DENECKE, M.A.; PANAK, P.J.; WEIGL, M.; FANGHÄNEL, T.;
R&D on partitioning at the German research centers Karlsruhe and Juelich
Proc. Internat. Conf. GLOBAL 2005 (Nuclear Energy Systems for Future Generation and Global Sustainability), Paper 059, Tsukuba, Japan, October 9-13, 2005

HAUSER, W.; GECKEIS, H.; GÖTZ, R.; FANGHÄNEL, T.; MORALES, T.;
Laser-Induced Breakdown Investigations on the Stability of Background Colloids in Natural Groundwater
MRS 2005, 29th International Symposium on the Scientific Basis of Nuclear Waste Management, September 12-16, 2005, Ghent, Belgium

KIENZLER, B.; BAUER, A.; LOIDA, A.; METZ, V.;
Vergleich der Kritikalitätsicherheit in der Nachbetriebsphase bei der Endlagerung in Salz und Ton
Workshop GEIST "Gegenüberstellung von Endlagerkonzepten im Salz und Ton", Peine 19. und 20.1.2005

KIENZLER, B.; METZ, V.; LÜTZENKIRCHEN, J.; FANGHÄNEL, T.;
Nuclear Waste Disposal: Geochemical Methods for Performance Assessment. Proceedings of Int'l Conf. GLOBAL 2005 Nuclear Energy Systems for Future Generation and Global Sustainability, Tsukuba, Japan, Oct 9-13, 2005

KIENZLER, B.; VEJMELKA, P.; RÖMER, J.; SCHILD, D.; JANNSON, M.;
Conclusions From In-Situ Actinide Migration Experiments in Äspö HRL
10th International Conference on Chemistry and Migration Behavior of Actinides and Fission Products in the Geosphere, Migration '05, September 18-23, 2005, Avignon, France,

KLENZE, R.; LINDQVIST-REIS, P.; SCHUBERT, G.; FANGHÄNEL, T.;
Hydratation des Cm(III) Aquoions bei erhöhten Temperaturen bis 200 °C
GdCH-Jahrestagung 2005, Heinrich-Heine Universität, Düsseldorf, 11. – 14. September, 2005

KLENZE, R.;
Fluorescence spectroscopy on aquatic actinides - Experimental results and theoretical needs
ACTINET – Theoretical User Lab Workshop
Forschungszentrum Karlsruhe, October 24th-25th 2005

KRUSE, K.;
Speziation von Mineral-Oberflächen in-situ unter Elektrolyten mit nichtlinear optischen Methoden
Erstes HGF Doktorandenseminar "Nukleare Sicherheitsforschung",
Karlsruhe, 9. –11 März 2005

LÉON, A.; ROTHE, J.; SCHILD, D.; FICHTNER, M.;
Comparative study of $NaAlH_4$ doped with $TiCl_3$ or Ti_{13}·6THF by ball milling using XAS and XPS.
Pierucci, S. [Hrsg.], 2nd Internat.Conf.on Hydrogen Era, Palermo, I, October 16-19, 2005 Milano : AIDIC Servizi S.r.l., (2005), 171-76, (Chemical Engineering Transactions ; 8) ISBN 88-901915-0-3

LOIDA A.; KELM, M.; KIENZLER B.; GECKEIS H.;
The Effect of Near Field Constraints on the Corrosion Behavior of High Burnup Spent Fuel
MRS 2005, 29th International Symposium on the Scientific Basis of Nuclear Waste Management, September 12-16, 2005, Ghent, Belgium

LOIDA A.; KIENZLER B.; GECKEIS H.; KIM,S.S.;
Radionuclide retention in compacted bentonite contacting high burnup spent fuel
E-MRS 2005 Spring Meeting, May31-June 3, 2005, Strasbourg, France

LUCKSCHEITER, B.; KIENZLER, B.;
Korrosionsverhalten von HAW-Gläsern und Radionuklid-Freisetzung unter den Bedingungen verschiedener Wirtsgesteine.
Workshop GEIST "Gegenüberstellung von Endlagerkonzepten im Salz und Ton", Peine 19. und 20.1.2005

LUCKSCHEITER, B.; KIENZLER, B.;
Kenntnisstand zum Korrosionsverhalten von HAW-Gläsern in wäßrigen Lösungen von Tonformationen.
Jahrestagung Kerntechnik 2005, Nürnberg, 10.-12.Mai 2005
Berlin : INFORUM GmbH (2005), 266-70 CD-ROM

LUCKSCHEITER, B.; NESOVIC, M.;
HLW-Glass dissolution and co-precipitation studies
MRS 2005, 29th International Symposium on the Scientific Basis of Nuclear Waste Management, September 12-16, 2005, Ghent, Belgium

LINDQVIST-REIS, P.; KLENZE, R.; FANGHÄNEL, T.;
Influence of temperature and ionic strength on the hydration of curium(III) in aqueous solution studied with TRLFS
Actinides 2005, Manchester, UK, July 4-8, 2005

MARQUARDT, C.M.; KIENZLER, B.; ALTMAIER, M.; BRENDLER, V.; BOSBACH, D.; NECK, V.; RICHTER, A.;
Sichtung, Zusammenstellung und Bewertung von Daten zur geochemischen Modellierung.
Workshop des BfS: Sicherheitstechnische Einzelfragen der Endlagerung, 28/29. September 2005, Hannover, Germany

MARQUARDT,C.M.; BUCKAU,G.; CLARET,F.; DARDENNE,K.; DENECKE,M.A.; GECKEIS,H.; PLASCHKE,M.; ROTHE,J.; SEIBERT,A.; SCHÄFER,T.; FANGHÄNEL,TH.
Huminstoffgetragener Radionuklidtransport: Ergebnisse aus den Untersuchungen am INE.
1. Fachgespräch: "Radionuklidmigration - aktueller Stand in der Endlagersicherheitsforschung" 26./27. April 2005, Karlsruhe, Germany

METZ, V.; LOIDA, A.; KIENZLER, B.;
Reaction path modelling of spent fuel corrosion in Brines: comparison with experimental results
MRS 2005, 29th International Symposium on the Scientific Basis of Nuclear Waste Management, September 12-16, 2005, Ghent, Belgium

METZ, V.; LÜTZENKIRCHEN, J.; KORTHAUS, E.; KIENZLER, B.;
Application of geochemical modelling in performance assesment: the quasi closed system Approach
MRS 2005, 29th International Symposium on the Scientific Basis of Nuclear Waste Management, September 12-16, 2005, Ghent, Belgium

METZ, V.; KIENZLER, B.; LÜTZENKIRCHEN, J.; VEJMELKA, P.;
Interaction of Np with cement corrosion products in Q-brine. International Workshop Mechanisms and modelling of waste/cement interactions, Meiringen, Schweiz, Mai 2005, S. 54.

METZ, V.;
Performance Assessment – Welchen Beitrag kann die Geochemie zum Langzeitsicherheitsnachweis leisten?
25 Jahre INE – Jubiläumsveranstaltung, Forschungszentrum Karlsruhe, 17. Juni 2005

NECK, V.; ALTMAIER, M.; FANGHÄNEL, T.;
Solubility of $AnO_2 \cdot xH_2O$(am) in carbonate solution and formation of ternary An(IV) hydroxide-carbonate complexes.
10th Int. Conf. on the Chemistry and Migration Behaviour of Actinides and Fission Products in the Geosphere, Avignon, France, Sept. 2005.

NECK, V.; ALTMAIER, M.; FANGHÄNEL, T.;
Hydrous PuO_{2+x}(s): Solubility and thermodynamic data.
10th Int. Conf. on the Chemistry and Migration Behaviour of Actinides and Fission Products in the Geosphere, Avignon, France, Sept. 2005.

NECK, V.; ALTMAIER, M.; FANGHÄNEL, T.;
Modelling of actinides in chloride solution: Ion interaction approach versus treatment as ion association (chloride complexation). OECD/NEA Working Session on the TDB-2 Guidelines, Forschungszentrum Karlsruhe, INE, February 21 - 22, 2005.

NECK, V.; FANGHÄNEL, T.;
Some limitations encountered in the use of the ionic strength correction procedures.
OECD/NEA Working Session on the TDB-2 Guidelines, Forschungszentrum Karlsruhe, INE, February 21 - 22, 2005.

NECK, V.; ALTMAIER, M.; FANGHÄNEL, T.;
Solubility and redox reactions of $PuO_2 \cdot xH_2O$(s) in the presence of oxygen.
1.) 12. Koordinierungsgespräch FZK-INE - PSI/LES, Karlsruhe, 10. - 11. März, 2005.
2.) 2nd ITU-INE joint seminar, Karlsruhe, June 7, 2005.
3.) 2nd FZK-INE - CEA/SECR Collaboration Meeting, Karlsruhe, October 18-19, 2005

PANAK, P.;
Kolloide
25 Jahre INE – Jubiläumsveranstaltung, Forschungszentrum Karlsruhe, 17. Juni 2005

PLASCHKE, M.; ROTHE, J.;
Röntgenspektromikroskopie zur ortsaufgelösten Identifizierung funktioneller Spezies in Huminstoffen
Status seminar of the Helmhotz Virtual Institute Functional Properties of Aquatic Interfaces, Karlsruhe, February 28, 2005

PLASCHKE, M.; ROTHE, J.; NABER, A.; BALDEA, I.; ALTMAIER, M.; DENECKE, M. A.; FANGHÄNEL, T.;
Near Edge X-ray Absorption Fine Structure (NEXAFS) of model compounds for the humic acid / actinide ion interaction
GdCH Jahrestagung 2005, Düsseldorf, Germany, 11.-14. September 2005

PLASCHKE, M.; ROTHE, J.; NABER, A.; SCHIMMELPFENNIG, B.; DENECKE, M. A.; FANGHÄNEL, T.;
XAFS of model compounds for the humic acid/ actinide ion interaction
4th ANKA Users Meeting with Inauguration of Two New Beamlines Karlsruhe, Karlsruhe, Germany, 06 - 07 October 2005/ Workshop des "Theoretical Userlabs within ACTINET", Forschungszentrum Karlsruhe, Germany, 24.-25. Oktober 2005

POINSSOT, CH.; GRAMBOW, B.; KELM, M.; SPAHIU, K.; MARTINEZ, A.; JOHNSON, L.; CERA, E.; DE PABLO, J.; QUINONES, J.; WEGEN, D.; LEMMENS, K.; MCMENAMIN, T.;
Mechanisms governing the release of radionuclides from spent nuclear fuel in geological repository: major outcomes of the European Project SFS
MRS 2005, 29th International Symposium on the Scientific Basis of Nuclear Waste Management, September 12-16, 2005, Ghent, Belgium

PUDEWILLS, A.;
Numerical modelling of the long term evolution of EDZ, Proc.of the First Inter. Seminar: ECOMINING-EUROPE IN THE 21ST CENTURY, 27-29 Oct. 2005, Sovata & Praid Salt Mine, Romania, Eds. St. E. Deak & G. Deak, pp. 110-115, EstFalia, 2004., Bucharest, ISBN 973-7681-03-7

RABUNG, T.; GECKEIS, H.; SCHILD, D.; MITCHELL, S.; FANGHÄNEL, T.;
Cm(III) Sorption onto Aluminum Oxides/Hydroxides.
10th International Conference on Chemistry and Migration Behavior of Actinides and Fission Products in the Geosphere (Migration '05) Avignon, France, Sept. 18 - 23,

RABUNG, T.; SCHILD, D.; GECKEIS, H.; KLENZE, R.; FANGHÄNEL, T.;
Fluoreszenz-Detektion der Cm(III) Sorption an Einkristall-Oberflächen.
Status seminar of the Helmhotz Virtual Institute Functional Properties of Aquatic Interfaces, Karlsruhe, February 28, 2005

RABUNG, T.;
Cm(III) Sorption an Aluminium Oxide/Hydroxide
Status seminar of the Helmhotz Virtual Institute Functional Properties of Aquatic Interfaces, Karlsruhe, September 2, 2005

RABUNG, T.;
Reaktionen an Grenzflächen
25 Jahre INE – Jubiläumsveranstaltung, Forschungszentrum Karlsruhe, 17. Juni 2005

RABUNG, T.; PIERRET, M.C.; BAUER, A.; GECKEIS, H.; BRADBURY, M.H.; BAEYENS, B.;
Eu(III)/Cm(III) sorption onto clay minerals: TRLFS studies and surface complexation modeling.
42nd Annual Meeting of The Clay Minerals Society; Workshop: Characterization of Solid/Water Interface Reactions of Metals and Actinides on Clays and Clay Minerals, Burlingten, Vermont, June 11, 2005

RAPP, B.; HERRMANN, D.; GUBER, A.; WELLE, A.; SCHILD, D.; JACOB, A.; DAUBER, M.; HOHEISEL, J.;
Mikrotiterplatte mit integrierter funktionalisierter Filterstruktur.
Mikrosystemtechnik Kongress, Freiburg, 10.-12.Oktober 2005

ROTH, G.;
Verglasung hochradioaktiver Flüssigabfälle – INE-Technologie und Anwendung in der VEK
25 Jahre INE – Jubiläumsveranstaltung, Forschungszentrum Karlsruhe, 17. Juni 2005

ROTHE, J; DENECKE, M. A.; DARDENNE, K.; FANGHÄNEL, T.;
The INE-Beamline for Actinide Research at ANKA
MIGRATION 2005, Avignon, France, September 18-23, 2005

ROTHE, J.; PLASCHKE, M.; NABER, A.;
Röntgenspektromikroskopie und konfokale Mikroskopie zur ortsaufgelösten Identifizierung funktioneller Spezies in Huminstoffen
Status seminar of the Helmhotz Virtual Institute Functional Properties of Aquatic Interfaces, Karlsruhe, September 2, 2005

SCHÄFER, T.; CLARET, F.; LEROTIC, M.; BUCKAU, G.; BAUER, A.; JACOBSEN, C.;
Source identification and characterization of humic and fulvic acids isolated from Callovo-Oxfordian argillite and opalinus clay.
Clays in Natural and Engineered Barriers for Radioactive Waste Confinement : 2nd Internat.Meeting, Tours, F, March 14-18, 2005

SCHILD, D.; MARQUARDT, C.M.; SEIBERT, A.; FANGHÄNEL, T.;
Pu-Humate Complexation in Natural Groundwater by XPS
ACTINIDES 2005 International Conference, July 4-8, 2005, Manchester, UK

SKOVBJERG,L.; CHRISTIANSEN, B.; UTSUNOMIYA, S.; PLASCHKE, M.; RÖMER, J.; GECKEIS, H.; BALIĆ-ŽUNIĆ, T.; EWING, R.; STIPP, S.;
Mechanism of Interaction of Green Rust Sulphate and Redox Reactive Radionuclides: - Clues from C, Se and Np
FUNMIG annual workshop, 28. Nov. - 1. Dec. 2005, Saclay, France

STUMPF, T.; TITS, J.; FANGHÄNEL, T.; WALTHER, C.; RABUNG, T.; WIELAND, W.;
Uptake of Trivalent Actinides (Cm(III)) by Hardened Cement Paste: A Time-Resolved Laser Fluorescence Spectroscopy (TRLFS) Study
Migration 2005, Avignon, September 18 - 23, 2005

STUMPF, T.; BUCKAU, G.; FANGHÄNEL, T.;
Koordination von dreiwertigen Actiniden durch Huminsäure: eine TRLFS Untersuchung
GDCh Jahrestagung 2005, Düsseldorf, September 11 - 14, 2005

WALTHER,C; CHO, H.R; MARQUARDT, C.M.; NECK, V.; SEIBERT, A.; YUN, J.I.; FANGHÄNEL,T.;
Redox behaviour of Pu(IV) in acidic solutions: Disproportionation or oxidation by O2 and subsequent equilibration of the redox couples Pu(V)/Pu(VI) and Pu(IV)/Pu(III) ?, Jahrestagung der Gesellschaft deutscher Chemiker, Fachgruppe Nuklearchemie, Düsseldorf, 11.-14. September 2005

YUN, J.-I.; KIM, M.A.; PANAK, P.J.; KIM, J.I.; FANGHÄNEL, T.;
Formation of aquatic actinide(IV) colloid and stabilization via interaction with An(III)/Ln(III)
10th International Conference on Chemistry and Migration Behavior of Actinides and Fission Products in the Geosphere, Migration '05, September 18-23, 2005, Avignon, France

WALTHER, C.; FUSS, M.; KOLTSOV, S.; BERGMANN, T.;
Investigation of actinide-oligomers and colloids by electrospray-mass-spectrometry.
Physik seit Albert Einstein : 69.Jahrestagung der DPG, Berlin, 4.-9.März 2005
Verhandlungen der Deutschen Physikalischen Gesellschaft, R.6, B.40(2005) MS 4.1

WEIGL, M.; GEIST, A.; MÜLLICH, U.; GOMPPER, K.;
Kinetics of Americium Extraction with 2,6-Di(5,6-dipropyl-1,2,4-triazin-3yl)pyridine"
International Solvent Extraction Conference (ISEC 2005): „Solvent Extraction for Sustainable Development"Peking, China19-23 September 2005

WEIGL, M.; PANAK, P.J.; DENECKE, M.A.; GEIST, A.;
"Chemistry and structure of organic ligands extracting selectively An(III) over Ln(III)"
Actinet-ThUL Workshop, Karlsruhe, 24-25 October 2005

WEIGL,M.; PANAK, P. J.; DENECKE, M. A.; GEIST, A.; GOMPPER, K.;
Strukturuntersuchungen an einem hochselektiven Komplexliganden zur Extraktion dreiwertiger Actiniden
DECHEMA/GVC-Gemeinschaftsausschuss „Extraktion", Frankfurt/M., 7.-8. März 2005

WEIGL, M.; PANAK, P.J.; DENECKE, M.A.; GEIST, A.;
"Structural Investigations on Partitioning Relevant Organic Ligands"
Actinides 2005, Manchester (UK), 3.-8. Juli 2005

Other publications

BUCKAU, G.;
Physico-Chemical Interpretation of Complexation/Binding Capacity or Effective Humate Ligand Concentration for the An(III) and An(VI) Humate Complexation", In: Humic Substances: Molecular Details and Application in Land and Water Conservation, Ed. E. Ghabbour, Taylor and Francis, 2005, 153-165 (ISBN 1-59169-031-5).

CHO, H.-R.; WALTHER, C.; ROTHE, J.; NECK, V.; DENECKE, M.A.; DARDENNE, K.; FANGHÄNEL, T.;
XAFS Investigation of the Formation and Structure of Zr(IV) Colloids
ANKA Annual Report 2005, pg 84-85.

CLARET, F.; RABUNG, T.; SCHÄFER, TH.; BUCKAU, G.;
Photodynamic Processes of Cm(III) with different Fulvic Acids, Annex 12 in: Humic Substances in Performance Assessment of Nuclear Waste Disposal: Actinide and Iodine Migration in the Far-Field (Third Technical Progress Report), Ed.: G. Buckau, Report FZKA 7070, Research Center Karlsruhe, 2005.

DENECKE, M.A.; ROTHE, J.; DARDENNE, K.; FANGHÄNEL, T.; BLANK, H.; MODROW, H.; HORMES, J.;
INE-Beamline – Status September 2005
ANKA Annual Report 2005, pg 152-153.

DENECKE, M.A.; GEIST, A.; WEIGL, M.; PANAK, P.J.; SCHIMMELPFENNIG, B.;
EXAFS Characterization of Am(III) Complexedwith 2,6-di (5,6-dipropyl1,2,4-triazin-3-yl)pyridine
ANKA Annual Report 2005, pg 86-87.

DENECKE, M.A.; JANSSENS, K.; DARDENNE, K;
Elemental distributions and U speciation in uranium-rich sediment samples from Heselbach, HASYLAB Annual Report 2005.

JANSSENS, K.; VEKEMANS, B.; DENECKE, M.A.; DARDENNE, K; RAUSCH, N.; SHOTYK, W.; FALKENBERG, G.;
Co-localization of heavy metals in peat samples from the Harjavalta smelter site (Finland) by means of confocal μ-XRF at BL L
HASYLAB Annual Report 2005.

GECKEIS, H.;
Research in actinide geochemistry: Do we need speciation information at the molecular level ?..
MRS 2005, 29th International Symposium on the Scientific Basis of Nuclear Waste Management, September 12-16, 2005, Ghent, Belgium, Book of Abstracts

GEIST, A.; WEIGL, M.; GOMPPER, K.;
A continuous DIAMEX Process in a hollow fibre module microplant
Proceedings of the International Solvent Extraction Conference (ISEC 2005): „Solvent Extraction for Sustainable Development" 659 – 664 Peking, China, 19-23 September 2005

HAUSER W.; GECKEIS H.; GÖTZ R.; FANGHÄNEL T.; MORALES, T.;
Laser-Induced Breakdown Investigations on the Stability of Background Colloids in Natural Groundwater
MRS 2005, 29th International Symposium on the Scientific Basis of Nuclear Waste Management, September 12-16, 2005, Ghent, Belgium, Book of Abstracts [64]

KIENZLER, B.; METZ, V.; LÜTZENKIRCHEN, J.; FANGHÄNEL, T.;
Nuclear Waste Disposal: Geochemical Methods for Performance Assessment. Proceedings of Int'l Conf. GLOBAL 2005 Nuclear Energy Systems for Future Generation and Global Sustainability, Tsukuba, Japan, Oct 9-13, 2005, Paper No. 034.

KIENZLER, B.; VEJMELKA, P.; RÖMER, J.; SCHILD, D.; JANNSON, M.;
Conclusions From In-Situ Actinide Migration Experiments in Äspö HRL
10th International Conference on Chemistry and Migration Behavior of Actinides and Fission Products in the Geosphere, Migration '05, September 18-23, 2005, Avignon, France, Book of Abstracts S. 39

KIM, J.I.; KIM, M.A.; PANAK, P.J.;
Actinides on the track of aquatic colloids: Speciation of colloid-borne An(III).

227th American Chemical Society Nat.Meeting, Anaheim, Calif., March 28 - April 1, 2004 Abstracts of Papers of the American Chemical Society, 227(2004) U98-U98 148- NUCL Part 2

KLENZE, R.; FANGHÄNEL, T.;
Langzeitsicherheit der Endlagerung: Aquatische Chemie der Actiniden
Nachrichten aus der Chemie, 53 (2005) 1004-1009

KLENZE, R.; FANGHÄNEL, T.; KIM, J.I.; BRENDLER, V.; HADERMANN, J.; GRENTHE, I.;BRUNO, J.; STIPP, S.L.S.; READ, D.; MISSANA, T.;
Aquatic Chemistry and Thermodynamics of Actinides and Fission Products Relevant to Nuclear Waste Disposal (ACTAF).
C. Davies (editor):Euradwaste ´04, "Radioactive Waste Management – Community Policy and Research Initiatives", Proceedings of the Sixth European Commission Conference on the Management and Disposal of Radioactive Waste, Luxembourg, 29-31 March 2004, p. 425-437

LOIDA, A.; KIENZLER, B.; GECKEIS, H.;KIM,S.S.;
Radionuclide retention in compacted bentonite contacting high burnup spent fuel
E-MRS 2005 Spring Meeting, May31-June 3, 2005, Strasbourg, France, Book of Abstracts [ ]

LOIDA A.; KELM M.; KIENZLER B.; GECKEIS H.;
The Effect of Near Field Constraints on the Corrosion Behavior of High Burnup Spent Fuel
MRS 2005, 29th International Symposium on the Scientific Basis of Nuclear Waste Management, September 12-16, 2005, Ghent, Belgium, Book of Abstracts [29]

LOISEAU, P.; CAURANT, D.; DENECKE, M.A.; ROTHE, J.; DARDENNE, K.; MAJÉRUS, O.; HIGEL, P.; ADVOCAT, T.;
Amorphisation and Recrystallisation Mechanisms of Zirconolite Ceramics Irradiated by Heavy Ions
ANKA Annual Report 2005, pg 88-89.

LUCKSCHEITER, B.; NESOVIC, M.;
HLW-Glass dissolution and co-precipitation studies
MRS 2005, 29th International Symposium on the Scientific Basis of Nuclear Waste Management, September 12-16, 2005, Ghent, Belgium, Book of Abstracts [87]

MARQUES FERNANDES, M.; STUMPF, T.; RABUNG, T.; BOSBACH, D.; FANGHÄNEL, T.; DARDENNE, K.; SCHÄFER, T.; DENECKE, M.A.;
EXAFS Investigation of Americium Incorporation Into Secondary Minerals
ANKA Annual Report 2005, pg 90-91.

METZ, V.; LOIDA, A.; KIENZLER, B.;
Reaction path modelling of spent fuel corrosion in Brines: comparison with experimental results
MRS 2005, 29th International Symposium on the Scientific Basis of Nuclear Waste Management, September 12-16, 2005, Ghent, Belgium, Book of Abstracts [155]

METZ, V.; LÜTZENKIRCHEN, J.; KORTHAUS, E.; KIENZLER, B.;
Application of geochemical modelling in performance assesment: the quasi closed system Approach
MRS 2005, 29th International Symposium on the Scientific Basis of Nuclear Waste Management, September 12-16, 2005, Ghent, Belgium, Book of Abstracts [28]

PANAK, P.J.; BREBAN, D.; DARDENNE, K.; ROTHE, J.; DENECKE, M.A.; KIM, M.A.; KIM, J.I.; FANGHÄNEL, T.;
Interaction of U(VI) with Silica and Aluminosilicate Colloids in "Statu Nascendi"
ANKA Annual Report 2005, pg 92-93.

PASHALIDIS, I.;COLOCASSIDOU, C.;COSTA, C.N.; EFSTATHIOU, A.M.; BUCKAU, G.;
IR (DRIFT) Spectroscopic Studies on Temperature Impact of Humic Acid, Annex 11 in: Humic Substances in Performance Assessment of Nuclear Waste Disposal: Actinide and Iodine Migration in the Far-Field (Third Technical Progress Report), Ed.: G. Buckau, Report FZKA 7070, Research Center Karlsruhe, 2005.

POINSSOT, CH.; GRAMBOW, B.; KELM, M.; SPAHIU, K.; MARTINEZ, A.; JOHNSON, L.; CERA, E.; DE PABLO, J.; QUINONES, J.; WEGEN, D.; LEMMENS, K.; MCMENAMIN, T.;
Mechanisms governing the release of radionuclides from spent nuclear fuel in geological repository: major outcomes of the European Project SFS
MRS 2005, 29th International Symposium on the Scientific Basis of Nuclear Waste Management, September 12-16, 2005, Ghent, Belgium, Book of Abstracts [22]

QUINTAS, A.; MAJERUS, O.; LOISEAU, P.; CAURANT, D.; DENECKE, M.A.; ROTHE, J.; DARDENNE, K.;
Influence of the Alkali Cation Type on the Incorporation of Neodynium in Borosilicate Glasses for Nuclear Waste Immobilization
ANKA Annual Report 2005, pg 94-95.

RABUNG, T.; GECKEIS, H.; SCHILD, D.; MITCHELL, S.; FANGHÄNEL, T.;
Cm(III) Sorption onto Aluminum Oxides/Hydroxides.
10th International Conference on Chemistry and Migration Behavior of Actinides and Fission Products in the Geosphere (Migration '05) Avignon, France, Sept. 18 - 23, 2005, Book of Abstracts, S. 102

RAPP, B.; HERRMANN, D.; GUBER, A.; WELLE, A.; SCHILD, D.; JACOB, A.; DAUBER, M.; HOHEISEL, J.;
Mikrotiterplatte mit integrierter funktionalisierter Filterstruktur.
Mikrosystemtechnik Kongress, Freiburg, 10.-12.Oktober 2005
Berlin [u.a.] : VDE Verl.; 2005, S.773-776, Inkl.CD-ROM, ISBN 3-8007-2926-1

ROTH, G.; WEISENBURGER, S.; FLEISCH, J.; WEISHAUPT, M.;
Process Technique and Safety Features of the German VEK Vitrification Plant Currently Under Commissioning, GLOBAL 2005, Tsukuba, Japan, Oct. 9-13, 2005, Proceedings (CD), Paper No. 296

ROTHE, J.; PLASCHKE, M.; DENECKE, M.A.; FANGHÄNEL, T. ;
Carbon K-edge spectromicroscopy of model substances for the study of humic acid actinide complexation.
227th American Chemical Society Nat.Meeting, Anaheim, Calif., March 28 - April 1, 2004 Abstracts of Papers of the American Chemical Society, 227(2004) U75-U75 4-NUCL Part 2

SCHÄFER T.; CLARET F.; LEROTIC M.; BUCKAU G.; RABUNG TH.; BAUER A.; JACOBSEN C.; “Source identification and characterization of humic and fulvic acids isolated from Oxfordian argillite and Opalinus clay”, In: Humic Substances: Molecular Details and Application in Land and Water Conservation, Ed. E. Ghabbour, Taylor and Francis, 2005, 43-62 (ISBN 1-59169-031-5).

SCHILD, D.; MARQUARDT, C.M.; SEIBERT, A.; FANGHÄNEL, T.;
Pu-Humate Complexation in Natural Groundwater by XPS
ACTINIDES 2005 International Conference, July 4-8, 2005, Manchester, UK
Book of Abstracts S. 82

SEIBERT, A.; ROTHE, J.; DARDENNE, K.; MARQUARDT, C.M.; DENECKE, M.A.;
Pu L3-XAFS Investigation of Colloidal Pu(IV)-humate Species
ANKA Annual Report 2005, pg 96-97.

WEISENBURGER, S.; GRÜNEWALD, W.; ROTH, G.; TOBIE, W.;
Overview and New Development concerning Measurement Methods of Glass Level in Large-Scale Radioactive Waste Glass Melters, GLOBAL 2005, Tsukuba, Japan, Oct. 9-13, 2005, Proceedings (CD), Paper No. 298

STUMPF, TH.; BUCKAU, G.; FANGHÄNEL, T.;
“Coordination of trivalent actinides by humic acids: A TRLFS study“, Annex 1 in: “Humic Substances in Performance Assessment of Nuclear Waste Disposal: Actinide and Iodine Migration in the Far-Field (Third Technical Progress Report)”, Ed.: G. Buckau, Report FZKA 7070, Research Center Karlsruhe, 2005.

SIMON, R.; MANGOLD, S.; STEININGER, R.; SCHUPPLER, S.; PELLEGRIN, E.; DENECKE, M. A.; ROTHE, J.;
Changes and Upgrades at the ANKA Spectroscopy Beamlines
ANKA Annual Report 2005, pg. 150-151.

SZYMCZAK, W.; WOLF, M.; CHANEL, V.; BUCKAU, G.;
“Molecular Mass and Size Distributions and of Europium Complexed Humic Substances Measured by TOF-SIMS and AFFFF”, Annex 4 in: “Humic Substances in Performance Assessment of Nuclear Waste Disposal: Actinide and Iodine Migration in the Far-Field (Third Technical Progress Report)”, Ed.: G. Buckau, Report FZKA 7070, Research Center Karlsruhe, 2005.

WEIGL, M.; PANAK, P.J.; DENECKE, M.A.; GEIST, A.;
"Chemistry and structure of organic ligands extracting selectively An(III) over Ln(III)"
Actinet-ThUL Workshop, Karlsruhe, 24-25 October 2005
Book of Abstracts

WEIGL, M.; PANAK, P.J.; DENECKE, M.A.; GEIST, A.;
“Structural Investigations on Partitioning Relevant Organic Ligands”
Actinides 2005, Manchester (UK), 3.-8. Juli 2005; Book of Abstracts

WEIGL, M.; GEIST, A.; MÜLLICH, U.; GOMPPER, K.;
Kinetics of Americium Extraction with 2,6-Di(5,6-dipropyl-1,2,4-triazin-3yl)pyridine”
Proceedings of the International Solvent Extraction Conference (ISEC 2005): „Solvent Extraction for Sustainable Development“164 – 168 Peking, China19-23 September 2005

WOLF M.; BUCKAU G.; CHANEL V.;
“Asymmetrical Flow Field-Flow Fractionation of Humic Substances: Comparison of Polyacrylic Acids and Polystyrene Sulfonates as Molar Mass Standards”, In: Humic Substances: Molecular Details and Application in Land and Water Conservation, Ed. E. Ghabbour, Taylor and Francis, 2005, 23-33 (ISBN 1-59169-031-5).